Expedition 344 summary[1]

R.N. Harris, A. Sakaguchi, K. Petronotis, A.T. Baxter, R. Berg, A. Burkett, D. Charpentier, J. Choi, P. Diz Ferreiro, M. Hamahashi, Y. Hashimoto, K. Heydolph, L. Jovane, M. Kastner, W. Kurz, S.O. Kutterolf, Y. Li, A. Malinverno, K.M. Martin, C. Millan, D.B. Nascimento, S. Saito, M.I. Sandoval Gutierrez, E.J. Screaton, C.E. Smith-Duque, E.A. Solomon, S.M. Straub, W. Tanikawa, M.E. Torres, H. Uchimura, P. Vannucchi, Y. Yamamoto, Q. Yan, and X. Zhao[2]

Chapter contents

[1] Harris, R.N., Sakaguchi, A., Petronotis, K., Baxter, A.T., Berg, R., Burkett, A., Charpentier, D., Choi, J., Diz Ferreiro, P., Hamahashi, M., Hashimoto, Y., Heydolph, K., Jovane, L., Kastner, M., Kurz, W., Kutterolf, S.O., Li, Y., Malinverno, A., Martin, K.M., Millan, C., Nascimento, D.B., Saito, S., Sandoval Gutierrez, M.I., Screaton, E.J., Smith-Duque, C.E., Solomon, E.A., Straub, S.M., Tanikawa, W., Torres, M.E., Uchimura, H., Vannucchi, P., Yamamoto, Y., Yan, Q., and Zhao, X., 2013. Expedition 344 summary. *In* Harris, R.N., Sakaguchi, A., Petronotis, K., and the Expedition 344 Scientists, *Proc. IODP,* 344: College Station, TX (Integrated Ocean Drilling Program). doi:10.2204/iodp.proc.344.101.2013
[2] **Expedition 344 Scientists' addresses.**

Abstract

The Costa Rica Seismogenesis Project (CRISP) was designed to elucidate processes that control nucleation and seismic rupture of large earthquakes at erosional subduction zones. The CRISP study area is located offshore the Osa Peninsula where the incoming Cocos Ridge has lifted the seismogenic zone to within reach of scientific drilling. This area is characterized by low sediment supply, a fast convergence rate, abundant plate interface seismicity, and a change in subducting plate relief along strike. In addition to elucidating processes at erosional convergent margins, this project is complementary to other deep fault drilling projects (e.g., The Nankai Trough Seismogenic Zone Experiment and the Japan Trench Fast Drilling Project).

Integrated Ocean Drilling Program (IODP) Expedition 344 is the second expedition of CRISP Program A (IODP Proposal 537A-Full5), a first step toward deep riser drilling through the seismogenic zone. The focus of CRISP Program A is on the shallow lithologic, hydrologic, stress, and thermal conditions that lead to unstable slip in the seismogenic zone. Together with IODP Expedition 334, the first expedition of CRISP Program A, these data provide exciting insights into the nature of seismogenesis and erosive plate boundaries.

Background

Seismogenesis at convergent margins

Convergent margins produce the world's largest earthquakes and devastating tsunamis, as most recently and tragically demonstrated by the 2011 Tohoku earthquake. Studies of interplate seismicity have shown that large earthquakes generally initiate within specific depth limits, generally between ~10 and 40 km (Byrne et al., 1988; Pacheco et al., 1993; Tichelaar and Ruff, 1993; Scholz, 2002), but the precise limits vary with temperature (Hyndman et al., 1997). This observation led to a conceptual model in which the subduction thrust is divided into three zones (e.g., Scholz, 1988). In the shallowest zone, plate convergence is accommodated by stable (aseismic) slip. Here, fault material is fresh, unconsolidated, and characterized by velocity strengthening. The middle section, where large earthquakes initiate, is characterized by unstable (stick-slip) behavior and is termed the seismogenic zone (Scholz, 2002). Fault zone rocks in this region have transitioned

doi:10.2204/iodp.proc.344.101.2013

from velocity-strengthening to velocity-weakening friction, and shear becomes localized. The onset of seismogenic behavior is correlated with the intersection of the 100°–150°C isotherm and the subduction thrust (Hyndman et al., 1997; Oleskevich et al., 1999). With increasing depth down the subduction thrust, the frictional characteristics undergo a second transition either due to the juxtaposition with the forearc mantle or because the rocks are heated to 350°–450°C and can no longer store elastic stresses needed for rupture. Transitional regions between the three zones have conditional stability and can host rupture but are generally not thought to be regions where large earthquakes initiate.

Although this three-zone two-dimensional view of the subduction thrust provides a reasonable framework, it is simplistic. Rupture models for large subduction earthquakes suggest significant fault plane heterogeneity in slip and moment release that in three dimensions is characterized as patchiness (Bilek and Lay, 2002). Additionally, we now know the transition zone from stable to unstable sliding is not simple but hosts a range of fault behaviors that includes creep events, strain transients, slow and silent earthquakes, and low-frequency earthquakes (Peng and Gomberg, 2010; Beroza and Ide, 2011; Ide, 2012).

Fundamentally unknown are the processes that change fault behavior from stable sliding to stick-slip behavior. Understanding these processes is important for understanding earthquakes, the mechanics of slip, and rupture dynamics. For a fault to undergo unstable slip, fault rocks must have the ability to store elastic strain, be velocity weakening, and have sufficient stiffness. Hypotheses for mechanisms leading to the transition between stable and unstable slip invoke temperature, pressure, and strain-activated processes that lead to downdip changes in the mechanical properties of rocks. These transitions are also sensitive to fault zone composition, lithology, fabric, and fluid pressures.

The composition of the material in the fault zone and its contrast with the surrounding wall rock play a key role in rock frictional behavior. The frictional state of the incoming sediment changes progressively with increasing temperature and pressure as it travels downdip. Important lithologic factors influencing friction are composition, fabric, texture, and cementation of rocks, as well as fluid pore pressure (Bernabé et al., 1992; Moore and Saffer, 2001; Beeler, 2007; Marone and Saffer, 2007; Collettini et al., 2009). For example, fault rocks with high phyllosilicate content are generally weaker than rocks with low phyllosilicate content (Ikari et al., 2011). Sediment properties including porosity, permeability, consolidation state, and alteration history also exert a strong influence on fault zone behavior. At erosive margins, where the plate boundary cuts into the overriding plate, the composition and strength of the upper plate is also important (McCaffrey, 1993).

Field observations and laboratory experiments suggest that a prerequisite for unstable sliding is that the incoming sediment is consolidated and lithified (Davis et al., 1983; Byrne et al., 1988; Marone and Scholz, 1988; Marone and Saffer, 2007; Fagereng and Sibson, 2010). This hypothesis posits that the updip limit of the seismogenic zone occurs near a threshold of consolidation and/or lithification in which fault zone behavior changes from distributed shear (stable sliding), where shear is accommodated by granular processes, to localized shear (unstable sliding) along discrete surfaces. Among other factors, the processes of lithification and consolidation are influenced by fault slip rate, mineralogy, and heat flow.

Pore pressure within the fault zone is a principal factor controlling effective stress and strength along the plate interface (Sibson, 1981; Scholz, 1988). Pore pressures in excess of hydrostatic pressures decrease the effective normal stress, thereby limiting the shear stress, and, coupled with the low consolidation and lithification state of sediment in the updip aseismic portion of the fault, may explain the lack of seismicity. A downdip decrease in pore fluid pressure increases the normal stress, leading to greater instability in plate sliding (Scholz, 1988).

Diagenetic and low-grade metamorphic reactions likely contribute to both lithification and consolidation processes, as well as changes in pore pressure (Moore and Saffer, 2001). These reactions lead to clay transformation, carbonate and zeolite cementation, the initiation of pressure solution, and quartz cementation. These processes lead to an increase in lithification, a decrease in fluid production that increases the effective stress, and strengthening of the overriding plate, which increases its ability to store elastic strain.

Variation in subducting plate relief has also been invoked as a cause for the change in the effective stress, the mechanics of the plate boundary, and the frictional stability of the fault zone (e.g., Scholz and Small, 1997). Detailed bathymetric and seismic data collection in several subduction zones has led to correlations between large earthquake rupture patterns and subducting features such as seamounts and ridges (Bilek et al., 2003; Bilek, 2007). Subducting oceanic ridges and seamounts have been suggested as asperities that can be the loci of earthquake nucleation (e.g., Lay and Kanamori, 1981; Lay et al., 1982; Ruff, 1992) or as barriers to along-strike earthquake rupture (Kodaira et al., 2000; Hirata et al., 2003;

Wang and Bilek, 2011). In fact, all of these processes may act in concert to change the frictional properties of the fault zone. Pore fluid pressure, fault rock mineralogy, diagenesis, consolidation, lithification, and subducting plate relief may all play an important role.

Chief among the many reasons that the active seismogenic zone is poorly understood is that it has been inaccessible to geologic sampling. Testing these hypotheses requires obtaining samples of fault zone material in the updip aseismic zone, in the transition zone, and within the seismogenic zone. Advances in drilling technology and the capabilities of the Japanese drilling vessel *Chikyu* make drilling into the transition and seismogenic zones possible.

Erosive and accretionary convergent margins

Fault behavior needs to be understood in the context of regional tectonics. Convergent margins may be divided into two end-member types that are termed erosive and accretionary plate boundaries (e.g., von Huene and Scholl, 1991; Clift and Vannucchi, 2004). The fundamental difference between these styles of subduction is the transfer of material between the overriding and downgoing plates. At accretionary margins, material above the décollement is transferred from the downgoing plate to the upper plate through either frontal accretion or underplating at the base of the forearc accretionary prism, leading to a net growth of the margin. Accretion rates vary between ~7 and 29 km^3/m.y. (Clift and Vannucchi, 2004). At erosive margins, all incoming sediment is subducted and the upper plate is eroded at its front and base such that the upper surface of the margin subsides and retreats (Lallemand et al., 1994). Basal erosion rates of 25–50 km^3/m.y. per kilometer of trench length are estimated for northeast Japan, northern Chile and Peru, Ecuador, Costa Rica, and Alaska (Scholl et al., 1980; von Huene and Lallemand, 1990; von Huene and Scholl, 1991; Ranero and von Huene, 2000; Collot et al., 2004; Clift and Vannucchi, 2004). The process by which subduction erosion occurs is unclear.

Catalogs of convergent margins (Clift and Vannucchi, 2004; Heuret et al., 2011) indicate subduction erosion is favored in regions where the incoming sediment thickness is <1 km and convergence rates exceed 60 mm/y. Conversely, subduction accretion is favored in areas where the incoming sediment thickness is >1 km and convergence rates are <60 mm/y. It is important to note that these are end-member models and in reality margins likely transition back and forth along strike and in time with phases of accretion, nonaccretion, and erosion.

One reason it is important to understand the contrasting behavior of erosive and accretionary margins is that the style of seismicity associated with each of these margins may differ. Notwithstanding the short instrumental record, Bilek (2010) suggests tsunami earthquakes are more likely to be generated at erosive margins. These events arise from slip in the shallowest portion of the subduction zone that produce large tsunamis relative to their seismic moment (Kanamori, 1972; Kanamori and Kikuchi, 1993; Satake and Tanioka, 1999; Polet and Kanamori, 2000; Abercrombie et al., 2001; Bilek and Lay, 2002; Ammon et al., 2006). These earthquakes generate large shallow slip on the subduction thrust that uplifts the seafloor, displacing the overlying water. In contrast, the largest events (M > 9) are more likely to be generated at accretionary margins (Bilek, 2010). This observation suggests the difference in seismic style between subduction accretion and erosion may be systematically different.

The Cocos Ridge and subducting Cocos plate

Offshore the western margin of Costa Rica, the oceanic Cocos plate subducts under the Caribbean plate, forming the southern end of the Middle America Trench (Fig. F1). Here, the Middle America Trench exhibits prominent variability that includes changes in the incoming plate age, convergence rate and obliquity, morphology, and slab dip. The age of the Cocos plate at the Middle America Trench decreases from 24 Ma offshore the Nicoya Peninsula to 14 Ma offshore the Osa Peninsula (Barckhausen et al., 2001). Subduction rates vary from 70 mm/y offshore Guatemala to 90 mm/y offshore southern Costa Rica (DeMets, 2001). Convergence obliquity across the trench varies from offshore Nicaragua, where it is as much as 25°, to nearly orthogonal convergence southeast of the Nicoya Peninsula (DeMets, 2001; Turner et al., 2007). The variations in plate age, convergence rate, and slab dip influence the thermal structure of the margin (Harris et al., 2010b), and the variation in the convergent obliquity has implications for slip partitioning as indicated by focal mechanisms and GPS displacement data (Lundgren et al., 1999; McCaffrey, 2002; Norabuena et al., 2004; Turner et al., 2007; LaFemina et al., 2009).

The bathymetry and morphology of the incoming Cocos plate varies substantially between the Nicoya and Osa Peninsulas (Fig. F1). This variation is a function of the plate's origin and subsequent history. The Cocos plate was formed at two ridges, the fast-spreading East Pacific Rise (EPR) and the slow-spreading Cocos-Nazca spreading center (CNS). The boundary separating EPR from CNS crust is a combination of a triple-junction

trace and a fracture zone, collectively comprising a "plate suture" (Barckhausen et al., 2001) (Fig. F1). EPR-generated crust is north of the plate suture and has a generally smoother morphology. CNS-generated crust is south of the plate suture and has a generally rougher morphology.

After the Cocos plate formed, it was intruded by Galapagos magmatism that generated the aseismic Cocos Ridge and many seamounts that together contribute to large variations in bathymetric relief. The Cocos Ridge is an overthickened welt of oceanic crust that stands ~2.5 km higher than the surrounding seafloor and has a maximum thickness of ~25 km, which is greater than three times normal ocean crust thickness (Walther, 2003). Northwest of the Cocos Ridge, seamounts 1–2 km high and 10–20 km in diameter cover ~40% of the seafloor (von Huene et al., 1995, 2000). The subduction of the Cocos Ridge and seamounts has caused substantial subduction erosion of the outer forearc (Ranero and von Huene, 2000). Additionally, the overthickened Cocos Ridge is more buoyant than normal oceanic crust and has uplifted the Osa Peninsula and the Quepos region (Gardner et al., 1992, 2001; Fisher et al., 1998; Sak et al., 2004). Cocos Ridge subduction is also manifested in changes to the dip and depth of the Wadati-Benioff Zone. The seismically active slab dips ~65° near the Nicaraguan border and shallows by a few degrees inboard of the Cocos Ridge. At depths below 60 km there is no seismically defined slab landward of the Cocos Ridge (Vergara Muñoz, 1988; Protti et al., 1994).

Upper plate and subaerial geology

Active subduction erosion from Guatemala to Costa Rica is indicated by drilling, seismic, and bathymetric data (Ranero and von Huene, 2000; Ranero et al., 2000; Vannucchi et al., 2001, 2003, 2004). Disrupted bathymetry at the base of the margin slope indicates frontal erosion (Fig. F1). These embayments are thought to mark the location where seamounts or other elevated bathymetric features have tunneled into the margin and indicate a net loss of material. Offshore the Osa Peninsula, the margin has a broad concavity centered on the Cocos Ridge, testifying to the removal of material through ridge subduction.

Basal erosion is suggested by shallow-water sedimentary rocks recovered at deep-water depths that lie unconformably on upper plate framework rock (Vannucchi et al., 2001). Drilling data offshore the Nicoya Peninsula suggest the margin has undergone basal erosion and subsidence since ~16 Ma (Vannucchi et al., 2001). Benthic fauna preserved in the slope apron sediment coupled with changes in facies are interpreted to suggest that a slow background subsidence of ~20 m/m.y. radically increased to ~600 m/m.y. initiating at the Miocene/Pliocene boundary at 2.4 Ma (Vannucchi et al., 2003). The short-term rate of removal of rock from the forearc is estimated to be 107–123 km^3/m.y. per kilometer of trench. This acceleration in subsidence may be linked to the arrival of the Cocos Ridge at the subduction zone (Vannucchi et al., 2003).

Seismic data along the margin show that it is composed of a thick slope sediment apron, a few hundred meters to ~2 km thick, unconformably overlying upper plate framework material (von Huene et al., 2000). In the Costa Rica Seismogenesis Project (CRISP) drilling area, the upper plate is underthrust by sediment and buttressed by a small frontal prism (Fig. F2). The frontal prism offshore the Osa Peninsula is ~6 km wide, a similar width to the frontal prism offshore the Nicoya Peninsula.

The subduction of the Cocos Ridge is thought to have caused (1) the cessation of the arc volcanism and uplift of the Talamanca Cordillera; (2) the inversion of the middle Eocene–Pliocene forearc basin, now exposed along the Fila Costeña, a fold-and-thrust belt with peak elevations of 1000–1500 m; and (3) the exhumation of the Late Cretaceous–early Eocene ophiolitic rocks cropping out along the Osa Peninsula Gulf and the middle Eocene–middle Miocene Osa Mélange. Geologic and GPS data reveal uplift and shortening is at a maximum directly inboard of the Cocos Ridge. Quaternary shortening exceeds 15 km (10–40 mm/y) across the Fila Costeña fold-and-thrust belt (Fisher et al., 2004; Sitchler et al., 2007). The Talamanca Cordillera, located between the Fila Costeña fold-and-thrust belt and the northern Panama deformation belt, exposes plutonic rocks as young as 6 Ma (MacMillan et al., 2004), implying rapid uplift.

Because of its influence on the upper plate, an outstanding issue for the tectonics of the region is the timing of the Cocos Ridge impinging on the Middle America Trench. Estimates range between ~1 Ma (Hey, 1977; Lonsdale and Klitgord, 1978), ~5 Ma (Sutter, 1985), and ~20–22 Ma (Lonsdale and Klitgord, 1978; van Andel et al., 1971). The 5 Ma age is based on the emplacement of adakitic arc rocks between 5.8 and 2.0 Ma (Abratis and Wörner, 2001) and thermochronological information on the uplift of the Talamanca Cordillera (Gräfe et al., 2002). However, marine deposition and volcanic flows in the Pliocene Terraba forearc basin directly inboard of the Cocos Ridge (Kolarsky et al., 1995) raise concerns about this model.

The lithology of the upper plate framework rock is not known. One hypothesis is that the upper plate basement is composed of a mélange of oceanic lithologies accreted to the overriding plate prior to

the current phase of subduction erosion (Fig. F2). This hypothesis posits that the basement is the offshore extension of the Caribbean Large Igneous Province (CLIP) and the Quepos and Osa terranes that crop out onshore (Ye et al., 1996; Kimura, Silver, Blum, et al., 1997; Vannucchi et al., 2001). The CLIP is composed of accreted oceanic islands and aseismic ridge terranes (Hauff et al., 1997, 2000; Sinton et al., 1997; Hoernle et al., 2002). The Quepos and Osa terranes are interpreted as accreted material derived from subducted edifices generated by the Galapagos hotspot (Hauff et al., 1997; Vannucchi et al., 2006). On land and close to the CRISP transect, the seawardmost unit is the Osa Mélange, which is dominated by basalt, radiolarite, and limestone (Vannucchi et al., 2006). Alternatively, upper plate basement may be composed of paleoaccretionary prism material. This hypothesis is consistent with the relatively low seismic velocities (3.5 km/s) observed below the erosional unconformity (Fig. F2B).

Within the upper plate basement, a major unknown is the nature of the high-amplitude landward-dipping reflectors cutting through the forearc (Fig. F2). These reflectors branch upward from the plate interface similar to "splay faults" in Nankai Trough (Park et al., 2002). These surfaces may represent old faults, related to a middle Eocene–middle Miocene accretionary event, now covered by the slope apron sediment. A few of them have offsets at the top of the forearc basement into the slope apron, indicating reactivation as normal faults. Similar reactivated normal faults are observed offshore the Nicoya Peninsula and Quepos terrane (McIntosh et al., 1993; Ranero and von Huene, 2000). These discontinuities across the forearc basement can offer preexisting planes of weakness and may play a role in focusing fluid flow drained from the deeper part of the margin. The nature and magnitude of permeability along these discontinuities is unknown. Identifying the nature and age of the landward-dipping reflectors is fundamental to understanding the tectonic history of the margin offshore Osa Peninsula and the process of subduction erosion.

Seismogenic zone and earthquakes

Costa Rica is a seismically active area with a history of Mw > 7 earthquakes and along-strike changes in the seismogenic zone (Protti et al., 1995; Newman et al., 2002). Offshore of the Osa Peninsula, the 20 August 1999 Mw 6.9 Quepos interplate thrust earthquake (Fig. F3) generated aftershocks recorded by a network of ocean-bottom seismometers (OBSs) and land seismometers deployed during the Costa Rica Seismogenic Zone Experiment (CRSEIZE) (DeShon et al., 2003). The 1999 Quepos earthquake initiated at the downdip extension of the incoming Quepos Plateau at a depth of 21 ± 4 km. This area coincides with the southern edge of the Costa Rica margin seamount province and bathymetrically elevated crust. These observations led Bilek et al. (2003) to suggest that this event represented rupture of topographic highs that act as asperities (Lay and Kanamori, 1980; Lay et al., 1982). Offshore the Osa Peninsula, earthquake hypocenters and aftershock clustering are located in regions of seismically imaged lower plate relief (Bilek et al., 2003; Husen et al., 2002; Protti et al., 1995).

Aftershocks to the 1999 Quepos earthquake delineate a plate dipping at 19° and are interpreted to mark the interface between the Cocos and Caribbean plates (DeShon et al., 2003). Most of the aftershocks occurred between 10 and 30 km depth and at a distance 30 to 95 km landward of the trench. DeShon et al. (2003) found that the sequence of aftershocks appeared to be influenced by the morphology of the downgoing plate, consistent with the suggestion of Bilek et al. (2003). The depth distribution of aftershocks yielded updip and downdip seismicity limits at depths of ~10 and 30 km below sea level (DeShon et al., 2003).

More recently, a 16 June 2002 Mw 6.4 event and its aftershocks were recorded by a temporary network of ocean-bottom hydrophones (OBHs) (Arroyo et al., 2011). This event nucleated 40 km west of the Osa Peninsula. Preliminary analysis shows this event to be a shallow underthrusting event that likely occurred on the plate boundary.

GPS measurements on land indicate interseismic strain accumulation on the plate interface and highlight the important influence that the subducting Cocos Ridge has on the tectonics of the area (Norabuena et al., 2004; LaFemina et al., 2009). Regional surface velocity data are consistent with the Cocos Ridge acting as a rigid indenter that leads to arc-parallel forearc motion (LaFemina et al., 2009).

Heat flow data

Values of surface heat flow vary greatly offshore Costa Rica and have important implications for the thermal state of the shallow subduction thrust and thermally mediated processes along the subduction thrust (Fig. F4). Regional heat flow measurements on the incoming Cocos plate reveal a large along-strike variation in heat flow (Von Herzen and Uyeda, 1963; Vacquier et al., 1967). EPR-generated crust of the Cocos plate has low heat flow values relative to the global mean for crust of the same age. The mean value and standard deviation of regional heat flow data on EPR seafloor are ~30 and 15 mW/m^2, respectively. Conductive predictions for seafloor of

ages between 24 and 14 Ma are ~100–130 mW/m^2 (Stein and Stein, 1992). In contrast, heat flow values on CNS-generated seafloor are close to the conductive prediction but above the global mean for crust of this age. These values exhibit large variability indicative of fluid flow with a mean and standard deviation of 110 and 60 mW/m^2, respectively.

In 2000 and 2001, heat flow studies specifically designed to investigate the nature of the thermal transition between cold EPR and warm CNS crust were undertaken (Fisher et al., 2003; Hutnak et al., 2007, 2008). Closely spaced heat flow values collocated with seismic reflection lines show a sharp transition (<5 km) between warm and cool seafloor seaward of the trench that generally corresponds to the area of the plate suture (Fig. **F4**). The sharp transition indicates a shallow source consistent with fluid flow in the upper oceanic crust. The thermal boundary between warm and unusually cool values deviates from the plate suture and appears to be influenced by the proximity of basement highs that penetrate the otherwise ~300–400 m thick sediment cover. This exposed basement on EPR accreted crust focuses discharge and efficiently ventilates the oceanic crust.

Probe measurements and bottom-simulating reflector (BSR) estimates of heat flow on the margin were analyzed by Harris et al. (2010a, 2010b). These profiles show strong variations along strike consistent with regional heat flow data on the incoming Cocos plate. Along the margin underthrust by EPR crust, heat flow is low (Langseth and Silver, 1996; Fisher et al., 2003; Hutnak et al., 2007), whereas along the margin underthrust by CNS crust, heat flow is generally high. The transition between the low and high heat flow generally correlates with the extension of the plate suture but is also influenced by the proximity of seamounts (Fisher et al., 2003) and appears relatively abrupt. High wavenumber variations in the heat flow data are interpreted as focused fluid flow through the margin near the deformation front (Harris et al., 2010a, 2010b).

Volatiles and fluids

Fluid flow pathways through the Costa Rica margin include the upper plate basement and overlying sediment, the décollement, and the underlying oceanic crust (e.g., Silver et al., 2000; Fisher et al., 2003; Hutnak et al., 2007; Sahling et al., 2008; Harris et al., 2010b). Along the entire Costa Rica margin, active fluid venting is indicated by elevated methane concentrations in the bottom water (Kahn et al., 1996; McAdoo et al., 1996; Bohrmann et al., 2002; Sahling et al., 2008). Chemoautotrophic and methanotrophic communities mark cold vents at numerous localities, but higher community abundances have been found where subducted seamounts have triggered fractures, slides, and slumps that break a low-permeability, shallow sediment carapace, allowing ascending fluids to feed the communities. These communities are particularly concentrated along headwall scarps (Kahn et al., 1996; Bohrmann et al., 2002; Sahling et al., 2008). Mud volcanoes and mud diapirs have also been found, particularly across the middle slope, and are associated with a high density of chemosynthetic vents. The chemistry of the pore fluids sampled at these midslope features is indicative of clay dehydration reactions at depth (Shipley et al., 1992; Bohrmann et al., 2002; Grevemeyer et al., 2004; Hensen et al., 2004; Sahling et al., 2008).

Along the décollement and the upper prism fault zone, coring and sampling during Ocean Drilling Program (ODP) Legs 170 and 205 offshore the Nicoya Peninsula revealed freshened pore waters containing elevated Ca, Li, and C_3–C_6 hydrocarbon concentrations and low K concentrations (Kimura, Silver, Blum, et al., 1997; Silver et al., 2000; Chan and Kastner, 2000; Morris, Villinger, Klaus, et al., 2003; Kastner et al., 2006). These fluids contrast with pore fluids from below the décollement and between the décollement and upper fault zone that have near-seawater chemistry (Kimura, Silver, Blum, et al., 1997; Morris, Villinger, Klaus, et al., 2003). Downhole temperatures measured during Legs 170 and 205 are too low to support in situ mineral dehydration and thermogenic hydrocarbon generation. Collectively, the geochemical data in the décollement offshore Nicoya Peninsula indicate an active fluid flow system with a fraction of the flow derived from depths within the subduction zone where temperatures are ~80°–150°C (Chan and Kastner, 2000; Silver et al., 2000; Kastner et al., 2006; Solomon et al., 2009). The sharpness of the geochemical anomalies in the décollement and the estimated temperature of the fluid suggest updip flow from a source region ~38–55 km landward of the trench at ~9–14 km depth, near the updip limit of the seismogenic zone (Harris and Wang, 2002; Spinelli et al., 2006; Kastner et al., 2006; Harris et al., 2010b).

The magnitude of the hydrological activity in a subducting oceanic plate setting is just beginning to be appreciated (Silver et al., 2000; Fisher et al., 2003; Hutnak et al., 2008; Spinelli and Wang, 2008; Solomon et al., 2009; Harris et al., 2010a, 2010b). Low heat flow values averaging ~30 mW/m^2 exist in the EPR-generated crust offshore the Nicoya Peninsula (Langseth and Silver, 1996; Fisher et al., 2003; Hutnak et al., 2007, 2008). These values reflect <30% of the expected value from conductive lithospheric cooling models for 24 Ma crust (Stein and Stein, 1994) and indicate effective hydrothermal cooling of

the upper oceanic crust. Seaward of the trench, recharge and discharge occur through exposed basement and seamounts (Fisher et al., 2003). This inference is corroborated by pore fluid chemical and isotopic profiles in basal sediment fluids that show a return to approximate seawater values near the upper part of the igneous basement (Chan and Kastner, 2000; Silver et al., 2000; Morris, Villinger, Klaus, et al., 2003). In addition to the cooling effect, the vigorous lateral flow of seawater must also alter and hydrate the igneous crust, affecting chemical and isotopic mass balances, as well as the transfer of volatiles through the subducting slab down to the depth of magma genesis.

Site survey data

The Central American margin offshore Costa Rica is one of the best studied subduction zones, with a wide spectrum of data from seismicity, land geology, volcanic petrology, geodesy, seismic imaging, submersible dives, and five deep-sea drilling and long-term monitoring cruises (Deep Sea Drilling Project Leg 84, ODP Legs 170 and 205, and Integrated Ocean Drilling Program (IODP) Expeditions 301T and 334). This margin has been the focus of two major scientific projects: the German Collaborative Research Center (SFB) 574 "Volatiles and fluids in subduction zones" (**sfb574.ifm-geomar.de/home/**) and the U.S. MARGINS National Science Foundation program (**www.nsf-margins.org/SEIZE/CR-N/CostaRica.html**). The supporting site survey data for IODP Expedition 344 are archived at the **IODP Site Survey Data Bank.**

More than 10,000 km of bathymetric imaging has been acquired (GeoMapApp and MARGINS Data Portal) (Fig. **F5**). The extensive multibeam bathymetric mapping shows variable seafloor morphology between the Nicoya and Osa Peninsulas (von Huene et al., 1995). The multibeam bathymetry is complemented by several deep-towed instrument traverses. The towed ocean bottom instrument (TOBI) sidescan sonar system of the Southampton Oceanography Centre was used during SO-163 in the spring of 2002 to detect active fluid flow at seafloor mounds and mass wasting offshore Costa Rica (Weinrebe and Ranero, 2003). Together with the results of the TOBI survey during the SO-144 cruise in 1999, much of the continental margin from Costa Rica to southeast Nicaragua was imaged with a resolution on the order of 10 m. Parts of that surveyed area were imaged with greater resolution using the Helmholtz-Center for Ocean Research Kiel (GEOMAR) DTS-1 deep-towed sidescan sonar system to map key areas with a resolution of better than 1 m (Klaucke et al., 2008; Petersen et al., 2009). Observations of the seafloor with a TV sled, gravity coring, and a TV-guided grab (Flüh et al., 2004) pinpointed areas of interest. Widespread mounds, some tens of meters high and a few hundred meters wide, have been monitored with current meters and hydrographic stations (Flüh et al., 2004). Outcropping carbonates on top and at the flanks indicate that these mounds are formed by authigenic precipitation at sites with abundant signs of fluid flow (Bohrmann et al., 2002; Hensen et al., 2004).

A local network of stations on land has recorded seismicity in the area over the last two decades (Figs. **F3, F5**). Several marine seismological networks of OBSs and OBHs have been deployed offshore Costa Rica. CRSEIZE, run by University of California Santa Cruz (USA), University of California San Diego (USA), Observatorio Vulcanologico y Sismologico de Costa Rica, and University of Miami (USA), established two seismic networks off the Osa and Nicoya Peninsulas. The first network was a 3 month (September–November 1999) onshore and offshore deployment between Quepos and the north shore of the Osa Peninsula, recording aftershocks from the 20 August 1999 Mw 6.9 underthrust earthquake. The second network operated onshore and offshore the Nicoya Peninsula from December 1999 to June 2000 (Newman et al., 2002; DeShon et al., 2003). CRSEIZE also included GPS campaigns across Costa Rica (Norabuena et al., 2004; LaFemina et al., 2009). German SFB 574 provided infrastructure for deploying OBS and land stations for >9 months (October 2002–August 2003) (Fig. **F3**) (Flüh et al., 2004).

Geophysical data acquisition in the Osa drilling area is extensive. The CRISP drilling sites are positioned on an OBS/OBH seismic refraction transect that crossed the onshore and offshore region of Costa Rica (Ye et al., 1996; Stavenhagen et al., 1998) (Fig. **F5**). These data were acquired in 1995/1996 during the Trans Isthmus Costa Rica Scientific Exploration of a Crustal Transect (TICOSECT) project. The TICOSECT transect is coincident with three multichannel seismic reflection surveys. The first was shot in 1978 (IG2903 vessel *Ida Green*), later reshot by Shell Oil (Kolarsky et al., 1995), and shot again in 1999 (BGR99 vessel *Prof. Polshkov*) with a long streamer and an industry acquisition system. The drilling sites have crosslines of industry and academic heritage. Transducer and high-resolution sparker coverage is available. Conventional heat probe transects that calibrate BSR-derived heat flow from the seismic records were acquired regionally and along the primary transect (Ranero et al., 2008; Harris et al., 2010a). Magnetic and gravity data cover the area (Barckhausen et al., 1998, 2001). GPS geodesy has been studied for more than a decade, and results show a locked Osa Peninsula area (LaFemina et al., 2009).

Seismic reflection data

Seismic reflection data offshore the Osa Peninsula are substantial (Fig. F6), mainly coming from R/V *Sonne* Cruises SO-76, SO-81 (Hinz et al., 1996; von Huene et al., 2000; Ranero and von Huene, 2000; Ranero et al., 2007), and BGR99 (Ranero et al., 2008). This combination of data greatly expanded swath mapping, seismic reflection, and refraction coverage from the area off the Nicoya Peninsula for ~250 km southeast where the crest of the Cocos Ridge is subducted. All seismic lines were collected with large tuned air gun arrays and multichannel streamers, as described in the original papers. Seismic data have been processed for signal enhancement including deconvolution and multiple attenuation, and were poststack time migrated. Selected sections are prestack depth migrated. All lines provide good imaging of the structure of the overriding plate, including the sediment cover strata, BSRs, and plate boundary reflections.

The seismic reflection data from Cruise SO-81 (Hinz et al., 1996) complement those acquired during Cruise BGR99. Cruise BGR99 records are processed in depth and the remainder in the time domain. The principal site survey line is flanked on either side by two lines at 1 km spacing, then by lines at 2, 5, and 10 km spacing (Fig. F6). Although these are the most revealing seismic images, other industry and academic acquired records in the area are numerous. Seismic reflection images collected between the Osa Peninsula and the Cocos Ridge (Fig. F6) show more stratified forearc basement and lower velocity material (by ~1 km/s) than in equivalent areas along the Nicoya transect.

In April and May of 2011, a 3-D seismic reflection data volume was acquired offshore Costa Rica, northwest of the Osa Peninsula and northwest of the Expedition 334 transect, together with high-resolution backscatter and multibeam data (Fig. F6). The goal of the 3-D seismic survey was to image the crustal structure and the plate-boundary fault from the trench into the seismogenic zone. The 3-D survey covers a distance of 55 km across the upper shelf, slope, and trench and extends 11 km along strike for a total survey area of 605 km^2. These data were acquired with the R/V *Langseth* using a 3300 $inch^3$ source shot every 50 m. Data were recorded by four 6 km long, 468-channel streamers with 150 m separation. When the Expedition 344 *Scientific Prospectus* was written (Harris et al., 2012), only preliminary results from processing 2-D seismic lines extracted from the 3-D volume and from initial 3-D volume processing were available (Bangs et al., 2011; Kluesner et al., 2011). Initial processing of the seismic data shows an upper plate structure with numerous faults, many extending down to the plate interface, and intense folding and faulting of the slope cover sequences (Bangs et al., 2011). Multibeam data across the shelf and slope correlate to faulting and folding sequences in the slope cover and deeper upper plate faulting seen in preliminary 2-D and 3-D seismic reflection images. The arcuate structure of the shelf edge and structural bulge seen in seismic data just landward of the shelf edge are consistent with a site of uplift over a subducting ridge (Kluesner et al., 2011).

Heat flow data

Heat flow data along seismic Line BGR99-7 (Fig. F5) are measured with marine probes and estimated from the depth of the BSR (Harris et al., 2010a). In general, probe and BSR values of heat flow agree (Fig. F7). Near the deformation front, high wavenumber variability indicative of fluid flow is observed. A simple analytical calculation suggests fluid flow rates of 7 to 15 mm/y. The high wavenumber variability is superimposed on a trend of decreasing landward heat flow consistent with the downward advection of heat with the subducting plate. Two-dimensional finite element thermal models of subduction were used to understand the heat flow data (Harris et al., 2010b). This analysis indicates that models using a conductive geotherm based on a plate model of lithospheric cooling produce values systematically lower than the heat flow data. Instead, the data are most consistent with a thermal model incorporating fluid flow within the upper oceanic crust of the subducting plate. These models predict much lower temperatures along the subduction thrust than the depth-extrapolated surface values used by Ranero et al. (2008).

Preliminary results from Expedition 334 (CRISP-A1)

The primary goal of Expedition 334 was to characterize the shallow upper plate at two sites along the BGR99-7 seismic reflection line (Fig. F2). Sites U1378 on the midslope and U1379 on the upper slope were characterized with logging-while-drilling (LWD) data and later cored, allowing samples of fluids and sediment to be collected. A third midslope location (Site U1380) was attempted but abandoned because of poor drilling conditions. In addition, the sediment and basement were cored on the incoming plate (Site U1381). These sites are briefly reviewed starting at the input site and continuing landward. Additional details are given in the Expedition 334 *Proceedings* volume (Vannucchi, Ujiie, Stroncik, Malinverno, and the Expedition 334 Scientists, 2012).

Site U1381 reveals the characteristics of the incoming sedimentary section and upper basement and serves as a reference site. This site is on the incoming Cocos plate, located ~6 km seaward of the trench on a local basement high. The primary objective at the site was to core basement material, and because of time constraints the entire sediment section was drilled using the rotary core barrel (RCB). Expedition 344 recored the sediment using the advanced piston corer (APC).

Midslope Site U1380 is 14.5 km landward of the trench (Fig. F2). Earthquake relocations (DeShon et al., 2003) and geodetic data (LaFemina et al., 2009) suggest this site is seaward of the locked portion of the plate interface. The site was cored between ~395 and 480 meters below seafloor (mbsf) during Expedition 334 as a contingency to Site U1378, which was drilled to ~524 mbsf (Expedition 334 Scientists, 2012a). During Expedition 334, both Sites U1380 and U1378 (1 km seaward) were abandoned before science goals were achieved, and a fundamental reason for returning to Site U1380 was to attain the science goals.

Scientific objectives

The CRISP program was designed to understand seismogenesis at erosional convergent margins. CRISP Program A is the first step toward deep riser drilling through the seismogenic zone. The principal objectives of CRISP Program A were to characterize the shallow lithologic, hydrologic, stress, deformation, physical property, and thermal conditions that lead to unstable slip in the seismogenic zone. The focus of this expedition is to document the lithology, deformation, and fluid system of the upper plate and to evaluate the subduction channel thickness. This information is necessary to better understand the structural environment and crustal stress that will be encountered during proposed deep riser drilling. Expedition 344 is a continuation of Expedition 334; they are Stages 1 and 2, respectively, of CRISP Program A. The primary goals for Expedition 344 were as follows.

1. Estimate the composition, texture, and physical properties of the décollement zone and upper plate material.

At erosive margins, the upper plate material is thought to constitute a primary input into the plate boundary. As the plate boundary migrates upward, upper plate material is incorporated into the subduction channel that feeds the seismogenic zone. The onset of seismogenic behavior along the subduction thrust is influenced by physical properties of the overriding plate material. Characterization of the décollement zone and upper plate basement will provide structural and mechanical constraints on the possible mechanical changes occurring at seismogenic depths. Sampling rocks of the upper plate basement beneath the upper slope is necessary to define drilling conditions for deep holes and to better understand this margin prior to CRISP Program B drilling.

2. Assess rates of sediment accumulation and margin subsidence/uplift in slope sediment.

The subduction of bathymetric features leading to both frontal and basal erosion of the upper plate are expected to be reflected in forearc tectonic processes. Rapid changes in sediment accumulation rates and margin subsidence are one manifestation of these processes. Rates of sediment accumulation will be documented with biostratigraphic and paleomagnetic methods. Margin uplift or subsidence can be documented by facies changes and careful studies of benthic foraminifers. Subsidence can also be indicated by progressive seaward tilting of sedimentary beds. The landward migration of the coastline and the arc magmatic front over time also reflect these processes.

3. Evaluate fluid/rock interaction, the hydrologic system, and the geochemical processes (indicated by composition and volume of fluids) active within the upper plate.

We expect that subduction of the Cocos Ridge caused fracturing of the upper plate, which modified the hydrological system and is now manifested in flow paths and fluid velocities, heat flow, and mass transport. Landward-dipping reflectors cutting through the upper plate have been interpreted to extend to the plate boundary. Geochemistry can open a window directly to the seismogenic zone through the analysis of solutes that can be related to chemical reactions occurring at the depth of seismogenesis.

Important feedback mechanisms exist between fluid pressure, temperature, and the strength of rocks. Temperature and fluid pressure exert important controls on the state of stress and friction. In turn, stress and deformation processes influence porosity and permeability, which have a fundamental influence on fluid pressure. Measuring the thermal and hydrologic regime is critical for understanding these feedback mechanisms. Fluid pressure and temperature may be measured in situ until a depth where the material is semiconsolidated. Laboratory analysis, as consolidation tests, can give indirect but realistic values of pore pressure.

4. Measure the stress field across the updip limit of the seismogenic zone.

The stress field may be inferred from borehole breakouts, anelastic strain recovery analysis (ASR), and sense of deformation. Borehole breakouts and ASR show a present stress state that can be compared with GPS crustal strain. The paleostress field from deposition to present is recorded in deformation of the rock. Structural analysis reveals the sense of shear, and the anisotropy of magnetic susceptibility can quantify the rock strain. Changes of stress field with Cocos Ridge subduction will be evaluated using structural analysis.

GPS data indicate high rates of strain in the vicinity of Osa Peninsula. Patterns of microearthquake epicenters suggest that relative plate motion in the seismogenic zone is accommodated by coseismic slip. CRISP Program A drilling will better define the orientation of the horizontal compressive stresses in the area. Downhole in situ heat flow measurements will improve our understanding of the thermal regime, allowing us to better estimate the temperature associated with the onset of seismicity as well as to develop viscoelastic models of deformation.

5. Study Cocos Ridge subduction and evolution of the Central American volcanic arc.

CRISP Program A is also a standalone project that provides data to solve long-standing problems related to tectonics of the region. These primary objectives included a better understanding of relationships between Cocos Ridge subduction to the tectonics of the upper plate and of the evolution of the Central American volcanic arc. These goals will be achieved through dating the impingement of the Cocos Ridge on the margin, recovery, dating and compositional characterization of tephra layers, and identifying potential late products of Central American arc volcanism.

Principal results

Site U1381 summary

Background and objectives

Fundamental to sampling and quantifying the material comprising the seismogenic zone of a convergent margin is an understanding of the nature of the sediment and oceanic crust entering the seismogenic zone and the hydrologic and the thermal state of the oceanic crust. Site U1381 serves as a reference site on the subducting aseismic Cocos Ridge.

Site U1381 is ~4.5 km seaward of the deformation front offshore Osa Peninsula and Caño Island, Costa Rica (Fig. F6). This site was chosen for multiple reasons. First, a clear seismic record of the plate stratigraphy and basement is present at this site (Fig. F8). The seismic section shows a 100 m thick sediment section resting on reflective basement interpreted as Cocos Ridge igneous crust. The sedimentary section is composed of pelagic and hemipelagic sediment (Expedition 334 Scientists, 2012d). Secondly, it is located on a local basement high. Basement relief often focuses fluid flow, so data from this site are likely to document the vigor of fluid flow in this area. Thirdly, Site U1381 is far enough away from the frontal thrust that it is expected to be reasonably free from the influence of downslope debris flows from the convergent margin slope. Finally, Site U1381 is located on the same seismic line as Sites U1412, U1380, and U1379 (Fig. F2). Paleomagnetic data constrain the age of this portion of Cocos Ridge to 14 Ma (Barckhausen et al., 2001).

During CRISP Expedition 334 in 2011, Site U1381 was cored using the RCB because the primary objective was oceanic crust and time constraints precluded APC drilling through the sediment section (Expedition 334 Scientists, 2012d). However, a disadvantage of the RCB system is that recovered soft sediment is usually highly disturbed. Thus a primary goal for revisiting this site was to core the sediment section with the APC to obtain more pristine samples and better document the nature of the sediment entering the seismogenic zone.

Operations

After a 403 nmi transit from Panama, the vessel stabilized over Site U1381 at 0620 h on 26 October 2012 (all times in text are ship local time, which is UTC – 6). Hole U1381C was spudded at 2015 h on 26 October (8°25.7027′N, 84°9.4800′W, 2064.6 m water depth; Table T1). Advancement for Hole U1381C was 103.8 mbsf, with 103.5 m cored with the APC and 0.3 m cored with the extended core barrel (XCB). Recovery with the APC was 108.70 m (105%), and recovery with the XCB was 0.33 m (110%). The advanced piston corer temperature tool (APCT-3) was deployed on Cores 344-U1381C-3H, 5H, 6H, and 7H, and four good temperature curves were recorded. The FlexIT orientation tool was deployed on Cores 344-U1381C-1H through 9H with good results. After reaching basement, the APC was changed to the XCB and a single short core was cut to confirm and recover basement material. Hole U1381C ended at 1545 h on 27 October, and a total of 33.5 h was spent at Site U1381.

Principal results

The cored interval in Hole U1381C comprises five units (Fig. F9). The top of the hole contains hemipelagic

sediment that is typical of an incoming plate location near a terrigenous source. The Unit I/II boundary is present in Core 344-U1381C-7H (55.93 mbsf) and is characterized by a change from greenish grayish silty clay with some nannofossils and terrigenous minerals to brownish grayish nannofossil-dominated ooze with abundant to common foraminifers and sections of abundant sponge spicules. This boundary was identified in smear slide and X-ray diffraction (XRD) data. The upper portion of Unit II is also characterized by a high abundance of tephra layers that reach 42 cm in thickness. Core description and smear slide data indicate a lithologic change in Core 344-U1381C-11H to finer grained nannofossil-rich clay with only some glass and feldspar components that marks the Unit II/III boundary (100.64 mbsf). The Unit III/IV boundary (103.20 mbsf) in Core 344-U1381C-12H again shows a drastic change in lithology to a pure clay/claystone. XRD data indicate mixing of smectite (probably saponite), pyrite, and to a lesser extent plagioclase. Sphalerite, calcite, and anhydrite are present as minor phases. Unit V starts at 103.55 mbsf in Core 344-U1381C-13X and consists of brecciated basalt. Alteration of the basaltic groundmass is slight to moderate, with smectite replacing interstitial glass and partially corroding plagioclase and clinopyroxene phenocrysts. Overall, this sediment reflects a sequence of hemipelagic siliceous ooze with terrigenous input, presumably remobilized from the slope sediment sequence, overlying sponge spicule–rich nannofossil calcareous ooze, pelagic calcareous ooze, and pelagic claystone. In addition, 84 tephra layers were recovered in Units I–IV.

The biostratigraphy of Hole U1381C was determined from calcareous nannofossils and radiolarians identified in core catcher samples from Cores 344-U1381C-1H through 11H. Biostratigraphic zones indicate that the base of Unit I is early Pleistocene (~1–2 Ma). Unit II represents the middle Miocene (~11–13 Ma), and based on nannofossil and radiolarian biostratigraphy, a ~9–11 m.y. hiatus separates Units I and II.

Benthic foraminifers are present throughout the cores, ranging from 1% to 5% of the total 125 µm sample size. Preservation is good, with little evidence of dissolution or breakage. Benthic foraminiferal assemblages from Unit I are substantially different than those in Unit II, indicating large paleoenvironmental changes related to organic carbon flux and bottom water ventilation. Of particular interest is the substantial presence of representatives of the *Stilostomella* extinction group in Sample 344-U1381C-6H-CC. These assemblages provide an alternative biostratigraphic datum to the calcareous nannofossils.

Thirty-five measurements of bedding were taken principally from tephra layers in Hole U1381C. Bedding is generally subhorizontal to gently dipping. In Unit III, near the bottom of the sedimentary succession, we observed a few deformation bands and mineral-filled extensional and shear fractures, which have a normal displacement component.

We collected and processed 28 whole-round (WR) core samples for interstitial water analyses and an additional 3 WR samples for helium analyses. In all cases, enough fluid was collected for shipboard and shore-based requests with 10 cm long WRs. Similar to Expedition 334 data from Hole U1381A, there is little variation in salinity, chloride, sodium, and potassium. Diagenesis of organic matter in the upper sediment is indicated by increases in alkalinity, ammonium, and phosphate and consumption of sulfate, which reaches a minimum value of 11 mM at ~40 mbsf. A concomitant calcium decrease indicates that carbonate precipitation is driven by the increase in alkalinity. The sulfate profile shows a reversal below ~40 mbsf, with a steady increase in concentration with depth. This observation is similar to that previously reported for Expedition 334 Hole U1381A and for the incoming sediment section offshore the Nicoya Peninsula. Overall, the concentration-depth profiles of Ca, SO_4, Li, Mn, and possibly Si indicate diffusional interaction with an altered seawater fluid in the oceanic basement.

We collected and analyzed 29 headspace samples for organic geochemistry analyses. Except for elevated values of hydrocarbons in the uppermost sample (at 1.5 mbsf), which has been attributed to drilling contamination, methane occurs only in trace amounts and no heavier hydrocarbons were detected.

Inorganic carbon distribution increases with depth in Hole U1381C, consistent with a change in lithology from the silty clay sediment of Unit I to the foraminiferal carbonate ooze of Unit II. The total organic carbon (TOC) concentration throughout the entire sediment section ranges from 1 to 2 wt%. The total nitrogen (TN) concentration ranges between 0.05 and 0.20 wt%.

Physical property measurements show high porosities (Unit I = 75%; Unit II = 78%) and low bulk densities (Unit I = 1.4 g/cm^3; Unit II = 1.3 g/cm^3), with little evidence for compaction. Magnetic susceptibility values stay fairly constant with depth but have intermittent peaks in Unit I and Unit II that correlate with tephra layers. Natural gamma radiation (NGR) gradually increases with depth and is highly variable around the Unit I/II boundary. Electrical conductivity values appear generally consistent with porosity trends. *P*-wave velocity measurements indicate slightly higher values in Unit II (1540 m/s) than in Unit I (1520 m/s), despite elevated porosities in Unit II, and *P*-wave velocity values are highest in Unit III

(1620 m/s). Vane shear and penetrometer measurements show strength values generally increase downhole throughout Units I and II. Thermal conductivity results are inversely correlated with porosity. Downhole temperature measurements are consistent with those obtained previously on Expedition 334 and suggest a thermal gradient of 231°C/km. The calculated heat flow of 185 mW/m^2 is higher than that predicted for 15 Ma crust, suggesting significant fluid flow in the underlying ocean crust.

Downhole variations in the natural remanent magnetization (NRM) intensity for archive-half cores correlate well with lithology in Hole U1381C. Paleomagnetic measurements indicate that the silty clay of Unit I (0–55.93 mbsf) has a mean NRM intensity on the order of 10^{-2} A/m, whereas the foraminifer-rich ooze in Unit II has a lower NRM intensity of 10^{-2} to 10^{-3} A/m. A number of higher NRM peaks appear in both Units I and II and can be tied directly to the presence of tephra layers. The measured NRM declinations of different cores are scattered, but upon correction with the FlexIT orientation data, declinations become close to magnetic north, indicating the remanence is of geomagnetic origin. Magnetic properties obtained from the archive section halves were confirmed by discrete sample measurements.

Characteristic remanent magnetization (ChRM) declinations and inclinations from discrete measurements were used to define magnetic polarity sequences for the oriented core section in Hole U1381C. At a low-latitude area such as Site U1381, a near 180° shift in declination in the cores is a more reliable sign of a polarity transition than a change in the magnetic inclination. For the upper part of Unit I, both pass-through and discrete sample measurements show signs of dominantly normal polarity of ChRM. An additional constraint is provided by an ash layer at ~25 mbsf, which is inferred to be the Ar-Ar dated (320 ka) Tiribí Tuff ash layer (Pérez et al., 2006). Thus, we interpret that the sediment from 0 to 49 mbsf was deposited within the Brunhes Chron (<0.78 Ma). In Sections 344-U1381C-6H-5 through 6H-7, we see dominantly reversed polarity in the section-half measurements. Discrete samples from this interval also show negative inclinations, and corrected declinations show a ~180° shift, consistent with the magnetization acquired in a reversed field. Thus, we tentatively conclude that the Brunhes/Matuyama boundary is at 49 mbsf in Section 344-U1381C-6H-3.

Site U1380 summary

Background and objectives

Site U1380 is located on the middle slope of the Costa Rica margin along seismic Line BGR99-7 (Fig. F6). Interplate earthquakes and geodetic measurements indicate that this site is seaward of the updip extent of seismicity and that the plate interface is not locked (Fig. F3). At Site U1380, the margin consists of a 550 m thick section of slope sediment overlying upper plate framework rock (Fig. F10). Hole U1380A was drilled during Expedition 334 to ~480 mbsf, but because of poor drilling conditions it was terminated prior to reaching the framework rock (Expedition 334 Scientists, 2012c). The primary goals for revisiting this site were to determine the nature, composition, and physical properties of the upper plate framework rock; to understand the nature of the landward-dipping seismic reflectors; and to estimate the state of stress. Seismic reflection Line BGR99-7 shows that this site is above the seaward edge of one of the high-amplitude reflectors.

Operations

After an 11.4 nmi transit from Site U1381, the vessel stabilized over Site U1380 at 1715 h on 27 October 2012. Hole U1380B was spudded at 0118 h on 28 October (8°35.9952′N, 84°4.3908′W, 502.7 m water depth; Table T1). The purpose of this hole was to conduct a jet-in test with a 14¾ inch tricone bit to verify the length of 16 inch casing that could be jetted into the formation with a reentry cone.

Hole U1380C was spudded at 1145 h on 29 October (8°35.9879′N, 84°4.3918′W, 502.7 m water depth; Table T1). The operations plan for this hole included a reentry system with two strings of casing to an undetermined depth, followed by RCB coring to 800 mbsf. The reentry cone and 16 inch casing string were installed to 48 mbsf. A 14¾ inch bit was used to drill the hole to 438 mbsf. The initial plan was to run 10¾ inch casing string to 430 mbsf. After drilling the 14¾ inch hole, it became impossible to keep the hole open to run casing to 430 mbsf. A new casing length of 405 m was selected to try to bridge a problematic zone from 337 to 396 mbsf. The hole was reamed and cleaned repeatedly prior to running casing. Eventually, the problematic zone was cemented and redrilled. After several days of hole cleaning, the 405 m long 10¾ inch casing string was run into the hole. With the end of the casing 18 m above the desired depth, we were unable to advance the casing any further and were forced to pull the casing back to the surface. To avoid disassembling the entire casing string, we secured the casing string to the moonpool doors and tripped back in the hole with a 9⅞ inch tricone bit and a 14¾ inch underreamer. We then attempted to ream the hole back to bottom. During this process, 391 m of casing parted just below sea level and followed the drill string down into the hole. To determine the condition of the casing string

inside the hole, we switched to a coring bottom-hole assembly (BHA) with an RCB bit and drilled down carefully from 336 to 438 mbsf. RCB coring commenced at 1745 h on 7 November and continued without interruption until 0400 h on 10 November to a total depth of 800 mbsf. Nonmagnetic RCB core barrels were used starting with Core 344-U1380C-11R. In an effort to improve recovery we started cutting half cores with Core 344-U1380C-25R. The total cored interval in Hole U1380C was 362.0 m, with 202.4 m recovered, for an overall recovery of 56%.

The hole was prepared for logging, the bit was dropped on the seafloor, and the triple combination (triple combo)–Ultrasonic Borehole Imager (UBI) logging string was rigged up. During the first logging attempt, the logging tools were unable to advance past 398 mbsf, which coincided with the estimated depth of the casing shoe. The tools were pulled from the hole, and the drill pipe was advanced to 467 mbsf without difficulty. The drill pipe was pulled back to 394 mbsf, and a reconfigured triple combo string without the UBI was run into the hole at 2310 h. This time the logging tools made it to 458 mbsf before encountering an obstruction. A review of the logs showed that the casing had slipped further down. After retrieving the logging tools, a BHA with a used RCB bit was deployed, the hole was washed down to 781 mbsf, the hole was conditioned for logging, and the bit was dropped in the bottom of the hole. The triple combo logging tool string was rigged up for the third time and run into the hole at 1310 h on 13 November. However, the logging tools encountered a similar obstruction at 462 mbsf. After several attempts to get the tools to reenter the open hole, logging operations were terminated. The hole was plugged with a 10 bbl cement plug, and the acoustic beacon was recovered. The drill string was pulled from the hole, clearing the rig floor at 0055 h on 14 November and ending Hole U1380C operations. A total of 17.3 days were spent on Site U1380.

Principal results

Hole U1380C was cored to investigate the lithostratigraphy and structural geology of the lower portions of the middle slope sequence and the uppermost portions of the basement, as interpreted in multichannel seismic reflection data. These data are summarized in Fig. **F11.** This hole deepens Site U1380, drilled during Expedition 334 (Expedition 334 Scientists, 2012c), and is a complementary hole to nearby Site U1378 where only the upper 539.9 m of the slope sediment was drilled during Expedition 334.

The majority of the sedimentary sequence consists of clayey siltstone (~59%) and silty claystone (~25%) with common interlayered centimeter- to decimeter-sized beds of fine- to medium-grained sandstone (~15%). The siltstone sedimentary sequence is disrupted by coarse-grained shell-rich sandstones, two conglomerates (~1%), and 25 tuff layers (<1%). Three lithostratigraphic units were distinguished based on lithologic compositional changes.

Unit I extends from 438 to 552.72 mbsf (Sections 344-U1380C-2R-1 to 13R-7, 55 cm) and is characterized by massive dark greenish gray silty clay and three sandstone-rich horizons with centimeter- to decimeter-sized sandy layers. These sandy layers are cemented with calcite and increase in abundance, thickness, and grain size with depth. Matrix components comprise lithic fragments (sedimentary and magmatic), feldspar, glass shards, and amphiboles. Biogenic components include rare nannofossils, diatoms, and foraminifers.

Unit II extends from 552.72 to 771.62 mbsf (Sections 344-U1380C-13R-7, 55 cm, to 47R-3, 106 cm) and is visually defined by a relatively sharp lithologic change into a greenish gray clayey siltstone with intercalated sandstone and conglomerate layers. Unit II is further divided into two subunits based on compositional and depositional variations. Subunit IIA is characterized by well-lithified siltstones and poorly to weakly lithified sand beds that contain abundant to common shell fragments. The matrix also contains abundant lithic fragments, feldspar, and zeolites, but the main mineralogical variation is the higher abundance of amphibole in this subunit. Low recovery hinders the precise measurement of the thickness of Subunit IIA (~11.38 m), but we assume that the missing material is composed of the same poorly lithified sand as the recovered sections. The lithologic boundary between Subunits IIA and IIB (123.24 m thick) in Core 344-U1380C-15R (564.10 mbsf) was not recovered. Subunit IIB is very dark greenish gray clayey siltstone characterized by two fining-upward sequences of centimeter- to decimeter-thick, medium- to coarse-grained sandstones and fine conglomerates. Matrix and sandstone components are predominantly terrigenous lithic fragments (magmatic more common than sedimentary), feldspar, glass, and rare heavy minerals. Biogenic material is mostly absent, and none was observed toward the bottom of the unit. Highly altered tuff layers in the lower parts of Cores 344-U1380C-30R (688.04 mbsf) and 47R (770.56 mbsf) are characterized by color changes from the dark greenish gray clayey siltstone to a reddish brown calcareous siltstone and by variations in the matrix mineralogy.

Both subunits of Unit II are characterized by normally graded sandstone beds that are often laminated, with abundant sapropel fragments that form

several centimeter-thick conspicuous horizons between the laminae. The conglomerates are very thickly bedded and contain poorly sorted, pebble-sized, matrix-supported lithic fragments. Upper contacts between fine- and coarse-grained sediment, when observed, are mostly gradational, whereas the lower contacts are erosional and commonly contain rip-up clasts, load clasts, and sand lenses. In general, Unit II is more indurated and lithified than Unit I.

Unit III (Cores 344-U1380C-47R through 52R) is a 29.44 m thick, fine-grained silty claystone with rare but thick (as thick as 1.20 m) intercalated fine- to coarse-grained sandstone. The matrix contains mostly terrigenous material dominated by lithic fragments and feldspar but is nearly devoid of biogenic material.

Unit I is a continuation of sediment cored in Hole U1380A during Expedition 334 (Expedition 334 Scientists, 2012c) and correlates well with Unit II from Hole U1378B (Expedition 334 Scientists, 2012a). The sedimentary succession recovered from Hole U1380C likely reflects an alternating, terrestrially sourced, turbiditic upper slope (Units I and III) to shelf (Unit II) sequence, eventually influenced by deltaic-derived sediments. The dynamic depositional environment is manifested by varying grain sizes that range up to pebble-sized conglomerates, especially in Unit II, and the cyclical increase in sandstone abundance throughout the sedimentary sequence.

Deformation structures increase gradually in Cores 344-U1380C-2R through 13R. Normal faults are present throughout the interval, with reverse faults increasing downhole. Deformation culminates in Cores 344-U1380C-11R through 13R with the development of pronounced foliation. Bedding is commonly steeply dipping. Deformation is moderate in Cores 344-U1380C-14R through 45R, and there is no foliation. Bedding remains steep until Core 344-U1380C-31R, and from Core 32R downhole it is subhorizontal to gently dipping. In the deeper cores there is an increase of discrete brittle shear zones.

The biostratigraphy of Hole U1380C was determined by nannofossils because core catcher samples were barren of radiolarians. Four biostratigraphic zones were identified. The interval from Sample 344-U1380C-2R-CC to 4R-CC is assigned to nannofossil Zones NN19–NN21. The second interval, between Samples 344-U1380C-5R-CC and 8R-CC, is assigned to Zone NN19. The third zone, NN18, is defined by the first downhole occurrence of *Discoaster brouweri*, which appears in Sample 344-U1380C-9R-CC. The fourth biostratigraphic zone encompasses Samples 344-U1380C-51R-CC through 52R-CC (791–797 mbsf) and is assigned to Zones NN15–NN17, based on the last occurrence (LO) of *Discoaster pentaradiatus*, the first occurrence (FO) of *Pseudoemiliania lacunosa* in Sample 344-U1380C-51R-CC, and the FO of *Discoaster asymmetricus* in Sample 344-U1380C-52R-CC. Therefore, the oldest sediment found at this hole is older than 2.4 Ma.

Benthic foraminifers were studied in 44 of the 52 core catcher samples collected. Benthic foraminifers vary from few (Samples 344-U1380C-2R-CC through 9R-CC) to present (Samples 344-U1380C-31R-CC through 52R-CC), and preservation ranges from moderate where abundance is higher to poor where foraminifers are present or rare. Overall, benthic foraminifer assemblages are characterized by species generally associated with organic carbon–rich environments and low bottom water oxygenation such as *Uvigerina peregrina*, *Epistominella smithi*, *Brizalina* spp., and *Hansenisca altiformis*. Downhole changes in benthic foraminifer assemblages are relatively subtle.

The most significant geochemical finding is the presence of fluid flow through a shear zone that extends from ~480 to 550 mbsf, at the boundary between lithostratigraphic Units I and II. The Cl, Li, and hydrocarbon data indicate that this fluid originated from a source depth where temperatures are >90°C. Below this horizon there is a marked increase in C_1/C_{2+} ratio toward a more biogenic signature of the gases, which is consistent with pore water data (Sr and Li) that indicate lower temperature volcanic tephra alteration reactions within the sediment of lithostratigraphic Unit II. Both the inorganic and organic carbon concentrations of the sediment are distinctly higher in lithostratigraphic Unit I than in the sediment underlying the 550 mbsf unconformity.

Within Unit I, magnetic susceptibility is generally low, NGR increases with depth to values of 38 cps, and bulk density and porosity appear to follow a steady compaction trend that is consistent with that observed in shallower sediment from Site U1378, located 1 km from Site U1380. *P*-wave velocity, thermal conductivity, and sediment compressive strength increase with depth.

Most of the physical properties show sharp changes at the Unit I/II boundary, near the major seismic reflector at 550 mbsf. Below this boundary, magnetic susceptibility becomes more variable and NGR counts decrease. Between 550 and 555 mbsf, bulk density increases from ~2.0 to 2.1 g/cm^3, porosity decreases from 43% to 35%, and thermal conductivity, *P*-wave velocity, and sediment strength increase.

A second major change in physical properties occurs at ~700 mbsf and is identified by a strong positive spike in magnetic susceptibility, a positive spike in *P*-wave velocity, and a slight negative excursion in NGR. In addition, bulk densities peak at 2.2 g/cm^3

and porosities reach their lowest values of 25% to 26%. This horizon could be correlated to a strong landward-dipping reflector at ~700 mbsf. Near the Unit II/III boundary (771.62 mbsf), there is a notable change in magnetic susceptibility, *P*-wave velocity, and thermal conductivity.

NRM measurements were made on all archive-half cores and on 60 discrete samples taken from the working halves in Hole U1380C. Archive-half cores were subjected to alternating field (AF) demagnetization up to 30 mT and discrete samples to stepwise thermal and AF demagnetization up to 475°C and 120 mT, respectively, in order to establish a reliable magnetostratigraphy at this site and to observe the magnetic properties of each lithology in the lithostratigraphic units recovered.

Several relatively well defined polarity intervals have been identified in downhole magnetostratigraphic records in spite of some samples showing unstable and ambiguous magnetization. Based on biostratigraphic data, we were able to tentatively correlate certain parts of the magnetic polarity interval recorded in the sediment with the geomagnetic polarity timescale. The Matuyama/Gauss Chron boundary (2.581 Ma) is tentatively placed at ~770 mbsf, based on both discrete sample and pass-through results.

Site U1412 summary

Background and objectives

Site U1412 (proposed Site CRIS-9A, located on seismic Line BGR99-7) targeted the frontal sedimentary prism at the base of the slope near the toe, the main subduction thrust, the underthrust sedimentary section beneath the subduction thrust, and the upper oceanic crust (Fig. **F6**). The scientific objectives were to (1) characterize the frontal sedimentary prism by documenting its lithology and age; (2) sample the décollement at a shallow depth to define the deformation style, stress, fault friction, and behavior; (3) characterize any diagenetic processes, microstructures, and potential sealing/healing processes; (4) characterize the physical properties of the subducting incoming and frontal prism sediments that are thought to mix with eroded upper plate material; and (5) determine the chemistry of pore waters within the wedge, décollement, and underthrust sections and characterize the fluid pathways.

Operations

After a 7.0 nmi transit from Site U1380, the vessel stabilized over Site U1412 at 0200 h on 14 November 2012. The original operations plan for Site U1412 called for two holes, an APC/XCB hole to ~500 mbsf and an RCB hole to 980 mbsf. Eventually, four holes were cored at this site. Coring conditions at this site were extremely difficult with below average recovery, and all four cored holes were abandoned short of the targeted depths because of poor hole conditions. Hole U1412A (8°29.3294′N, 84°7.6686′W, 1921 m water depth; Table **T1**) was spudded at 1520 h on 14 November. This was an APC/XCB drilled hole to 200.3 mbsf. APCT-3 formation temperature measurements were taken with Cores 344-U1412A-3H, 5H, 7H, and 8H. The FlexIT orientation tool was deployed with Cores 344-U1412A-1H through 15H. Core 344-U1412A-25X reached 200.3 mbsf before the hole became too unstable to continue coring. The vessel was offset 350 m in a south-southwest direction in an attempt to find a more favorable coring location. Hole U1412B (8°29.1599′N, 84°7.7512′W, 1965 m water depth; Table **T1**) was spudded at 2350 h on 16 November. This hole was drilled without recovery to 149.1 mbsf, and Core 344-U1412B-20X reached 304.3 mbsf before deteriorating hole conditions forced us to stop coring. Logging with the triple combo tool string was attempted on 20 November, but the tools could not exit the BHA and the drill string became stuck. After freeing the drill string, the logging tools were laid out and the hole was abandoned. Because this hole did not reach the depth objective, a third hole was attempted 50 m to the northeast. Hole U1412C (8°29.1700′N, 84°7.7467′W, 1965 m water depth; Table **T1**) was spudded at 0730 h on 21 November. This hole was drilled without recovery to 300 mbsf, and Core 344-U1412C-10R reached 387 mbsf. After several hours spent trying to clean the hole and getting stuck, the decision was made to abandon Hole U1412C and proceed to Site U1413. After coring objectives were completed at Site U1413, the vessel returned to Site U1412. Hole U1412D (8°29.1402′N, 84°7.7793′W, 1973 m water depth; Table **T1**) was spudded at 0850 h on 1 December. This hole was drilled without recovery to 350.4 mbsf. We were only able to recover Cores 344-U1412D-2R and 3R before the hole collapsed.

A total of 55 cores were recovered at this site: 16 APC cores, 28 XCB cores, and 11 RCB cores. The APC cored interval was 114.9 m, with 115.5 m recovered (101%), the XCB cored interval was 240.6 m, with 82.8 m recovered (34%), and the RCB cored interval was 105.8, with 48.8 m recovered (46%). The overall recovery for Site U1412 was 54%. The total time spent on Site U1412 was 277.5 h or 11.56 days (60.25 h in Hole U1412A, 104.5 h in Hole U1412B, 71.25 h in Hole U1412C, and 41.5 h in Hole U1412D).

Principal results

Site U1412 was drilled to investigate the lithostratigraphy and structural geology of the slope-toe sequence

and the uppermost portions of the basement, as interpreted in multichannel seismic reflection data (Fig. F12). The primary goal of this site was to penetrate the décollement and investigate the fluid flow regime within the sediment as well as the oceanic crust.

Three units were distinguished in the sedimentary rocks (Fig. F13). Unit I is predominantly dark greenish to greenish gray clay (33%) with small variations in grain size to silt (16%) and silty clay (17%) and contains eight tephra layers. This is terrigenous-influenced sediment. Unit I shows indications for gas expansion and gas hydrate dissociation. Unit II is light to dark grayish brown calcareous nannofossil ooze with varying amounts of diatoms and sponge spicules. Primary sedimentary structures could not be observed because of very strong drilling disturbance. Unit III is a sequence of grayish green clayey siltstone with minor interlayered sandstone and contains five dark grayish tephra layers. The Unit III matrix composition is dominated by terrigenous clay and contains nannofossils as well as radiolarian and diatom fragments. Hole U1412D sediment is slightly more clayey, highly bioturbated, and shows a decrease in the biogenic components.

The change in lithology at this site from terrigenous input to Miocene calcareous ooze to Pleistocene hemipelagic sediment likely reflects accretion of large slivers of the incoming plate.

Nannofossil biostratigraphy indicates that the upper portion of Hole U1412A is Zone NN19 (0.4–1.89 Ma). A major change from Pleistocene to Miocene is recorded in Core 344-U1412B-8X, consistent with the lithostratigraphic boundary between Units I and II (204.74 mbsf). In Hole U1412C, Samples 344-U1412C-2R-CC through 5R-CC are indicative of the middle Miocene. A major age inversion is recorded between Cores 344-U1412B-5R and 6R, with the reappearance of Pleistocene assemblages. Benthic foraminifers are common in the upper sections of Hole U1412A and include *Uvigerina peregrina*, *Uvigerina auberiana*, *Cibicidoides pachyderma*, *Melonis affinis*, and *Cassidulina carinata*. A substantial change in foraminiferal assemblages occurs starting with Core 344-U1412B-7X and is characterized by *Globocassidulina subglobosa*, *Cibicidoides pachyderma* var. *bathyalis*, *Hansenisca altiformis*, and *Planulina renzi*. The latter species last appeared in the middle Miocene, which agrees with the nannofossil and radiolarian biostratigraphy.

Hole U1412A has subhorizontal to gently dipping bedding at the very top of the drilled section. Steeply dipping normal faults are common in the lower part of the section. Hole U1412C has steeply dipping bedding, normal and reverse faults, and intervals of brecciated sediment, in some cases with fragments where striated and polished surfaces are developed. The fault zone with well-developed foliation located at 330 to 342 mbsf coincides with an age reversal from Miocene to Pleistocene. Such large accumulated displacement implies that the fault zone has been highly active and has experienced multiple events.

The upper sections of sediment reflect changes associated with organic matter diagenesis. The sulfate–methane transition zone (SMTZ) occurs at 14.73 mbsf, and high-resolution headspace samples were collected below this depth for shore-based geomicrobiology studies. The decrease in calcium and magnesium concentrations at the SMTZ depth reflects precipitation of authigenic carbonates. The presence of gas hydrate in the sediment was inferred from discrete chloride anomalies and excursions to low C_1/C_{2+} ratios between 60 and 85 mbsf, consistent with observations of mousse-like texture in sediment. We observe decreasing concentrations in alkalinity, boron, and magnesium, whereas calcium, barium, strontium, and lithium concentrations increase with depth. There is, however, not enough resolution in the sample coverage from lithostratigraphic Units II and III to delineate in situ diagenetic reactions or fluid migration pathways. In general, methane concentrations increase rapidly below 14.1 mbsf, consistent with the depth of the SMTZ at this site. The gas composition of the headspace and void gas is consistent with a biogenic methane source. However, an observed decrease to ~400 in the C_1/C_{2+} ratios of headspace and void gas samples and a few occurrences of propane in Unit III point to a mixture of biogenic gas and thermogenic hydrocarbons that migrated from depth.

Physical properties measured indicate that bulk density values increase and porosity values decrease in the upper 30 m. Both properties remain stable to the base of Unit I in Hole U1412A, with average bulk density and porosity values of 1.69 g/cm^3 and 60%, respectively. Bulk density and porosity values in Unit III show considerable variability but suggest slightly more compaction (higher bulk density and lower porosity) than at the base of Unit I. In Unit I, background magnetic susceptibility is low, with some high excursions. NGR is relatively stable throughout Unit I and higher and more scattered within Unit III. Strength increases in the upper 30 m and then remains stable until Unit III, where it is higher and more scattered. Formation factor was measured in the uppermost 110 m, and values vary between 1.5 and 4. Thermal conductivity and *P*-wave measurements were rare and scattered because of gas disturbance. Measured *P*-wave velocities are low, varying

between 1500 and 1600 m/s. Thermal conductivity ranges from 0.7 to 1.3 W/(m·K). A least-squares linear fit to the downhole temperature data yields a gradient of 114°C/km.

We measured the NRM of archive section halves and demagnetized them in an alternating field up to 40 mT. There are more significant variations in NRM intensity within lithostratigraphic Unit I than in Units II and III. We demagnetized 61 discrete samples to verify the section data. We recognized seven magnetozones in Hole U1412A and interpreted them to include the Brunhes Chron and the Jaramillo, Cobb Mountain, and Olduvai Subchrons. Our magnetostratigraphic data suggest extremely high sediment accumulation rates for Hole U1412A, similar to those found in Hole U1379C during Expedition 334. Paleomagnetic measurements of nine discrete samples from Hole U1412B display a change from normal to reversed polarity at ~167 mbsf. Changes in the inclination sign are also observed for the seven samples studied from Hole U1412C. Two discrete samples from Hole U1412D were measured for shipboard structural analyses. Based on the small number of samples, no magnetostratigraphic interpretations are available at this time.

Site U1413 summary

Background and objectives

Site U1413 (proposed Site CRIS-13B) targeted the upper slope of the Costa Rica margin (Fig. **F6**). This site is within the 3-D seismic data set along Line 2466 and crossing Line 4882 (Fig. **F14**). Interplate earthquake relocations (Fig. **F3**) and interpretation of geodetic measurements show that this site is located above the seismogenic zone (Bilek et al., 2003; LaFemina et al., 2009). The primary purpose of drilling Site U1413 was to determine the nature, composition, and physical properties of the slope sediment. This site is also designed as a "pilot hole" in preparation for proposed deeper CRISP Program B drilling at this location. Science objectives at Site U1413 included (1) documenting the lithology and physical properties, (2) determining the stress orientation of the margin above the seismogenic zone, and (3) constraining the fluid-flow regime. Documenting periods of subsidence and uplift provides important information about the process of tectonic erosion that characterizes the Costa Rica margin. One technique for estimating the relative motion of the margin is through stratigraphic correlations of multiple sites.

Operations

After a 15.0 nmi transit from Site U1412, the vessel stabilized over Site U1413 at 2330 h on 23 November 2012. The original operations plan for Site U1413 called for two holes: an APC/XCB hole to ~600 mbsf and an RCB hole to 1430 mbsf. Eventually, three holes were cored at this site. Hole U1413A (8°44.4593′N, 84°6.8095′W, 540 m water depth; Table **T1**) was spudded at 0635 h on 24 November. This was an APC/XCB hole to 189.1 mbsf. APCT-3 formation temperature measurements were taken with Cores 344-U1413A-3H, 5H, 6H, 7H, and 8H. The FlexIT orientation tool was deployed with Cores 344-U1413A-1H through 18H. Hole U1413B (8°44.4593′N, 84°6.7992′W, 540 m water depth; Table **T1**) was spudded at 0055 h on 26 November. This was a shallow hole to 25.6 mbsf drilled primarily for geochemical analyses. Hole U1413C (8°44.4482′N, 84°6.7993′W, 540 m water depth; Table **T1**) was spudded at 0940 h on 26 November. This hole was drilled without recovery to 178.0 mbsf, was cored with the RCB system to 582.2 mbsf, and was terminated to allow time to complete other expedition objectives. Following coring, three logging runs were conducted on 30 November with the triple combo, UBI, and Formation MicroScanner (FMS) tool strings.

A total of 71 cores were recovered at this site: 21 APC cores, 8 XCB cores, and 42 RCB cores. The APC cored interval was 166.2 m, with 171.2 m recovered (103%). The XCB cored interval was 48.5 m, with 43.7 m recovered (90%). The RCB cored interval was 404.2 m, with 313.9 m recovered (78%). The overall recovery at Site U1413 was 85%. The total time spent on Site U1413 was 170.25 h or 7.1 days (48.5 h in Hole U1413A, 5.75 h in Hole U1413B, and 116.0 h in Hole U1413C).

Principal results

Site U1413 was drilled to investigate the lithostratigraphy and structural geology of the upper slope sequence as a preliminary study for future deep riser drilling.

Three lithostratigraphic units (Fig. **F15**) were distinguished in the sediment of Holes U1413A–U1413C, with an overall abundance of silty clay to clay (32.1%), clayey silt to sandy silt (53.3%), silty sand to sand (14.4%), and tephra (0.2%). The 44.6 m thick Unit I recovered in Holes U1413A and U1413B is dominated by dark greenish gray silty clay with multiple centimeter-sized turbidite sequences of fine-sand laminae. A slump/slide event was identified in the uppermost ~3.5 m of this unit. The lithology changes into a brownish green chaotic mixture of silty clay and dark gray sands in the lowermost part of Core 344-U1413A-5H. Ten tephra layers were also identified in Unit I. Lithostratigraphic Unit II, starting at 44.60 mbsf, is characterized by a well-consolidated light greenish gray calcareous clayey silt(stone) with

occasional variations to silty clay, as well as minor sand(stone) layers. Unit II exhibits moderate variability in the amount and extent of calcareous cementation with depth. In addition, this unit contains several horizons of lithified and reworked rounded carbonate mud clasts. Fourteen tephra layers were identified in Unit II. Near the bottom of Hole U1413A (Section 344-U1413A-20X-1), a chaotic layer of intermixed sand and calcareous clayey silt, not associated with a lithologic change, most likely represents a mass transport deposit (MTD) interval. Unit II continues in Hole U1413C to 366.45 mbsf with the same lithology, but heavy minerals, shell fragments, and occasional sandstone layers with sapropel and leaf fragments become more abundant with depth. The boundary between Units II and III (Section 344-U1413C-21R-3, 117 cm) is marked by the first appearance of an 18 m thick package of alternating sandstones and siltstones with common to abundant organic matter (sapropel) and shell and gastropod fragments. The matrix of the siltstone and sandstone is characterized by abundant magmatic and sedimentary lithic fragments, common feldspar, and volcanic glass fragments. Foraminifers are the most abundant components of the biogenic material. After a relatively thin siltstone interval (~42 m), the remainder of the hole (426.8–578.8 mbsf) consists of massive fine- to medium-grained sandstones that contain three tephra layers. The sandstones are normally graded and range from decimeter- to meter-thick layers with occasional internal laminations, particularly in the uppermost part of the section. Some cores in Unit III are particularly rich in gastropods and reworked, well-rounded carbonate clasts. These lithostratigraphic units can be correlated to some of the units found at Sites U1378 and U1379 during Expedition 334.

Biostratigraphy at Site U1413 was mainly constrained by calcareous nannofossils. The upper section of Hole U1413A (Samples 344-U1413A-1H-CC through 14H-CC) is assigned to Nannofossil Zone NN21. In Samples 344-U1413A-15H-CC through 19X-CC, the age is less well constrained and is assigned to Zones NN20–NN21 (1.89 Ma to present). The first appearance of *Pseudoemiliania lacunosa*, which defines the top of Zone NN19, is found in Sample 344-U1413A-20X-CC. The LO of *Helicosphaera sellii* is observed in Sample 344-U1413C-15R-CC and is assigned to 1.34 Ma. Radiolarians are present in the upper section of Hole U1413A, but few biostratigraphically useful species were found.

Benthic foraminifers were dominant and well preserved in Samples 344-U1413A-1H-1W to 19X-CC, but they range from common to few in the lower section of Hole U1413A and throughout Hole U1413C, with most of the foraminiferal samples showing signs of mechanical breakage. Benthic foraminiferal assemblages show remarkable changes downhole. The uppermost 150 m of sediment is characterized by an assemblage composed of *Brizalina bicostata*, *Cassidulina tumida*, and *Cancris inflatus*. These species are absent in the rest of the cored interval. From 160 mbsf (Sample 344-U1413A-20X-CC) to 478 mbsf (Sample 344-U1413C-32X-CC), there is a completely different assemblage composed of *Brizalina spissa*, *Epistominella smithi*, *Uvigerina* cf. *excellens*, and *Hansenisca altiformis*. The lower part of Hole U1413C (Samples 344-U1413C-36R-CC through 42R-CC) is characterized by the appearance of *Brizalina* cf. *dilatata*, which together with *Uvigerina peregrina* dominates the assemblages and constitutes as much as 80% of all foraminifers.

Faulting-related deformation starts to be present and abundant below 180 mbsf. Deformation is additionally localized along brecciated fault zones at 181, 230, 237–239, 365, 529–532, and 567 mbsf. Both normal and reverse faults were observed. Dip angles of these faults vary from subhorizontal to subvertical.

We collected 106 interstitial water samples from Site U1413. Hole U1413B was dedicated to high-resolution studies of the biogeochemical processes just below the SMTZ, which at this site occurs at 16 mbsf. Pore fluid profiles of sulfate, alkalinity, and ammonium concentrations in the uppermost ~150 m of Holes U1413A and U1413B reflect organic matter remineralization but are significantly impacted by sediment slumps at ~45 and ~150 mbsf. Calcium and magnesium concentrations decrease from seawater values at the seafloor to minima of 1.1 and 39.8 mM, respectively, at the lithostratigraphic Unit I/II boundary (44.60 mbsf), reflecting precipitation of authigenic carbonates. Cl concentrations decrease with depth to ~500 mbsf, but below this depth the Cl profile shows a trend of increasing concentrations reaching ~96% of seawater value. The reason for the lower than modern seawater Cl value throughout the cored section but in particular in the upper ~150 m is as yet unclear. Methane increases below the SMTZ, and the C_1/C_2 ratio in the upper 50 m indicates a biogenic origin for the gas. Below this depth, the C_1/C_2 ratio decreases steadily with depth and shows a marked decrease to values <100 below 480 mbsf, indicating a thermogenic component from a deeper source.

Site U1413 porosity values decrease (and bulk densities increase) rapidly from 0 to 180 mbsf and more gradually below 180 mbsf. Magnetic susceptibility excursions appear to coincide with sand-rich layers that contain detrital magnetite. *P*-wave velocities average 1600 m/s above 20 mbsf. There are only a few scattered measurements between 20 and 200 mbsf because of core disturbance, and values average 1960 m/s below 200 mbsf. Thermal conductivity in-

creases from 0.9 to 1.25 W/(m·K) from the seafloor to 200 mbsf and then gradually increases to 1.35 W/(m·K) at the bottom of Hole U1413C. Three temperature measurements yield a gradient of 49°C/km and a heat flow of 56 mW/m^2. Sediment strength generally increases from the seafloor to 140 mbsf. Below 140 mbsf, values are scattered but show an overall gradual increase. Formation factor increases rapidly within the upper 20 m and more gradually below 20 mbsf.

We performed split-core measurements of NRM and AF demagnetization of discrete samples to observe the magnetic properties of each lithostratigraphic unit recovered at Site U1413. In order to verify the section data, we demagnetized and measured 119 discrete samples using a progressive AF demagnetization technique. Based on biostratigraphic data, we were able to tentatively correlate certain parts of the magnetic polarity interval recorded in the sediment with the geomagnetic polarity timescale. In particular, the polarity shift from reversed to normal at 485 mbsf in Section 344-U1413C-42R-4 may represent the beginning of the Olduvai normal polarity subchron (1.778 Ma). The sediment accumulation rate for the uppermost 480 m of sediment in Hole U1413C is 269.97 m/m.y.

Downhole logging measurements were taken in Hole U1413C with three tool strings: a slick triple combo (without the radioactive source because of poor hole conditions), a UBI, and an FMS tool string. The tool strings could not be lowered below 187 mbsf because of a borehole obstruction; the last two tool strings were chosen to focus on the ultrasonic and resistivity imaging of borehole breakouts. Three logging units were distinguished. Logging Unit 1 (93–148 mbsf) contains clear borehole breakouts imaged by low reflection amplitudes and large traveltimes in the UBI ultrasonic log and by the orientation of the FMS pair of arms that measure the larger borehole radius. The orientation of the breakouts shows that the minimum principal horizontal stress is oriented approximately north–south. In contrast, the borehole is nearly circular and in gauge (~10 inch diameter) in logging Unit 2 (148–169 mbsf), which also has a higher natural radioactivity and higher resistivity than Unit 1, suggesting a more consolidated formation. The borehole is washed out in all directions in logging Unit 3 (169–184 mbsf), and low measured values of natural radioactivity and resistivity are likely artifacts caused by hole enlargement.

Site U1414 summary

Background and objectives

The primary objective of Expedition 344 was to sample and quantify the material comprising the seismogenic zone of an erosive subduction margin. Fundamental to this objective is an understanding of the nature of the sediment and oceanic crust entering the seismogenic zone, the hydrologic system, and the thermal state of the igneous oceanic crust. Site U1414 (proposed Site CRIS-19A) serves as a secondary reference site on the flank of the subducting aseismic Cocos Ridge (Fig. F6).

Site U1414 is located within the 3-D seismic volume (Fig. F6) and is ~1 km seaward of the deformation front offshore the Osa Peninsula. Site U1414 is located near Line 2497 and crossing Line 2562 (Fig. F16). This site was chosen for multiple reasons. First, a clear seismic record of the plate stratigraphy is present at this site. The seismic section shows a 400 m thick sediment section resting on reflective basement interpreted as Cocos Ridge igneous crust. Secondly, the sedimentary section is thought to be composed of pelagic and hemipelagic sediments that may contain the Pleistocene to mid-Miocene sediment missing at Site U1381 as documented by biostratigraphy and a gap in the Costa Rica tephra record. Thirdly, a reflector of interest exists about two-thirds of the way through the sediment column. Finally, this site presented an opportunity to sample igneous basement.

The primary science goals at Site U1414 included (1) documenting the presence or absence of the hiatus observed at Site U1381, (2) documenting the presence or absence of tephras during the hiatus found at Site U1381, and (3) documenting the composition and alteration state of basement. Finally, because of oblique convergence of subduction at the Middle America Trench, sediment at Site U1414 likely reflects the sediment now under seismic Line BGR99-7. Documenting the physical state and water content of this sediment was an important objective.

Operations

After a 5.8 nmi transit from Site U1412, a positioning beacon was deployed at 0010 h and the vessel stabilized over Site U1414 at 0015 h on 3 December 2012. Hole U1414A (8°30.2304′N, 84°13.5298′W, 2459 m water depth; Table T1) was spudded at 0805 h. Cores 344-U1414A-1H through 22H were taken from 0 to 200.1 mbsf with the APC. APCT-3 formation temperature measurements were taken with Cores 344-U1414A-3H, 5H, 7H, and 9H. The coring system was switched to the XCB after having to drill over Core 344-U1414A-22H. Cores 344-U1414A-23X through 35X were taken from 200.1 to 311.9 mbsf, and XCB coring was terminated after penetration rates and recovery drastically decreased. The APC/XCB assembly was raised to just below the seafloor, a free-fall funnel was deployed, and the remainder of the drill string was brought to the surface.

An RCB BHA was then assembled with a new bit and lowered to just above the seafloor. Hole U1414A was reentered, and Cores 344-U1414A-36R through 63R were recovered with the RCB by 1205 h on 9 December, including 96 m of igneous basement. Coring was terminated so that logging could begin.

In preparation for logging, the hole was swept clean with mud and the bit was released. The end of the drill string was set at 96 mbsf, and the logging tools were rigged up. The first logging run was with the triple combo–UBI tool string and reached a depth of 421 mbsf, where it encountered an obstruction. The second logging run was with the FMS-sonic tool string, and it reached the same depth. Logging activities were completed by 1200 h on December 10. The remainder of the drill string was pulled to the surface while the R/V *JOIDES Resolution* began a slow move toward land in dynamic positioning mode. The BHA cleared the rig floor at 1955 h on 10 December, ending Site U1414. The *JOIDES Resolution* picked up speed at 2015 h and continued the 95 nmi transit to Puntarenas, Costa Rica. First line ashore was at 0502 h on 11 December 2012, ending Expedition 344.

A total of 63 cores were recovered at this site: 22 APC cores, 13 XCB cores, and 28 RCB cores. The APC cored interval was 200.1 m, with 206.16 m recovered (103%). The XCB cored interval was 111.8 m, with 94.1 m recovered (84%). The RCB cored interval was 159.7 m, with 84.5 m recovered (53%). The overall recovery for Site U1414 was 81%. The total time spent on Site U1414 was 193 h or 8.0 days.

Principal results

The lithology of the upper part of Hole U1414A (Fig. F17) is characterized by a predominantly monotonous, terrigenous sequence of soft, light greenish gray hemipelagic silty clay to clay with some small sand layers in the uppermost part of Unit I (Subunit IA) and an increasing amount of calcareous nannofossils in the lower part (Subunit IB). Terrigenous material (lithic fragments, glass shards, and minerals) decreases with depth. The Unit I/II boundary at 145.34 mbsf separates greenish gray nannofossil-rich clay sediment from calcareous ooze. Unit II (145.3–309.4 mbsf) is a 164 m thick moderately consolidated interval that is characterized in the upper part by nannofossil calcareous ooze. In the lower part calcareous nannofossil ooze alternates with biosilica-rich calcareous ooze. Unit III (309.4–375.3 mbsf) is a 66 m thick interval that is characterized by a sequence of lithified, calcareous, and siliceous cemented silt- and sandstone that probably lost biogenic components as a result of diagenetic remobilization but still preserves the original sedimentary structures such as bedding and bioturbation. Tephra layers and pods are rare (1%), but despite their dark brown to black macroscopic appearance, the glass shards are mainly transparent under the microscope, implying an evolved rather than a mafic volcanic origin. Overall, 35 tephra layers were recovered in Units I–III.

Igneous basement, encountered at 375.2 mbsf, comprises a ~65 m thick sequence of massive basalt (Cores 344-U1414A-45R through 58R) overlying a 1.5 m thick interval of intercalated sediment. Below the sediment is a second (at least ~30 m thick) massive basaltic interval (Cores 344-U1414A-58R through 63R). We tentatively identify eight units. Based on changes in lava morphology, the presence of chilled margins, texture and phenocryst abundance we identify 8 units. Massive and thin sheet flows (Units 1–6) lie above the intercalated sediment (Unit 7). This is, in turn, above a massive flow (Unit 8).

Igneous Units 1–6 and 8 are massive and microcrystalline and exhibit groundmass textures including intersertal, intergranular, vesicular, porphyritic, and subophitic. Seriate and rare variolitic and glassy textures were observed in the uppermost 5 cm of Unit 2. Groundmass comprises plagioclase (44%–63%), clinopyroxene (14%–31%), magmatic opaques (4%–36%), and partially to completely replaced olivine (0%–8.6%). Mesostasis is typically hyalophitic and intersertal. Phenocryst abundance ranges from aphyric to highly plagioclase phyric, with phenocrysts typically more abundant in coarser grained intervals and the middle and uppermost portions of each unit. Unit 4 exhibits porphyritc texture throughout, comprising ~30% of the groundmass. Plagioclase, clinopyroxene, and olivine are all identified as phenocryst phases within Site U1414 basement. Olivine, however, is absent in Units 3, 4, and 6. Megacrysts of plagioclase up to 20 mm in size are observed in the lower portion of Unit 8.

Alteration of basement rocks at Site U1414 is the result of interaction with either seawater or modified "hydrothermal" fluids that partially replace groundmass and phenocryst mineralogy, fill fractures and vesicles, and form breccia. Overall alteration is slight to moderate; however, more intense alteration is concentrated around veins, vein-flanking alteration halos, vesicles, and chilled margins. Secondary mineralogy includes expanding clay minerals saponite and smectite, carbonate, silicates, secondary sulfides, and zeolite. No oxidative alteration assemblages, such as iron-oxyhydroxides or cleadonite, were observed. Cross-cutting relationships observed within veins and vesicles at Site U1414 suggest initial precipitation of expanding clays followed by sulfides and carbonate. The timing of quartz and zeolite remains uncertain. A number of veins at Site U1414

exhibit pressure-induced brecciation along the vein margins and multiple episodes of calcium carbonate precipitation. The most intense alteration observed at Site U1414 is a jigsaw-puzzle breccia in the uppermost 70 cm of Unit 3. The breccia comprises highly altered, subangular basaltic clasts and a smectite matrix. Rare chlorite (or chlorite/smectite) was tentatively identified within mesostasis between Sections 344-U1414A-48R-4 and 49R-1. Overall, our observations suggest that Site U1414 was subjected to an oxygen-starved alteration regime in which access to seawater was restricted.

Biostratigraphy in Hole U1414A is constrained by radiolarians and nannofossils. Nannofossils have moderate preservation overall, with evidence of recrystallization downhole. Radiolarians are well preserved overall, with intervals of poor preservation between Samples 344-U1414A-17H-CC and 21H-CC. The presence of *Pseudoemiliania lacunosa* and *Collosphaera tuberosa* indicates that the upper ~120 m was deposited in the Pleistocene. Radiolarian and nannofossil assemblages at the base of Hole U1414A constrain the age of the oldest sediment to the mid-Miocene.

Foraminiferal work was conducted on 34 core catcher samples. Generally, the abundance of benthic foraminifers varied from common to few, with a few particular intervals where benthic foraminifers were only present. Preservation was good to moderate except for some samples contained in lithologic Subunit IIB, where foraminiferal preservation was poor with tests showing signs of recrystallization.

Overall, two main benthic foraminiferal assemblages can be distinguished in this hole. The upper assemblage (0–140 mbsf) includes *Globobulimina* group species *Uvigerina auberiana* and, as accessory species, *Uvigerina* cf. *senticosa*, *Cassidulina carinata*, and *Melonis affinis*. The lower assemblage (140–320 mbsf) is composed of species belonging to the "*Cibicides*" group, *Globocassidulina subglobosa*, *Pullenia* spp., and *U.* cf. *senticosa*. In Sample 344-U1414A-12H-CC, we found the LO of the *Stilostomella* group species, which indicates an age older than 0.6 Ma for that group. The base of the hole (Samples 344-U1414A-30H-CC through 34H-CC) contains specimens of *Planulina renzi*. This species died out during the mid-Miocene. This is in agreement with the biostratigraphic constraints for that interval.

Site U1414 has subhorizontal to gently dipping bedding. Few faults, generally normal, were observed in Units I and II. Unit III is characterized by strong foliation and veins. Unit III is slightly metamorphosed. Some shear zones are also recognized.

We completed chemical analyses on 61 interstitial water samples collected from Hole U1414A. The pore fluid composition in the uppermost 80 m shows trends characteristic of organic matter remineralization. In addition, coincident minima in ammonium and sulfate concentrations at 37 mbsf suggest that there may be favorable conditions for sulfate-reducing ammonium oxidation. The feasibility of this metabolic pathway in marine sediment was recently documented for the first time in sediment from the Bay of Bengal, India.

The sulfate concentration-depth profile at this site is also unusual in that it displays a second minimum at 330 mbsf, which corresponds to a sharp minimum in calcium and a maximum in barium concentrations. These data suggest lateral flow of a sulfate-depleted fluid, which originated from microbial oxidation of methane and/or other organic carbon sources landward of Site U1414 and migrated updip through the upper sediment of Unit III. The calcium minimum thus likely reflects a combination of in situ carbonate formation caused by the ongoing sulfate reduction and a contribution from the laterally migrating fluid having low calcium concentration. Similarly, the barium concentration, which mirrors the sulfate profile at depth, is controlled by the stability of the mineral barite ($BaSO_4$); thus, the increase in barium may reflect both in situ marine barite dissolution at the sulfate minimum plus barium contribution from the laterally migrating low-sulfate fluid. Postcruise isotopic analyses of the carbon species, solid-phase barite and carbonate analyses, and numerical modeling will be required to determine the origin and history of the fluid flow at depth in this input sediment section.

The incoming sediment also displays changes in composition driven by the nature of the lithology and associated diagenetic reactions. Lithologic changes at this site are apparent in the silica profile, which is characterized by typical silicate mineral diagenesis. The gradual increase in the amount of biogenic opal in the sediment from the silty clay/sand–dominated Unit I through the nannofossil-rich clay in Subunit IB is apparent as a monotonic increase in dissolved silica. The change from the nannofossil-rich clay of Subunit IB to the nannofossil-rich calcareous ooze of Subunit IIA coincides with a sharp decrease in Si concentrations. Another marked increase in Si concentrations across the lithologic Subunit IIA/IIB boundary reflects a change in fluid-rock reactions in Subunit IIB that are dominated by opal-A solubility at the in situ temperature of ~35°–45°C. Near the base of Subunit IIB is a distinct decrease in Si concentrations, which coincides with a clear decrease in dissolved K concentrations, consistent with clinoptilolite formation, a K-Si-rich zeolite, which is also apparent in the XRD data.

Bulk density and porosity data are complicated by the combination of lithologic changes and varia-

tions in diagenesis. Compaction is slight in Unit I, with porosity values of 69% at 145 mbsf. Below 145 mbsf, porosity values decrease to 54% and then gradually increase to >75% near 225 mbsf before decreasing to the base of the hole. Background magnetic susceptibility values generally decrease with depth, reaching near-zero values below 350 mbsf. Excursions generally correspond to tephra layers. NGR values are generally stable in the upper 110 m, rise to a peak at 130 mbsf, and then decrease with depth to the Unit II/III boundary. NGR values are scattered in Unit III, with a peak near 350 mbsf. *P*-wave velocities from the split cores decrease in the upper 25 m and then gradually increase with depth. Overall, *P*-wave velocities in Unit I are low, averaging 1520 m/s. A local maximum at ~190 mbsf corresponds to a bulk density maximum and porosity minimum. *P*-wave velocities between 300 and 340 mbsf average 1850 m/s and then sharply increase to 3260 m/s below 340 mbsf. Thermal conductivity shows variations consistent with bulk density. Strength values rise steadily in Unit I and Subunit IIA. Four downhole temperature measurements yield a thermal gradient of 168°C/km.

We measured the NRM and performed AF demagnetization on all archive section halves and several discrete samples from Site U1414. In general, variations in NRM intensity follow changes in lithology, especially in the light green calcareous ooze of Hole U1414A. We demagnetized 55 discrete samples collected from the working halves with AF demagnetization up to 120 mT, with the main objective of recognizing the characteristic remanent magnetization. The upper part of Hole U1414A is characterized by a short interval with normal polarities and then a longer reversed interval followed by three normal intervals. The Brunhes Chron, if present, is very short or condensed in the uppermost ~10 m. Between 94 and 114 mbsf, four samples with homogeneous characteristics confirm the presence of a normal polarity interval. However, most of the samples from the middle part of Hole U1414A show reversed polarity. The lower part of the hole (below 282 mbsf) includes six samples with normal polarity, separated by only one sample with reversed shallow inclination.

The logging program in Hole U1414A included two runs with the triple combo–UBI and FMS-sonic tool strings. Logs were collected from 96 to ~410 mbsf and include spectral gamma radiation, bulk density, electrical resistivity, *P*- and *S*-wave velocity, and ultrasonic and resistivity images of the borehole wall. We distinguished four logging units in Hole U1414A. Logging Unit 1 (94–259 mbsf) is characterized by total gamma ray values that decrease from between ~40 gAPI at 120 mbsf to ~10 gAPI at the base of the unit. Bulk density, resistivity, and elastic wave velocities are generally low in this unit and show a decreasing trend toward the base of the unit, where the bulk density is 1.5 g/cm^3, resistivity is 0.5 Ωm, and *P*- and *S*-wave velocities are 1.6 and 0.4 km/s, respectively. Logging Unit 2 (259–335 mbsf) displays an increase with depth of bulk density (1.6–1.8 g/cm^3), resistivity (0.5–1 Ωm), *P*-wave velocity (1.7–2.1 km/s), and *S*-wave velocity (0.5–0.7 km/s). NGR values are generally 10–30 gAPI. Logging Unit 3 (335–375 mbsf) contains larger variations in physical properties, with gamma ray values ranging between 20 and 60 gAPI, bulk densities between 1.8 and 2.2 g/cm^3, resistivities between 1 and 10 Ωm, *P*-wave velocities between 2 and 4 km/s, and *S*-wave velocities between 0.5 and 2.7 km/s. Finally, logging Unit 4 (375–410 mbsf) corresponds to the volcanic basement at Site U1414 and displays very low natural radioactivity (10 gAPI or less) and high values of bulk density (2.3–2.8 g/cm^3), resistivity (2–100 Ωm), *P*-wave velocity (3.2–6.7 km/s), and *S*-wave velocity (1.7–3.8 km/s).

Preliminary scientific assessment

Expedition 344 was superlative, and with the exception of not reaching the décollement and the underthrust sediment at the toe site (U1412), exceeded expectations. We recovered material across the Costa Rica erosive convergent margin offshore the Osa Peninsula. Material was recovered from the incoming Cocos plate (Sites U1381 and U1414), the toe of the margin (Site U1412), the midslope region (Site U1380), and the upper slope region (Site U1413).

Recovery was very good at the incoming plate sites, good at the midslope and upper slope sites, and poor at the toe site. At Sites U1381 and U1414 we collected 76 cores with a recovery of 86%, at Sites U1380 and U1413 we collected 122 cores with a recovery of 75%, and at Site U1412 we collected 55 cores with a recovery of 54% (see **"Principal results"** for details).

The overarching goal of Expedition 344 was a better understanding of seismogenesis at erosive convergent margins through shallow drilling. A second objective was to better understand erosive convergent margins. In this respect, Expedition 344 has given us an increased understanding of subduction erosion that has led to important new insights. Most of the science objectives were achieved. Below we assess these objectives and highlight major results.

1. Estimate the composition, texture, and physical properties of the upper plate material.

Slope sediment was recovered at Sites U1380 and U1413. Seismic reflection data over both sites show

that the slope sediment unconformably overlies a lower unit. The lower unit at Site U1380 was identified as upper plate basement prior to drilling. Both of these slope sites are divided into three units. Unit I at Sites U1380 and U1413 consists of slope sediment and is characterized silty clay and fine sandstones. Unit II at both sites is characterized by clayey siltstone lithified to varying degrees with calcite cement. Sands are present in these units and tend to be less well lithified. At Site U1380, Unit III consists of silty claystone with intercalated massive coarse sandstones that are well lithified with calcite cement. At Site U1413, Unit III consists of fine- to medium-grained sandstone and siltstone. Units I and III of Site U1380 and all units of Site U1413 represent terrestrially sourced upper slope sequences. Unit II of Site U1380 represents a terrestrially sourced shelf sequence. High sediment accumulation rates throughout the depositional interval were observed at both sites. Observed organic debris and thin normally graded sands with sharp erosional bases indicate deposition within the distal facies of a clastic turbidite sequence. Carbonate cements are ubiquitous at these sites.

The upper part of Hole U1380C (438–551 mbsf) is characterized by abundant faults and fractures and steeply dipping bedding planes, whereas the lower part of this hole (551–797 mbsf) is characterized by less steeply dipping beds. Two structural domains are also identified at Site U1413. The upper domain (0–180 mbsf) is characterized by subhorizontal to gently dipping bedding planes, and the lower domain (180–582.2 mbsf) is characterized by a downhole increase in bedding dips and an abundance of fault structures.

Physical properties show a strong, sharp change at the boundary between upper slope sediment and upper plate framework rock. In the upper plate framework rock, magnetic susceptibility becomes more variable; NGR counts decrease; bulk density increases; porosity decreases; and thermal conductivity, *P*-wave velocity, and sediment strength increase.

A major result is that the upper plate material drilled at Site U1380 is not a mélange of oceanic material or the offshore extension of the Caribbean large igneous complex but forearc basin material consisting of lithic sedimentary units.

2. Assess rates of sediment accumulation and margin subsidence in slope sediment.

Expedition 344 successfully recovered slope sediment at Sites U1380 and U1413. Preliminary biostratigraphic and paleomagnetic ages from Sites U1380 and U1413 indicate high sediment accumulation rates in the terrestrially sourced slope sequence. Estimates of slope accumulation rates at Site U1380 vary between ~290 and 590 m/m.y. At Site U1413, mass transport deposits make accumulation rates more complicated, but rates vary between 380 and 432 m/m.y. These accumulation rates are remarkably high and could be due to enhanced erosion rates caused by the subduction of the Cocos Ridge or alternatively by subducting bathymetry that may erode the margin, creating lows that are then filled. These rates are the same order of magnitude as those determined during Expedition 334 at Sites U1378 and U1379 (Expedition 334 Scientists, 2012a, 2012b) and an order of magnitude larger than those determined offshore the Nicoya Peninsula (Kimura, Silver, Blum, et al., 1997).

Onshore research of sedimentary facies and benthic foraminifers in slope sediment at Sites U1380 and U1413 will be used to assess margin subsidence and evolution. Expedition 344 was successful at obtaining the material necessary for these onshore studies. An important preliminary implication of the high accumulation rates is that this margin has undergone high rates of vertical motion.

3. Evaluate fluid/rock interaction, the hydrologic system, and geochemical processes as indicated by the composition and pore fluids within the upper plate.

Fluids play a large role in subduction zone processes and dynamics. Thus, understanding their pathways as they enter and exit subduction zones is of fundamental importance and was an important goal of this expedition. The flow of fluids influences the thermal regime, as well as solute budgets and their transfer between the ocean, volcanic arc, and mantle. The distribution of fluid pressure within subduction zones influences flow velocities, effective stress, and fault strength. The chemistry of fluids advected toward the surface can be used to infer reactions occurring at depth and their potential role in seismogenesis.

Solute concentrations indicative of fluid flow were observed in three different environments. These environments include the upper basement of the incoming Cocos plate at Site U1381, within sediment above basement at Site U1414, and associated with a shear zone within the lower slope at Site U1380.

At midslope Site U1380, the presence of fluid flow through a shear zone that extends from ~480 to 550 mbsf, at the boundary between lithostratigraphic Units I and II, is indicated by anomalous values of Cl, Li, and hydrocarbon data. These tracers indicate that this fluid originated from a source depth where temperatures are ~80°–90°C. At upper slope Site U1413, no unequivocal evidence for fluid flow was observed.

At input Site U1381, concentration-depth profiles of Ca, SO_4, Li, Mn, and possibly Si solutes indicate the

diffusion of fluids with seawater-like chemistry in the igneous basement. In fact, vigorous flow in the subducting oceanic basement is suggested by anomalously high heat flow measured at these sites. In contrast, at Site U1414, the cemented sandstone unit at the base of the sediment may inhibit diffusion between the sediments and the subducting basement. Here, the lateral flow of fluids just above the sandstone is indicated by sulfate and calcium minima at ~330 mbsf. This pattern reflects a lateral flow of sulfate-depleted fluids that likely originated from oxidation of methane and/or other organic carbon sources landward of Site U1414 and migrated updip above the sandstone layer.

At toe Site U1412, borehole stability was an issue that precluded crossing the décollement and recovering the underthrust sediment and igneous basement. The geochemistry of pore fluids largely indicates in situ diagenetic reactions. Lithium concentration values indicate diffusive interaction with a fluid originating from a source depth where temperatures are ~80°–90°C. The direct lack of evidence for fluid flow, however, is likely due to the lack of recovered sediment.

Pore fluids in the uppermost ~50 m at all margin sites drilled during Expedition 344 are dominated by reactions associated with the cycling of organic carbon. Within the uppermost 50 m of the sites drilled on the slope, active sulfate reduction, biogenic methane production, and precipitation of authigenic carbonates were observed. The depth of the SMTZ varies from site to site, with the shallowest SMTZ occurring at ~14 mbsf at Site U1412. At input Sites U1381 and U1414, there is no methane production and sulfate is controlled by organic matter catabolic reactions.

4. Estimate the stress field along the CRISP transect.

In the CRISP study area, paleostress is assessed through the structural analysis of faults, present-day in situ stress is estimated from borehole breakout data, and anelastic strain recovery measurements are estimated on recovered whole rounds.

At Site U1380, kinematic fault analysis indicates a paleoextensional stress regime with maximum and minimum compressive stresses oriented to the vertical and northeast–southwest, respectively. Both normal and reverse faults were observed at Site U1413, indicating multiple generations of faulting.

Preliminary analysis of ultrasonic images and four-arm caliper data reveal an interval of breakouts between 148 and 169 mbsf, indicating a minimum compressive stress oriented approximately north–south. This stress orientation corresponds to an upper slope extensional stress regime and is consistent with upper slope extension found at Site U1379 during Expedition 334.

5. Better understand the impact of Cocos Ridge subduction, the evolution of the Central American volcanic arc, and the development of the volcanic gap inboard of the Cocos Ridge.

A fundamental question is whether Central American volcanism ceased with the arrival of the Cocos Ridge and how volcanism evolved subsequent to the arrival of the ridge. Expeditions 334 and 344 drilled into the sediment and basalt of the Cocos Ridge for the first time. At Site U1381, 109 m of sediment and 84 tephras were recovered. At Site U1414, 375 m of sediment and 35 tephras were recovered, as well as 96 m of basaltic crust. The gap in the tephra record between mid- to late Pleistocene and middle Miocene documented at Site U1381 has likely been recovered at Site U1414. Biostratigraphic analysis shows that sediment containing ~20 felsic tephra layers during this time period was recovered. Analyses of these tephra will yield new insights into the evolution of Central American volcanism.

References

Abercrombie, R.E., Antolik, M., Felzer, K., and Ekström, G., 2001. The 1994 Java tsunami earthquake: slip over a subducting seamount. *J. Geophys. Res.: Solid Earth,* 106(B4):6595–6607. **doi:10.1029/2000JB900403**

Abratis, M., and Wörner, G., 2001. Ridge collision, slab-window formation, and the flux of Pacific asthenosphere into the Caribbean realm. *Geology,* 29(2):127–130. **doi:10.1130/0091-7613(2001)029<0127:RCSWFA>2.0.CO;2**

Ammon, C.J., Kanamori, H., Lay, T., and Velasco, A.A., 2006. The 17 July 2006 Java tsunami earthquake. *Geophys. Res. Lett.,* 33(24):L24308. **doi:10.1029/2006GL028005**

Arroyo, I.G., Grevemeyer, I., von Huene, R., Husen, S., Ranero, C.R., and Behrmann, J.H., 2011. Interplate seismicity at the CRISP site: the 2002 Osa earthquake sequence [presented at the 2011 American Geophysical Union Fall Meeting, San Francisco, CA, 5–9 December 2011]. (Abstract PP11B-1787) **http://www.agu.org/meetings/fm11/waisfm11.html**

Bangs, N.L., McIntosh, K.D., Silver, E.A., Ranero, C.R., Kluesner, J.W., von Huene, R., Cavanaugh, S., Graf, S., Cameselle, A.L., Baracco, A.M., and Nuñez, E., 2011. Preliminary results of the CRISP 3D seismic experiment, offshore Costa Rica [presented at the 2011 American Geophysical Union Fall Meeting, San Francisco, CA, 5–9 December 2011]. (Abstract T21B-2341) **http://www.agu.org/meetings/fm11/waisfm11.html**

Barckhausen, U., Ranero, C.R., von Huene, R., Cande, S.C., and Roeser, H.A., 2001. Revised tectonic boundaries in the Cocos plate off Costa Rica: implications for the segmentation of the convergent margin and for plate tectonic models. *J. Geophys. Res.: Solid Earth,* 106(B9):19207–19220. **doi:10.1029/2001JB000238**

Barckhausen, U., Roeser, H.A., and von Huene, R., 1998. Magnetic signature of upper plate structures and sub-

ducting seamounts at the convergent margin off Costa Rica. *J. Geophys. Res.: Solid Earth,* 03(B4):7079–7094. **doi:10.1029/98JB00163**

Beeler, N.M., 2007. Laboratory-observed faulting in intrinsically and apparently weak materials: strength, seismic coupling, dilatancy, and pore-fluid pressure. *In* Dixon, T.H., and Moore, J.C. (Eds.), *The Seismogenic Zone of Subduction Thrust Faults:* New York (Columbia Univ. Press), 370–449.

Bernabé, Y., Fryer, D.T., and Hayes, J.A., 1992. The effect of cement on the strength of granular rocks. *Geophys. Res. Lett.,* 19(14):1511–1514. **doi:10.1029/92GL01288**

Beroza, G.C., and Ide, S., 2011. Slow earthquakes and nonvolcanic tremor. *Annu. Rev. Earth Planet. Sci.,* 39(1):271–296. **doi:10.1146/annurev-earth-040809-152531**

Bilek, S.L., 2007. Influence of subducting topography on earthquake rupture. *In* Dixon, T.H., and Moore, J.C. (Eds.), *The Seismogenic Zone of Subduction Thrust Faults:* New York (Columbia Univ. Press), 123–146.

Bilek, S.L., 2010. The role of subduction erosion on seismicity. *Geology,* 38(5):479–480. **doi:10.1130/focus052010.1**

Bilek, S.L., and Lay, T., 2002. Tsunami earthquakes possibly widespread manifestations of frictional conditional stability. *Geophys. Res. Lett.,* 29(14):1673. **doi:10.1029/2002GL015215**

Bilek, S.L., Schwartz, S.Y., and DeShon, H.R., 2003. Control of seafloor roughness on earthquake rupture behavior. *Geology,* 31(5):455–458. **doi:10.1130/0091-7613(2003)031<0455:COSROE>2.0.CO;2**

Bohrmann, G., Heeschen, K., Jung, C., Weinrebe, W., Baranov, B., Cailleau, B., Heath, R., Hühnerbach, V., Hort, M., Masson, D., and Trummer, I., 2002. Widespread fluid expulsion along the seafloor of the Costa Rica convergent margin. *Terra Nova,* 14(2):69–79. **doi:10.1046/j.1365-3121.2002.00400.x**

Byrne, D.E., Davis, D.M., and Sykes, L.R., 1988. Loci and maximum size of thrust earthquakes and the mechanics of the shallow region of subduction zones. *Tectonics,* 7(4):833–857. **doi:10.1029/TC007i004p00833**

Chan, L.-H., and Kastner, M., 2000. Lithium isotopic compositions of pore fluids and sediments in the Costa Rica subduction zone: implications for fluid processes and sediment contribution to the arc volcanoes. *Earth Planet. Sci. Lett.,* 183(1–2):275–290. **doi:10.1016/S0012-821X(00)00275-2**

Clift, P., and Vannucchi, P., 2004. Controls on tectonic accretion versus erosion in subduction zones: implications for the origin and recycling of the continental crust. *Rev. Geophys.,* 42(2):RG2001. **doi:10.1029/2003RG000127**

Collettini, C., Niemeijer, A., Viti, C., and Marone, C., 2009. Fault zone fabric and fault weakness. *Nature (London, U. K.),* 462(7275):907–910. **doi:10.1038/nature08585**

Collot, J.-Y., Marcaillou, B., Sage, F., Michaud, F., Agudelo, W., Charvis, P., Graindorge, D., Gutscher, M.-A., and Spence, G., 2004. Are rupture zone limits of great subduction earthquakes controlled by upper plate structures? Evidence from multichannel seismic reflection data acquired across the northern Ecuador–southwest Colombia margin. *J. Geophys. Res.: Solid Earth,* 109(B11):B11103. **doi:10.1029/2004JB003060**

Davis, D., Suppe, J., and Dahlen, F.A., 1983. Mechanics of fold-and-thrust belts and accretionary wedges. *J. Geophys. Res.: Solid Earth,* 88(B2):1153–1172. **doi:10.1029/JB088iB02p01153**

DeMets, C., 2001. A new estimate for present-day Cocos-Caribbean plate motion: implications for slip along the Central American volcanic arc. *Geophys. Res. Lett.,* 28(21):4043–4046. **doi:10.1029/2001GL013518**

DeShon, H.R., Schwartz, S.Y., Bilek, S.L., Dorman, L.M., Gonzalez, V., Protti, J.M., Flueh, E.R., and Dixon, T.H., 2003. Seismogenic zone structure of the southern Middle America Trench, Costa Rica. *J. Geophys. Res.: Solid Earth,* 108(B10):2491. **doi:10.1029/2002JB002294**

Expedition 334 Scientists, 2012a. Site U1378. *In* Vannucchi, P., Ujiie, K., Stroncik, N., Malinverno, A., and the Expedition 334 Scientists, *Proc. IODP,* 334: Tokyo (Integrated Ocean Drilling Program Management International, Inc.). **doi:10.2204/iodp.proc.334.103.2012**

Expedition 334 Scientists, 2012b. Site U1379. *In* Vannucchi, P., Ujiie, K., Stroncik, N., Malinverno, A., and the Expedition 334 Scientists, *Proc. IODP,* 334: Tokyo (Integrated Ocean Drilling Program Management International, Inc.). **doi:10.2204/iodp.proc.334.104.2012**

Expedition 334 Scientists, 2012c. Site U1380. *In* Vannucchi, P., Ujiie, K., Stroncik, N., Malinverno, A., and the Expedition 334 Scientists, *Proc. IODP,* 334: Tokyo (Integrated Ocean Drilling Program Management International, Inc.). **doi:10.2204/iodp.proc.334.105.2012**

Expedition 334 Scientists, 2012d. Site U1381. *In* Vannucchi, P., Ujiie, K., Stroncik, N., Malinverno, A., and the Expedition 334 Scientists, *Proc. IODP,* 334: Tokyo (Integrated Ocean Drilling Program Management International, Inc.). **doi:10.2204/iodp.proc.334.106.2012**

Fagereng, A., and Sibson, R.H., 2010. Melange rheology and seismic style. *Geology,* 38(8):751–754. **doi:10.1130/G30868.1**

Fisher, A.T., Stein, C.A., Harris, R.N., Wang, K., Silver, E.A., Pfender, M., Hutnak, M., Cherkaoui, A., Bodzin, R., and Villinger, H., 2003. Abrupt thermal transition reveals hydrothermal boundary and role of seamounts within the Cocos plate. *Geophys. Res. Lett.,* 30(11):1550–1553. **doi:10.1029/2002GL016766**

Fisher, D.M., Gardner, T.W., Marshall, J.S., Sak, P.B., and Protti, M., 1998. Effect of subducting seafloor roughness on forearc kinematics, Pacific coast, Costa Rica. *Geology,* 26(5):467–470. **doi:10.1130/0091-7613(1998)026<0467:EOSSFR>2.3.CO;2**

Fisher, D.M., Gardner, T.W., Sak, P.B., Sanchez, J.D., Murphy, K., and Vannucchi, P., 2004. Active thrusting in the inner forearc of an erosive convergent margin, Pacific coast, Costa Rica. *Tectonics,* 23(2):TC2007. **doi:10.1029/2002TC001464**

Flüh, E.R., Söding, E., and Suess, E., 2004. RV *Sonne* Cruise Report SO173/1, 3, and 4—Subduction II: the Central American continental margin. *GEOMAR Rep.,* 115.

Gardner, T., Marshall, J., Merritts, D., Bee, B., Burgette, R., Burton, E., Cooke, J., Kehrwald, N., Protti, M., Fisher, D., and Sak, P., 2001. Holocene forearc block rotation in

response to seamount subduction, southeastern Península de Nicoya, Costa Rica. *Geology,* 29(2):151–154. doi:10.1130/0091-7613(2001)029<0151:HFBRIR>2.0.CO;2

Gardner, T.W., Verdonck, D., Pinter, N.M., Slingerland, R., Furlong, K.P., Bullard, T.F., and Wells, S.G., 1992. Quaternary uplift astride the aseismic Cocos Ridge, Pacific coast, Costa Rica. *Geol. Soc. Am. Bull.,* 104(2):219–232. doi:10.1130/0016-7606(1992)104<0219:QUATAC>2.3.CO;2

Gräfe, K., Frisch, W., Villa, I.M., and Meschede, M., 2002. Geodynamic evolution of southern Costa Rica related to low-angle subduction of the Cocos Ridge: constraints from thermochronology. *Tectonophysics,* 348(4):187–204. doi:10.1016/S0040-1951(02)00113-0

Grevemeyer, I., Kopf, A.J., Fekete, N., Kaul, N., Villinger, H.W., Heesemann, M., Wallmann, K., Spiess, V., Gennerich, H.-H., Muller, M., and Weinrebe, W., 2004. Fluid flow through active mud dome Mound Culebra offshore Nicoya Peninsula, Costa Rica: evidence from heat flow surveying. *Mar. Geol.,* 207(1–4):145–157. doi:10.1016/j.margeo.2004.04.002

Harris, R., Sakaguchi, A., and Petronotis, K., 2012. Costa Rica Seismogenesis Project, Program A Stage 2 (CRISP-A2): sampling and quantifying lithologic inputs and fluid inputs and outputs of the seismogenic zone. *IODP Sci. Prosp.,* 344. doi:10.2204/iodp.sp.344.2012

Harris, R.N., Grevemeyer, I., Ranero, C.R., Villinger, H., Barckhausen, U., Henke, T., Mueller, C., and Neben, S., 2010a. Thermal regime of the Costa Rican convergent margin, 1. Along-strike variations in heat flow from probe measurements and estimated from bottom-simulating reflectors. *Geochem., Geophys., Geosyst.,* 11(12):Q12S28. doi:10.1029/2010GC003272

Harris, R.N., Spinelli, G., Ranero, C.R., Grevemeyer, I., Villinger, H., and Barckhausen, U., 2010b. Thermal regime of the Costa Rican convergent margin, 2. Thermal models of the shallow Middle America subduction zone offshore Costa Rica. *Geochem., Geophys., Geosyst.,* 11(12):Q12S29. doi:10.1029/2010GC003273

Harris, R.N., and Wang, K., 2002. Thermal models of the Middle America Trench at the Nicoya Peninsula, Costa Rica. *Geophys. Res. Lett.,* 29(21):2010–2013. doi:10.1029/2002GL015406

Hauff, F., Hoernle, K., Schminke, H.-U., and Werner, R., 1997. A mid-Cretaceous origin for the Galápagos hotspot: volcanological, petrological and geochemical evidence from Costa Rican oceanic crustal segments. *Geol. Rundsch.,* 86(1):141–155. doi:10.1007/PL00009938

Hauff, F., Hoernle, K., Tilton, G., Graham, D.W., and Kerr, A.C., 2000. Large volume recycling of oceanic lithosphere over short time scales: geochemical constraints from the Caribbean large igneous province. *Earth Planet. Sci. Lett.,* 174(3–4):247–263. doi:10.1016/S0012-821X(99)00272-1

Hensen, C., Wallmann, K., Schmidt, M., Ranero, C.R., and Suess, E., 2004. Fluid expulsion related to mud extrusion off Costa Rica—a window to the subducting slab. *Geology,* 32(3):201–204. doi:10.1130/G20119.1

Heuret, A., Lallemand, S., Funiciello, F., Piromallo, C., and Faccenna, C., 2011. Physical characteristics of subduction interface type seismogenic zones revisited. *Geochem., Geophys., Geosyst.,* 12(1):Q01004. doi:10.1029/2010GC003230

Hey, R., 1977. Tectonic evolution of the Cocos-Nazca spreading center. *Geol. Soc. Am. Bull.,* 88(12):1404–1420. doi:10.1130/0016-7606(1977)88<i:TEOTCS>2.0.CO;2

Hinz, K., von Huene, R., Ranero, C.R., and the PACOMAR Working Group, 1996. Tectonic structure of the convergent Pacific margin offshore Costa Rica from multichannel seismic reflection data. *Tectonics,* 15(1):54–66. doi:10.1029/95TC02355

Hirata, K., Geist, E., Satake, K., Tanioka, Y., and Yamaki, S., 2003. Slip distribution of the 1952 Tokachi-Oki earthquake (*M* 8.1) along the Kuril Trench deduced from tsunami waveform inversion. *J. Geophys. Res.: Solid Earth,* 108(B4):2196. doi:10.1029/2002JB001976

Hoernle, K., van den Bogaard, P., Werner, R., Lissinna, B., Hauff, F., Alvarado, G., and Garbe-Schönberg, D., 2002. Missing history (16–71 Ma) of the Galápagos hotspot: implications for the tectonic and biological evolution of the Americas. *Geology,* 30(9):795–798. doi:10.1130/0091-7613(2002)030<0795:MHMOTG>2.0.CO;2

Husen, S., Kissling, E., and Quintero, R., 2002. Tomographic evidence for a subducted seamount beneath the Gulf of Nicoya, Costa Rica: the cause of the 1990 Mw = 7.0 Gulf of Nicoya earthquake. *Geophys. Res. Lett.,* 29(8):1238. doi:10.1029/2001GL014045

Hutnak, M., Fisher, A.T., Harris, R., Stein, C., Wang, K., Spinelli, G., Schindler, M., Villinger, H., and Silver, E., 2008. Large heat and fluid fluxes driven through mid-plate outcrops on ocean crust. *Nat. Geosci.,* 1(9):611–614. doi:10.1038/ngeo264

Hutnak, M., Fisher, A.T., Stein, C.A., Harris, R., Wang, K., Silver, E., Spinelli, G., Pfender, M., Villinger, H., MacKnight, R., Costa, P.P., DeShon, H.R., and Diamente, C., 2007. The thermal state of 18–24 Ma upper lithosphere subducting below the Nicoya Peninsula, northern Costa Rica margin. *In* Dixon, T.H., and Moore, J.C. (Eds.), *The Seismogenic Zone of Subduction Thrust Faults:* New York (Columbia Univ. Press), 86–122.

Hyndman, R.D., Yamano, M., and Oleskevich, D.A., 1997. The seismogenic zone of subduction thrust faults. *Isl. Arc,* 6(3):244–260. doi:10.1111/j.1440-1738.1997.tb00175.x

Ide, S., 2012. Variety and spatial heterogeneity of tectonic tremor worldwide. *J. Geophys. Res.: Solid Earth,* 117(B3):B03302. doi:10.1029/2011JB008840

Ikari, M.J., Marone, C., and Saffer, D.M., 2011. On the relation between fault strength and frictional stability. *Geology,* 39(1):83–86. doi:10.1130/G31416.1

Kahn, L.M., Silver, E.A., Orange, D., Kochevar, R., and McAdoo, B., 1996. Surficial evidence of fluid expulsion from the Costa Rica accretionary prism. *Geophys. Res. Lett.,* 23(8):887–890. doi:10.1029/96GL00732

Kanamori, H., 1972. Mechanism of tsunami earthquakes. *Phys. Earth Planet. Inter.,* 6(5):346–359. doi:10.1016/0031-9201(72)90058-1

Kanamori, H., and Kikuchi, M., 1993. The 1992 Nicaragua earthquake: a slow tsunami earthquake associated with

subducted sediments. *Nature (London, U. K.),* 361(6414):714–716. **doi:10.1038/361714a0**

Kastner, M., Solomon, E., Wei, W., Chan, L.-H., and Saether, O.M., 2006. Data report: chemical and isotopic compositions of pore fluids and sediments from across the Middle America Trench, offshore Costa Rica. *In* Morris, J.D., Villinger, H.W., and Klaus, A. (Eds.), *Proc. ODP, Sci Results*, 205: College Station, TX (Ocean Drilling Program), 1–21. **doi:10.2973/odp.proc.sr.205.208.2006**

Kimura, G., Silver, E.A., Blum, P., et al., 1997. *Proc. ODP, Init. Repts.,* 170: College Station, TX (Ocean Drilling Program). **doi:10.2973/odp.proc.ir.170.1997**

Klaucke, I., Masson, D.G., Petersen, C.J., Weinrebe, W., and Ranero, C.R., 2008. Multifrequency geoacoustic imaging of fluid escape structures offshore Costa Rica: implications for the quantification of seep processes. *Geochem., Geophys., Geosyst.*, 9(4):Q04010. **doi:10.1029/2007GC001708t**

Kluesner, J.W., Silver, E.A., von Huene, R., Bangs, N.L., McIntosh, K.D., Ranero, C.R., Orange, D., Cavanaugh, S., Graf, S., Baracco, A.M., and Cameselle, A.L., 2011. Detailed surface structure in high-resolution bathymetry and backscatter from the CRISP 3-D seismic experiment, offshore Costa Rica [presented at the 2011 American Geophysical Union Fall Meeting, San Francisco, CA, 5–9 December 2011]. (Abstract T21B-2336) **http://www.agu.org/meetings/fm11/waisfm11.html**

Kodaira, S., Takahashi, N., Nakanishi, A., Miura, S., and Kaneda, Y., 2000. Subducted seamount imaged in the rupture zone of the 1946 Nankaido earthquake. *Science,* 289(5476):104–106. **doi:10.1126/science.289.5476.104**

Kolarsky, R.A., Mann, P., and Montero, W., 1995. Island arc response to shallow subduction of the Cocos Ridge, Costa Rica. *In* Mann, P. (Ed.), *Geologic and Tectonic Development of the Caribbean Plate Boundary in Southern Central America*. Spec. Pap.—Geol. Soc. Am., 295:235–262. **doi:10.1130/SPE295-p235**

LaFemina, P., Dixon, T.H., Govers, R., Norabuena, E., Turner, H., Saballos, A., Mattioli, G., Protti, M., and Strauch, W., 2009. Fore-arc motion and Cocos Ridge collision in Central America. *Geochem., Geophys., Geosyst.,* 10(5):Q05S14. **doi:10.1029/2008GC002181**

Lallemand, S.E., Schnürle, P., and Malavieille, J., 1994. Coulomb theory applied to accretionary and nonaccretionary wedges: possible causes for tectonic erosion and/or frontal accretion. *J. Geophys. Res.: Solid Earth,* 99(B6):12033–12055. **doi:10.1029/94JB00124**

Langseth, M.G., and Silver, E.A., 1996. The Nicoya convergent margin—a region of exceptionally low heat flow. *Geophys. Res. Lett.,* 27(8):891–894. **doi:10.1029/96GL00733**

Lay, T., and Kanamori, H., 1980. Earthquake doublets in the Solomon Islands. *Phys. Earth Planet. Inter.,* 21(4):283–304. **doi:10.1016/0031-9201(80)90134-X**

Lay, T., Kanamori, H., and Ruff, L., 1982. The asperity model and the nature of large subduction zone earthquakes. *Earthquake Predict. Res.,* 1(1):3–71.

Lonsdale, P., and Klitgord, K.D., 1978. Structure and tectonic history of the eastern Panama Basin. *Geol. Soc. Am. Bull.,* 89(7):981–999. **doi:10.1130/0016-7606(1978)89<981:SATHOT>2.0.CO;2**

Lundgren, P., Protti, M., Donnellan, A., Heflin, M., Hernandez, E., and Jefferson, D., 1999. Seismic cycle and plate margin deformation in Costa Rica: GPS observations from 1994 to 1997. *J. Geophys. Res.: Solid Earth,* 104(B12):28915–28926. **doi:10.1029/1999JB900283**

MacMillan, I., Gans, P.B., and Alvarado, G., 2004. Middle Miocene to present plate tectonic history of the southern Central American volcanic arc. *Tectonophysics*, 392(1–4)325–348. **doi:10.1016/j.tecto.2004.04.014**

Marone, C., and Saffer, D.M., 2007. Fault friction and the upper transition from seismic to aseismic faulting. *In* Dixon, T.H., and Moore, J.C. (Eds.), *The Seismogenic Zone of Subduction Thrust Faults:* New York (Columbia Univ. Press), 346–369.

Marone, C., and Scholz, C.H., 1988. The depth of seismic faulting and the upper transition from stable to unstable slip regimes. *Geophys. Res. Lett.,* 15(6):621–624. **doi:10.1029/GL015i006p00621**

McAdoo, B.G., Orange, D.L., Silver, E.A., McIntosh, K., Abott, L., Galewsky, J., Kahn, L., and Protti, M., 1996. Seafloor structural observations, Costa Rica accretionary prism. *Geophys. Res. Lett.,* 23(8):883–886. **doi:10.1029/96GL00731**

McCaffrey, R., 1993. On the role of the upper plate in great subduction zone earthquakes. *J. Geophys. Res.: Solid Earth,* 98(B7):11953–11966. **doi:10.1029/93JB00445**

McCaffrey, R., 2002. Crustal block rotations and plate coupling. *In* Stein, S., and Freymueller, J. (Eds.), *Plate Boundary Zones*. Geodyn. Ser., 30:101–122. **doi:10.1029/GD030p0101**

McIntosh, K., Silver, E., and Shipley, T., 1993. Evidence and mechanisms for forearc extension at the accretionary Costa Rica convergent margin. *Tectonics,* 12(6):1380–1392. **doi:10.1029/93TC01792**

Moore, J.C., and Saffer, D., 2001. Updip limit of the seismogenic zone beneath the accretionary prism of southwest Japan: an effect of diagenetic to low-grade metamorphic processes and increasing effective stress. *Geology,* 29(2):183–186. **doi:10.1130/0091-7613(2001)029<0183:ULOTSZ>2.0.CO;2**

Morris, J.D., Villinger, H.W., Klaus, A., et al., 2003. *Proc. ODP, Init. Repts.,* 205: College Station, TX (Ocean Drilling Program). **doi:10.2973/odp.proc.ir.205.2003**

Newman, A.V., Schwartz, S.Y., Gonzalez, V., DeShon, H.R., Protti, J.M., and Dorman, L.M., 2002. Along-strike variability in the seismogenic zone below Nicoya Peninsula, Costa Rica. *Geophys. Res. Lett.,* 29(20):1977. **doi:10.1029/2002GL015409**.

Norabuena, E., Dixon, T.H., Schwartz, S., DeShon, H., Newman, A., Protti, M., Gonzalez, V., Dorman, L., Flueh, E.R., Lundgren, P., Pollitz, F., and Sampson, D., 2004. Geodetic and seismic constraints on some seismogenic zone processes in Costa Rica. *J. Geophys. Res.: Solid Earth,* 109(B11):B11403. **doi:10.1029/2003JB002931**

Oleskevich, D.A., Hyndman, R.D., and Wang, K., 1999. The updip and downdip limits to great subduction earthquakes: thermal and structural models of Cascadia, south Alaska, SW Japan, and Chile. *J. Geophys. Res.: Solid*

Earth, 104(B7):14965–14992. doi:10.1029/1999JB900060

Pacheco, J.F., Sykes, L.R., and Scholz, C.H., 1993. Nature of seismic coupling along simple plate boundaries of the subduction type. *J. Geophys. Res.: Solid Earth,* 98(B8):14133–14159. doi:10.1029/93JB00349

Park, J.-O., Tsuru, T., Kodaira, S., Cummins, P.R., and Kaneda, Y., 2002. Splay fault branching along the Nankai subduction zone. *Science,* 297(5584):1157–1160. doi:10.1126/science.1074111

Peng, Z., and Gomberg, J., 2010. An integrated perspective of the continuum between earthquakes and slow-slip phenomena. *Nat. Geosci.,* 3(9):599–607. doi:10.1038/ngeo940

Pérez, W., Alvarado, G.E., and Gans, P.B., 2006. The 322 ka Tiribí Tuff: stratigraphy, geochronology and mechanisms of deposition of the largest and most recent ignimbrite in the Valle Central, Costa Rica. *Bull. Volcanol.,* 69(1):25–40. doi:10.1007/s00445-006-0053-x

Petersen, C.J., Klaucke, I., Weinrebe, W., and Ranero, C.R., 2009. Fluid seepage and mound formation offshore Costa Rica revealed by deep-towed sidescan sonar and sub-bottom profiler data. *Mar. Geol.,* 266(1–4):172–181. doi:10.1016/j.margeo.2009.08.004

Polet, J., and Kanamori, H., 2000. Shallow subduction zone earthquakes and their tsunamigenic potential. *Geophys. J. Int.,* 142(3):684–702. doi:10.1046/j.1365-246x.2000.00205.x

Protti, M., Gündel, F., and McNally, K., 1994. The geometry of the Wadati-Benioff Zone under southern Central America and its tectonic significance: results from a high-resolution local seismographic network. *Phys. Earth Planet. Inter.,* 84(1–4):271–287. doi:10.1016/0031-9201(94)90046-9

Protti, M., Gündel, F., and McNally, K., 1995. Correlation between the age of the subducted Cocos plate and the geometry of the Wadati-Benioff Zone under Nicaragua and Costa Rica. *In* Mann, P. (Ed.), *Geologic and Tectonic Development of the Caribbean Plate Boundary in Southern Central America*. Spec. Pap.—Geol. Soc. Am., 295:309–326. doi:10.1130/SPE295-p309

Ranero, C.R., Grevemeyer, I., Sahling, U., Barckhausen, U., Hensen, C., Wallmann, K., Weinrebe, W., Vannucchi, P., von Huene, R., and McIntosh, K., 2008. Hydrogeological system of erosional convergent margins and its influence on tectonics and interplate seismogenesis. *Geochem., Geophys., Geosyst.,* 9(3):Q03S04. doi:10.1029/2007GC001679

Ranero, C.R., and von Huene, R., 2000. Subduction erosion along the Middle America convergent margin. *Nature (London, U. K.),* 404(6779):748–752. doi:10.1038/35008046

Ranero, C.R., von Huene, R., Flueh, E., Duarte, M., Baca, D., and McIntosh, K., 2000. A cross section of the convergent Pacific margin of Nicaragua. *Tectonics,* 19(2):335–357. doi:10.1029/1999TC900045

Ranero, C.R., von Huene, R., Weinrebe, W., and Barckhausen, U., 2007. Convergent margin tectonics: a marine perspective. *In* Bundschuh, J., and Alvarado, G.E. (Eds.), *Central America: Geology, Resources and Hazards:* London (Taylor and Francis), 239–265.

Ruff, L.J., 1992. Asperity distributions and large earthquake occurrence in subduction zones. *Tectonophysics,* 211(1–4):61–83. doi:10.1016/0040-1951(92)90051-7

Sahling, H., Masson, D.G., Ranero, C.R. Hühnerbach, V., Weinrebe, W., Klaucke, I., Bürk, D., Brückmann, W., and Suess, E., 2008. Fluid seepage at the continental margin offshore Costa Rica and southern Nicaragua. *Geochem., Geophys., Geosyst.,* 9(5):Q05S05. doi:10.1029/2008GC001978

Sak, P.B., Fisher, D.M., and Gardner, T.W., 2004. Effects of subducting seafloor roughness on upper plate vertical tectonism: Osa Peninsula, Costa Rica. *Tectonics,* 23(1):TC1017. doi:10.1029/2002TC001474

Satake, K., and Tanioka, Y., 1999. Sources of tsunami and tsunamigenic earthquakes in subduction zones. *Pure Appl. Geophys.,* 154(3–4):467–483. doi:10.1007/s000240050240

Scholl, D.W., von Huene, R., Vallier, T.L., and Howell, D.G., 1980. Sedimentary masses and concepts about tectonic processes at underthrust ocean margins. *Geology,* 8(12):564–568. doi:10.1130/0091-7613(1980)8<564:SMACAT>2.0.CO;2

Scholz, C.H., 1998. Earthquakes and friction laws. *Nature (London, U. K.),* 391(6662):37–42. doi:10.1038/34097

Scholz, C.H., 2002. *The Mechanics of Earthquakes and Faulting* (2nd. ed): New York (Cambridge Univ. Press).

Scholz, C.H., and Small, C., 1997. The effect of seamount subduction on seismic coupling. *Geology,* 25(6):487–490. doi:10.1130/0091-7613(1997)025<0487:TEOSSO>2.3.CO;2

Shipley, T.H., McIntosh, K.D., Silver, E.A., and Stoffa, P.L., 1992. Three-dimensional seismic imaging of the Costa Rica accretionary prism: structural diversity in a small volume of the lower slope. *J. Geophys. Res.: Solid Earth,* 97(B4):4439–4459. doi:10.1029/91JB02999

Sibson, R.H., 1981. Controls on low-stress hydro-fracture dilatancy in thrust, wrench and normal fault terrains. *Nature (London, U. K.),* 289(5799):665–667. doi:10.1038/289665a0

Silver, E., Kastner, M., Fisher, A., Morris, J., McIntosh, K., and Saffer, D., 2000. Fluid flow paths in the Middle America Trench and Costa Rica margin. *Geology,* 28(8):679–682. doi:10.1130/0091-7613(2000)28<679:FFPITM>2.0.CO;2

Sinton, C.W., Duncan, R.A., and Denyer, P., 1997. Nicoya Peninsula, Costa Rica: a single suite of Caribbean oceanic plateau magmas. *J. Geophys. Res.: Solid Earth,* 102(B7):15507–15520. doi:10.1029/97JB00681

Sitchler, J.C., Fisher, D.M., Gardner, T.W., and Protti, M., 2007. Constraints on inner forearc deformation from balanced cross sections, Fila Costeña thrust belt, Costa Rica. *Tectonics,* 26(6):TC6012. doi:10.1029/2006TC001949

Solomon, E.A., Kastner, M., Wheat, C.G., Jannasch, H., Robertson, G., Davis, E.E., and Morris, J.D., 2009. Long-term hydrogeochemical records in the oceanic basement and forearc prism at the Costa Rica subduction

zone. *Earth Planet. Sci. Lett.,* 282(1–4):240–251. doi:10.1016/j.epsl.2009.03.022

Spinelli, G.A., Saffer, D.M., and Underwood, M.B., 2006. Hydrogeologic responses to three-dimensional temperature variability, Costa Rica subduction margin. *J. Geophys. Res.: Solid Earth,* 111(B4):B04403. doi:10.1029/2004JB003436

Spinelli, G.A., and Wang, K., 2008. Effects of fluid circulation in subduction crust on Nankai margin seismogenic zone temperatures. *Geology,* 36(11):887–890. doi:10.1130/G25145A.1

Stavenhagen, A.U., Flueh, E.R., Ranero, C., McIntosh, K.D., Shipley, T., Leandro, G., Shulze, A., and Danobeitia, J.J., 1998. Seismic wide-angle investigations in Costa Rica: a crustal velocity model from the Pacific to the Caribbean coast. *Zb. Geol. Paläontol.*, 1997(3–6):393–408.

Stein, C.A., and Stein, S., 1992. A model for the global variation in oceanic depth and heat flow with lithospheric age. *Nature (London, U. K.),* 359(6391):123–129. doi:10.1038/359123a0

Stein, C.A., and Stein, S., 1994. Constraints on hydrothermal heat flux through the oceanic lithosphere from global heat flow. *J. Geophys. Res.: Solid Earth,* 99(B2):3081–3095. doi:10.1029/93JB02222

Sutter, F.R., 1985. Sección geológica del Pacífico al Atlántico a través de Costa Rica. *Rev. Geol. Am. Cent.*, 2:23–32. http://www.geologia.ucr.ac.cr/revista/revista/to_pdf/revista/02/02-RIVIER.pdf

Tichelaar, B.W., and Ruff, L.J., 1993. Depth of seismic coupling along subduction zones. *J. Geophys. Res.: Solid Earth,* 98(B2):2017–2037. doi:10.1029/92JB02045

Turner, H.L., III, LaFemina, P., Saballos, A. Mattioli, G.S., Jansma, P.E., and Dixon, T., 2007. Kinematics of the Nicaraguan forearc from GPS geodesy. *Geophys. Res. Lett.,* 34(2):L02302. doi:10.1029/2006GL027586

Vacquier, V., Sclater, J.G., and Correy, C.E., 1967. Studies of the thermal state of the Earth: heat flow, Eastern Pacific. *Bull. Earthquake Res. Inst.,* 45:375–393.

van Andel, T.H., Heath, G.R., Malfait, B.T., Heinrichs, D.F., and Ewing, J.I., 1971. Tectonics of the Panama Basin, eastern equatorial Pacific. *Geol. Soc. Am. Bull.,* 82(6):1489–1508. doi:10.1130/0016-7606(1971)82[1489:TOTPBE]2.0.CO;2

Vannucchi, P., Fisher, D.M., Bier, S., and Gardner, T.W., 2006. From seamount accretion to tectonic erosion: formation of Osa mélange and the effects of Cocos Ridge subduction in southern Costa Rica. *Tectonics*, 25(4):TC2004. doi:10.1029/2005TC001855

Vannucchi, P., Galeotti, S., Clift, P.D., Ranero, C.R., and von Huene, R., 2004. Long-term subduction-erosion along the Guatemalan margin of the Middle America Trench. *Geology,* 32(7):617–620. doi:10.1130/G20422.1

Vannucchi, P., Ranero, C.R., Galeotti, S., Straub, S.M., Scholl, D.W., and McDougall-Ried, K., 2003. Fast rates of subduction erosion along the Costa Rica Pacific margin: implications for nonsteady rates of crustal recycling at subduction zones. *J. Geophys. Res.: Solid Earth,* 108(B11):2511. doi:10.1029/2002JB002207

Vannucchi, P., Scholl, D.W., Meschede, M., and McDougall-Reid, K., 2001. Tectonic erosion and consequent collapse of the Pacific margin of Costa Rica: combined implications from ODP Leg 170, seismic offshore data, and regional geology of the Nicoya Peninsula. *Tectonics,* 20(5):649–668. doi:10.1029/2000TC001223

Vannucchi, P., Ujiie, K., Stroncik, N., Malinverno, A., and the Expedition 334 Scientists, 2012. *Proc. IODP,* 334: Tokyo (Integrated Ocean Drilling Program Management International, Inc.). doi:10.2204/iodp.proc.334.2012

Vergara Muñoz, A., 1988. Seismicity of the Panama Block, I. Magnitudes and spatial distribution of epicentres. *Tectonophysics,* 145(3–4):213–224. doi:10.1016/0040-1951(88)90196-5

Von Herzen, R.P., and Uyeda, S., 1963. Heat flow through the eastern Pacific Ocean floor. *J. Geophys. Res.,* 68(14):4219–4250. doi:10.1029/JZ068i014p04219

von Huene, R., Bialas, J., Flueh, E., Cropp, B., Csernok, T., Fabel, E., Hoffmann, J., Emeis, K., Holler, P., Jeschke, G., Leandro M., C., Perez Fernandez, I., Chavarria S., J., Florez H., A., Escobedo Z., D., Leon, R., and Barrios L., O., 1995. Morphotectonics of the Pacific convergent margin of Costa Rica. *In* Mann, P. (Ed.), *Geologic and Tectonic Development of the Caribbean Plate Boundary in Southern Central America*. Spec. Pap.—Geol. Soc. Am., 295:291–307. doi:10.1130/SPE295-p291

von Huene, R., and Lallemand, S., 1990. Tectonic erosion along the Japan and Peru convergent margins. *Geol. Soc. Am. Bull.,* 102(6):704–720. doi:10.1130/0016-7606(1990)102<0704:TEATJA>2.3.CO;2

von Huene, R., Ranero, C.R., Weinrebe, W., and Hinz, K., 2000. Quaternary convergent margin tectonics of Costa Rica, segmentation of the Cocos plate, and Central American volcanism. *Tectonics,* 19(2):314–334. doi:10.1029/1999TC001143

von Huene, R., and Scholl, D.W., 1991. Observations at convergent margins concerning sediment subduction, subduction erosion, and the growth of the continental crust. *Rev. Geophys.,* 29(3):279–316. doi:10.1029/91RG00969

Walther, C.H.E., 2003. The crustal structure of the Cocos Ridge off Costa Rica. *J. Geophys. Res.: Solid Earth,* 108(B3):2136. doi:10.1029/2001JB000888

Wang, K., and Bilek, S.L., 2011. Do subducting seamounts generate or stop large earthquakes? *Geology,* 39(9):819–822. doi:10.1130/G31856.1

Weinrebe, W., and Ranero, C.R. (Eds.), 2003. FS/RV *Sonne* Cruise Report SO173/2: Seduction, Part A. Seismogenesis and tectonic erosion during subduction: Middle America margin. *GEOMAR Rep.,* 116. https://ftp.ifm-geomar.de/users/wweinrebe/SO-173-2/Geomar-Report-116.pdf

Ye, S., Bialas, J., Flueh, E.R., Stavenhagen, A., von Huene, R., Leandro, G., and Hinz, K., 1996. Crustal structure of the Middle America Trench off Costa Rica from wide-angle seismic data. *Tectonics,* 15(5):1006–1021. doi:10.1029/96TC00827

Publication: 11 December 2013
MS 344-101

Figure F1. Topographic and bathymetric map of the Costa Rica area, showing location of Expedition 344 drilling area. Seafloor bathymetry is based on satellite gravimetry and swath mapping (Barckhausen et al., 2001; Fisher et al., 2003; von Huene et al., 2000). Note the collision of Cocos Ridge with the trench offshore of the Osa Peninsula. This process brings the seismogenic zone within reach of IODP riser drilling capabilities. DSDP = Deep Sea Drilling Project, ODP = Ocean Drilling Program. Inset shows tectonic setting of Central America, including the plates that interact in this region: North America (NA), Caribbean (CA), South America (SA), Nazca (NZ), Cocos (CO), and Pacific (PA). EPR = East Pacific Rise, CNS = Cocos-Nazca spreading center.

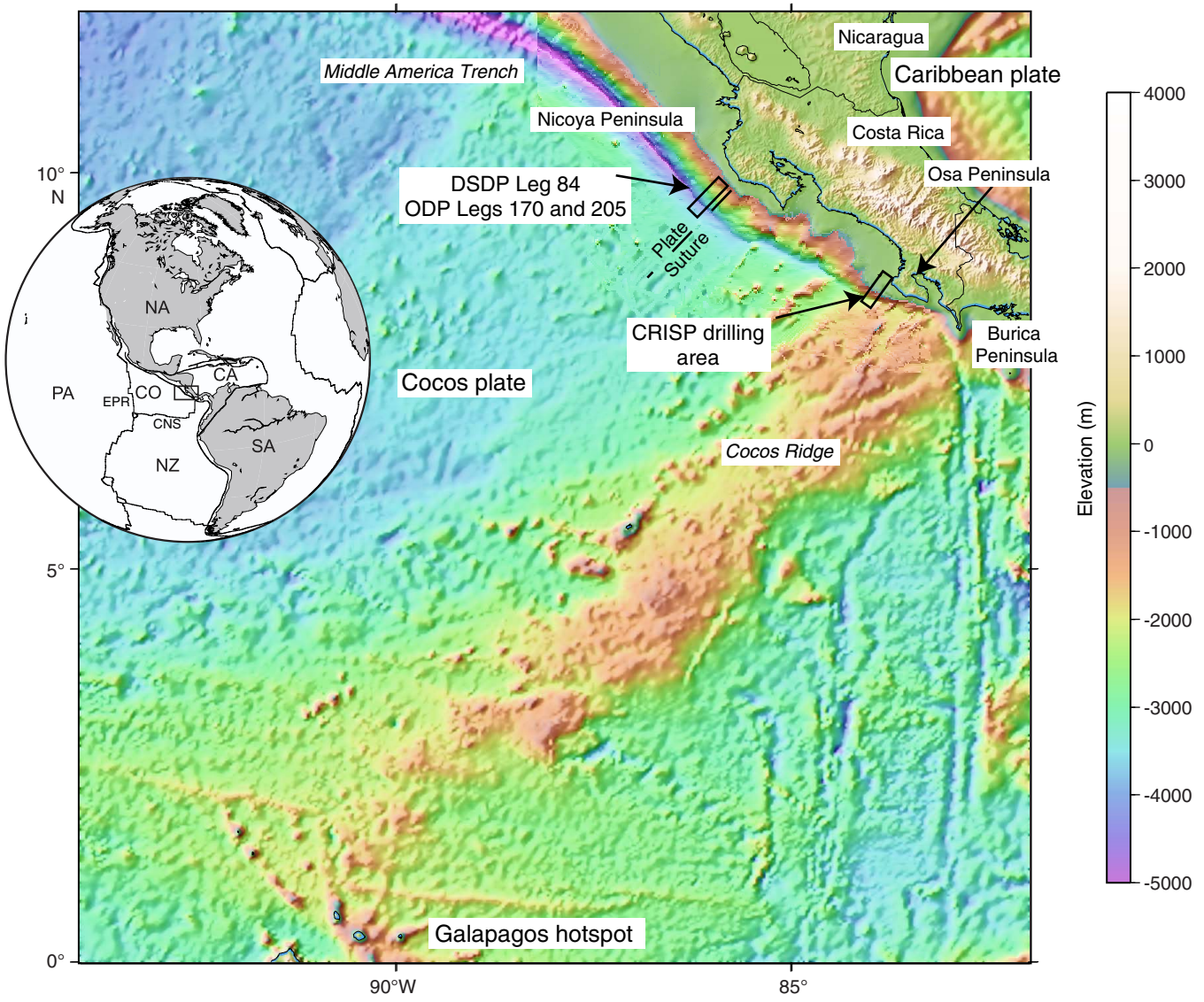

Figure F2. A. Seismic Line BGR99-7 showing location of Expedition 344 drill sites. Prestack depth migration (C.R. Ranero, unpubl. data) is at a vertical exaggeration of 1.3×. **B.** Interpreted wide-angle seismic section from Stavenhagen et al. (1998). Schematic figure through Osa Peninsula margin showing Sites U1381, U1412, U1378, U1380, and U1379. v = *P*-wave velocity.

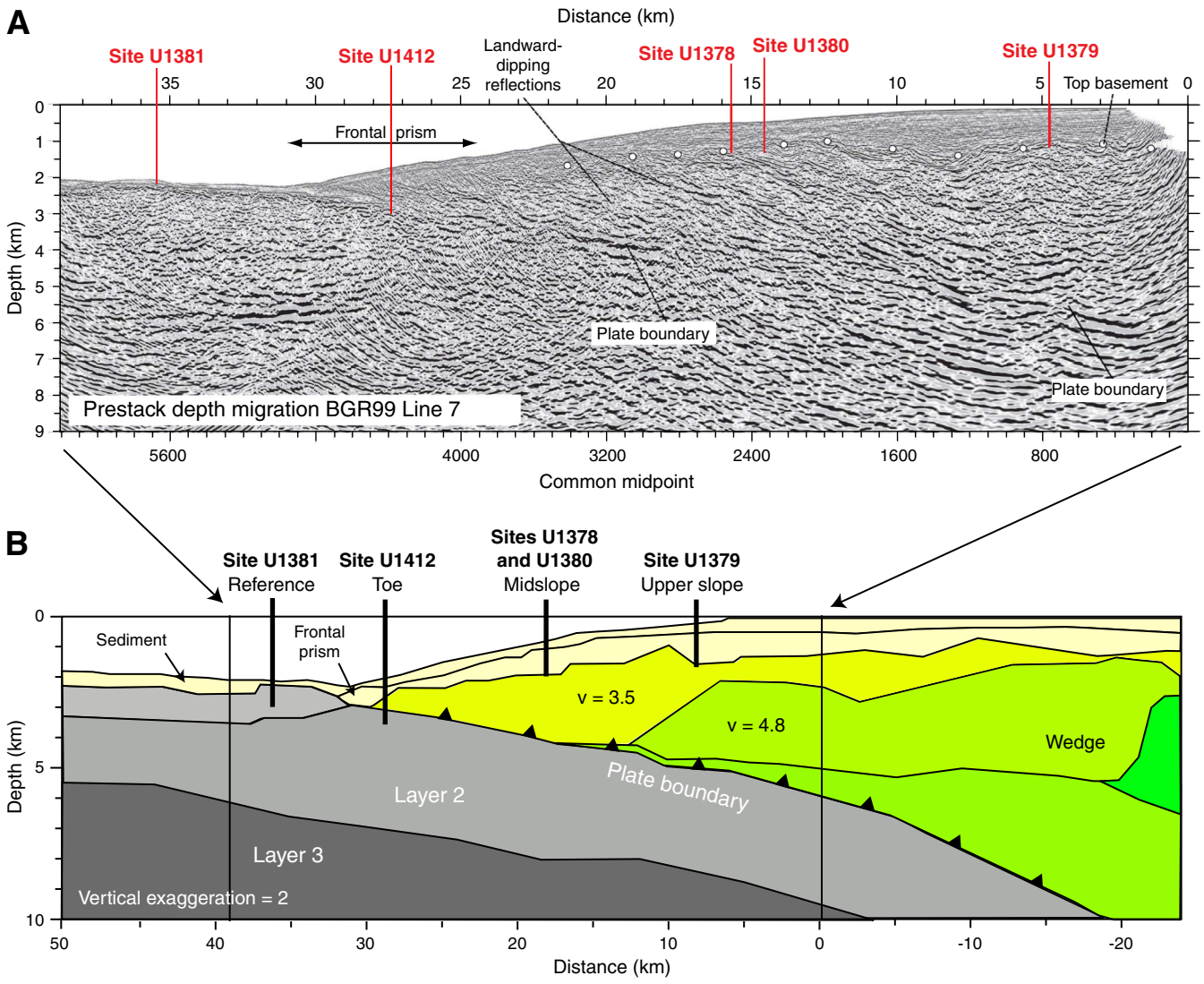

Figure F3. Seismicity along the Costa Rica margin with Expedition 344 site locations. Small black circles show seismicity recorded by Sismologica Nacional between 1992 and 2007. Focal mechanisms correspond to large earthquakes (Mw > 6.4) nucleated in the seismogenic zone over the past 25 y. Red circles show aftershocks from the 2002 Osa event, and beige circles show aftershocks from the 1999 Quepos event (modified from Arroyo et al., 2011). Triangles, squares, and diamonds show various seismic networks.

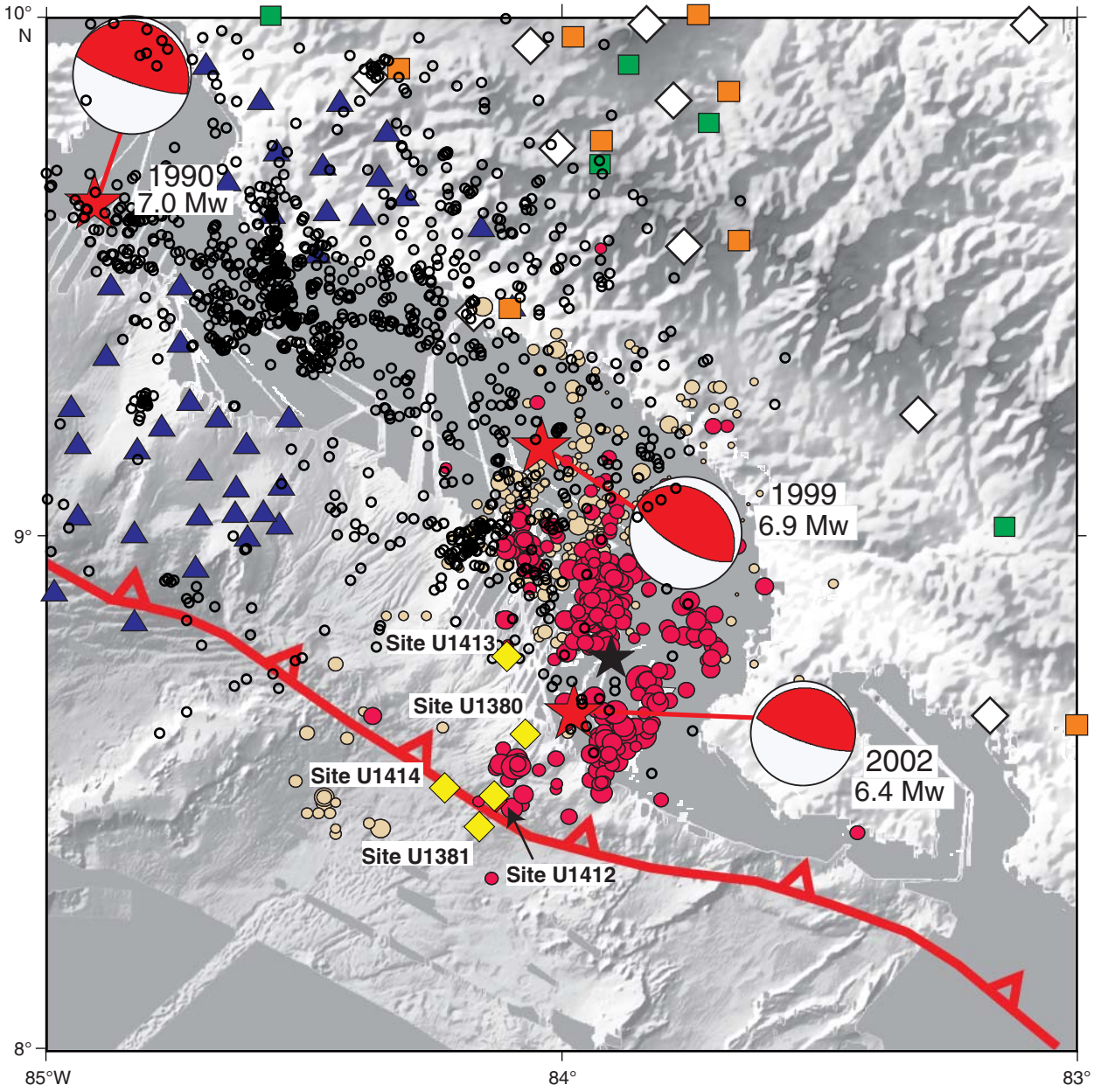

Figure F4. Heat flow data offshore Costa Rica. Color-coded circles indicate heat flow values (Von Herzen and Uyeda, 1963; Vacquier et al., 1967; Langseth and Silver, 1996; Fisher et al., 2003; Hutnak et al., 2007; Harris et al., 2010a). Stars show locations of heat flow measurements from Expedition 334 and ODP Leg 170 drill sites. Dashed red line indicates the position of the thermal transition between areas of relatively low and high heat flow. East Pacific Rise (EPR)-generated crust to the north of the triple junction and fracture zone traces has heat flow suppressed by roughly 70%, whereas Cocos-Nazca spreading center (CNS)-generated crust to the south generally has heat flow that matches conductive lithospheric cooling models (Hutnak et al., 2007, 2008).

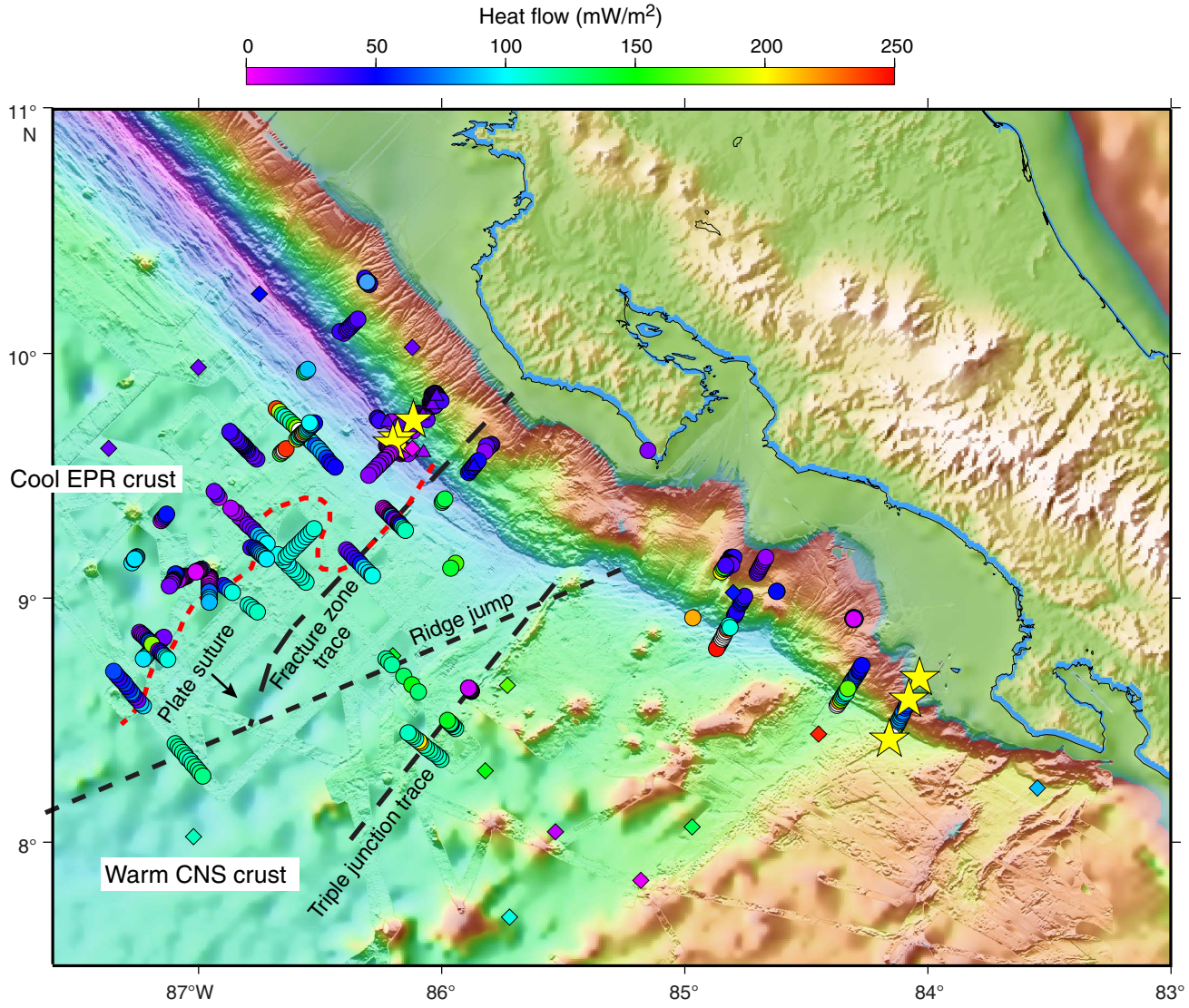

Figure F5. Central America Focus Site activity map (2008) (media.marine-geo.org/image/central-america-focus-site-activity-map-2008-0/). OBS = ocean-bottom seismometer, BSR = bottom-simulating reflector.

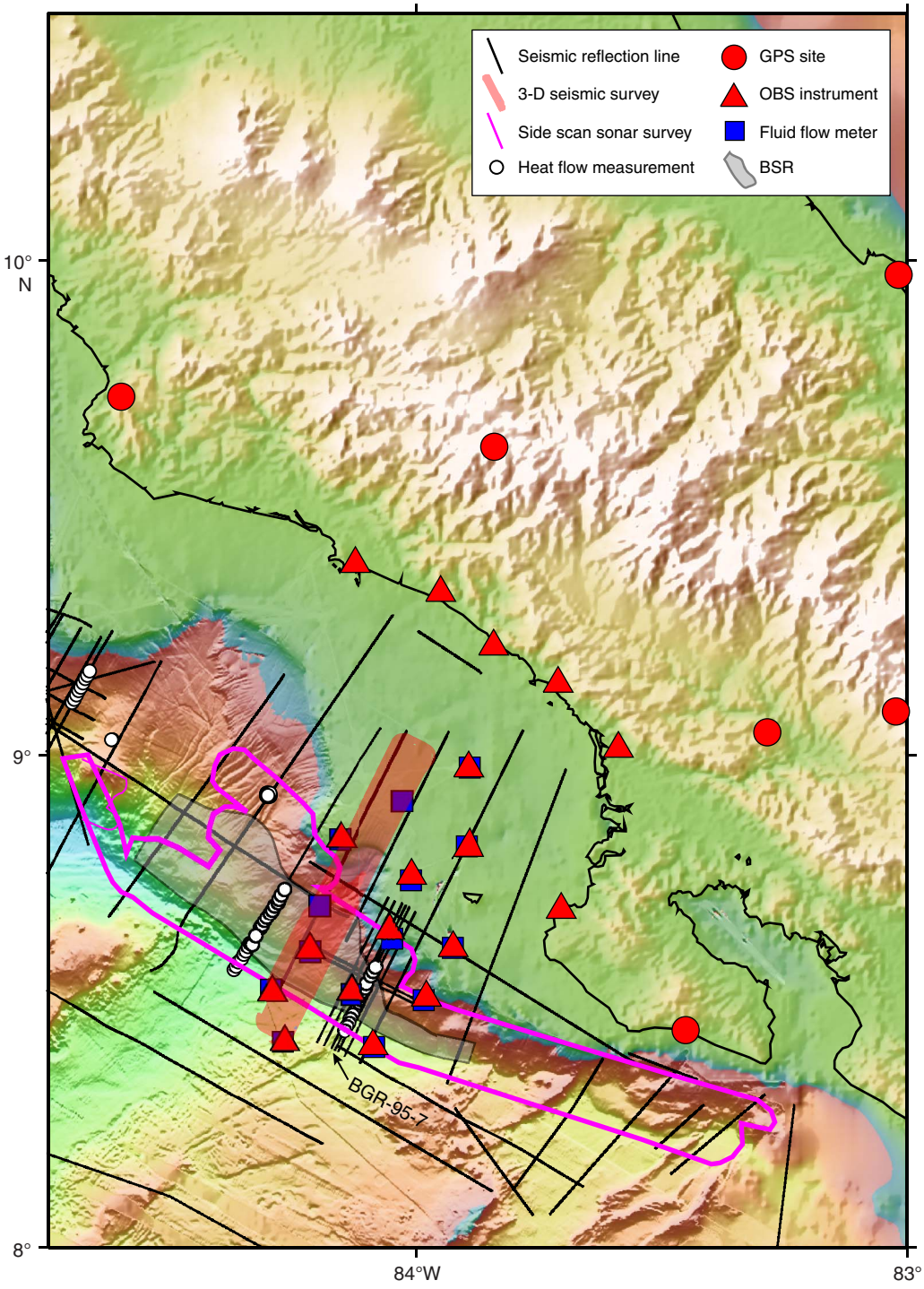

Figure F6. Location of Expedition 344 drill sites. Red diamonds denote Expedition 344 sites (U1380, U1381, and U1412–U1414) and yellow diamonds denote Expedition 334 sites not occupied during Expedition 344 (U1378 and U1379). Red lines = 3-D seismic survey, black lines = seismic reflection lines. Numbers along the short and long axes of the 3-D survey represent inlines and crosslines, respectively.

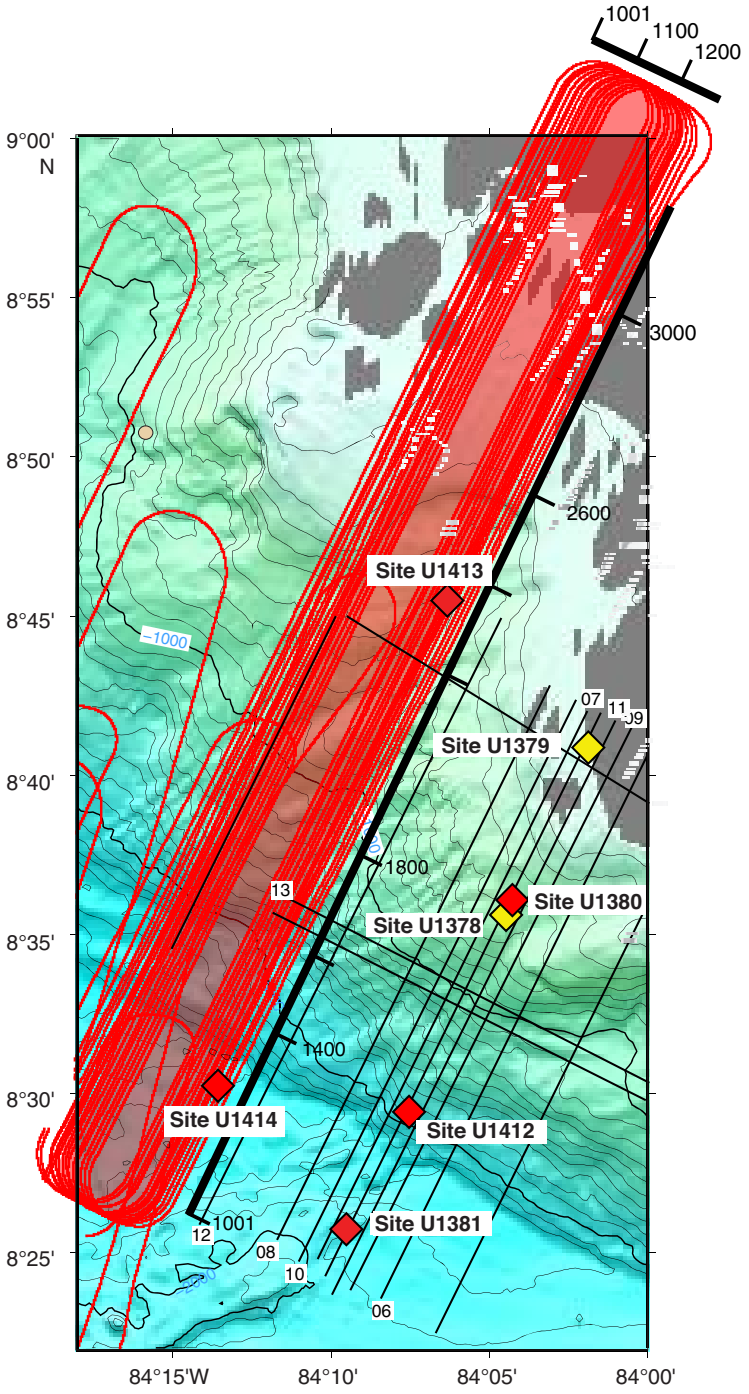

Figure F7. Heat flow and thermal models along seismic reflection Line BGR99-7, with Expedition 334 and 344 sites marked. Red solid circles show seafloor probe observations of heat flow, and blue circles show heat flow derived from bottom-simulating reflectors (BSRs) (Harris et al., 2010a). Red lines correspond to heat flow predictions based on two-dimensional thermal models described in Harris et al. (2010b). The dashed line corresponds to a subducting plate with no upper crustal fluid flow. The solid line corresponds to a subducting plate that incorporates upper crustal fluid flow.

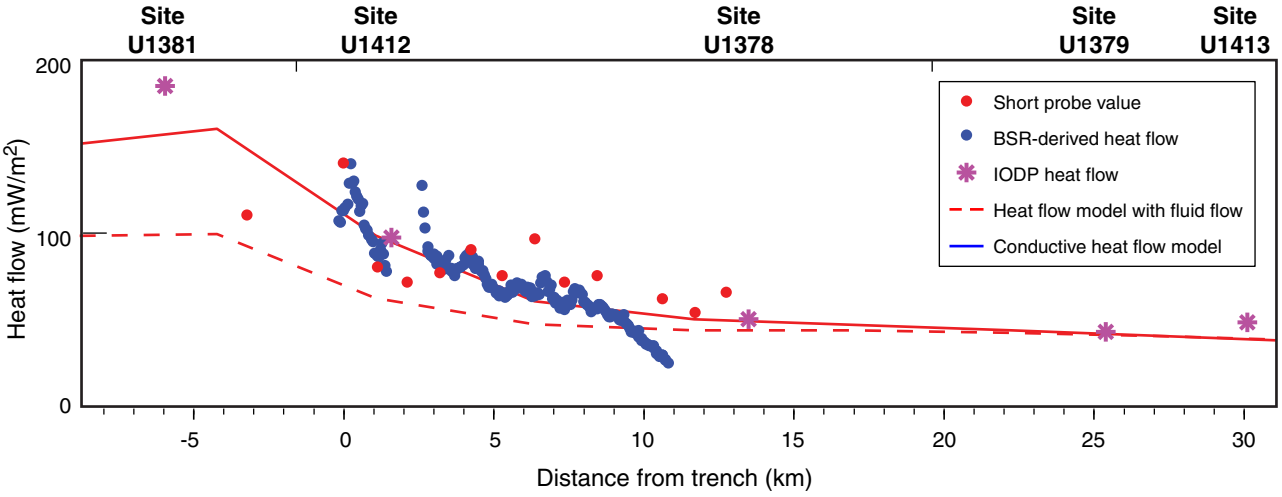

Figure F8. Detail of poststack time-migrated seismic Line BGR99-7 centered at Site U1381. Prestack depth migration from C.R. Ranero (unpubl. data).

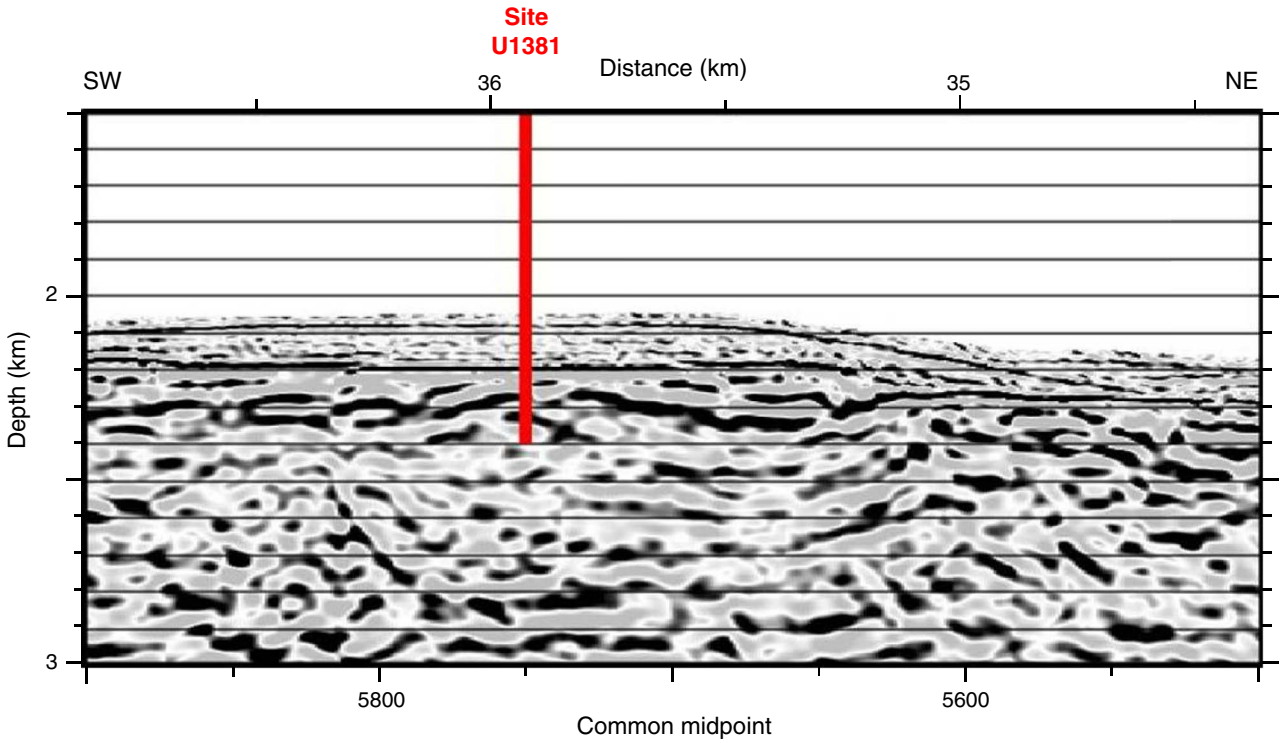

Figure F9. Summary of lithostratigraphic, biostratigraphic, paleomagnetic, physical property, and geochemical data, Site U1381. Nanno = nannofossil, MS = magnetic susceptibility. WRMSL = Whole-Round Multisensor Logger, MAD = moisture and density.

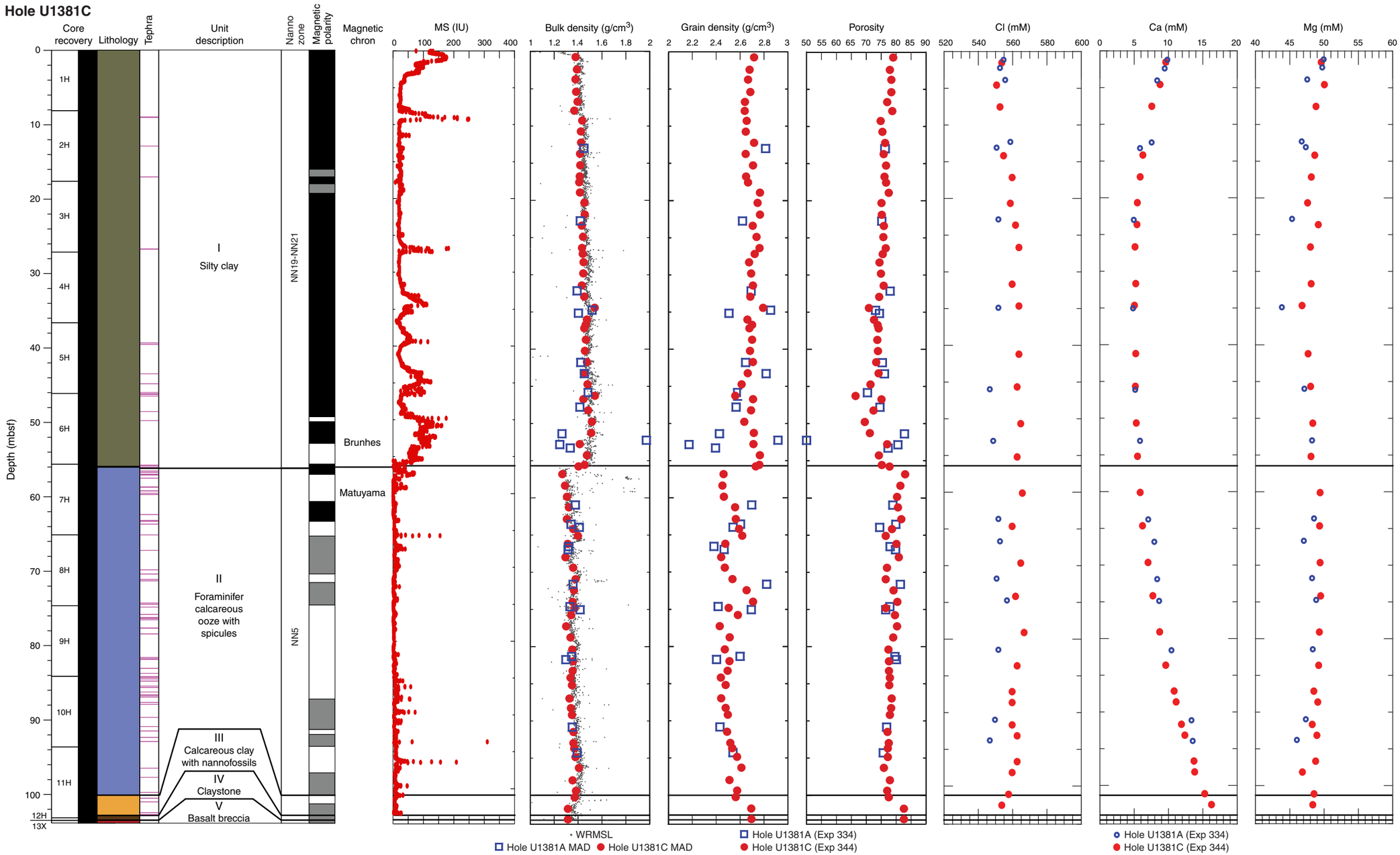

Figure F10. Detail of poststack time-migrated seismic Line BGR99-7 centered at Site U1380. Prestack depth migration from C.R. Ranero (unpubl. data).

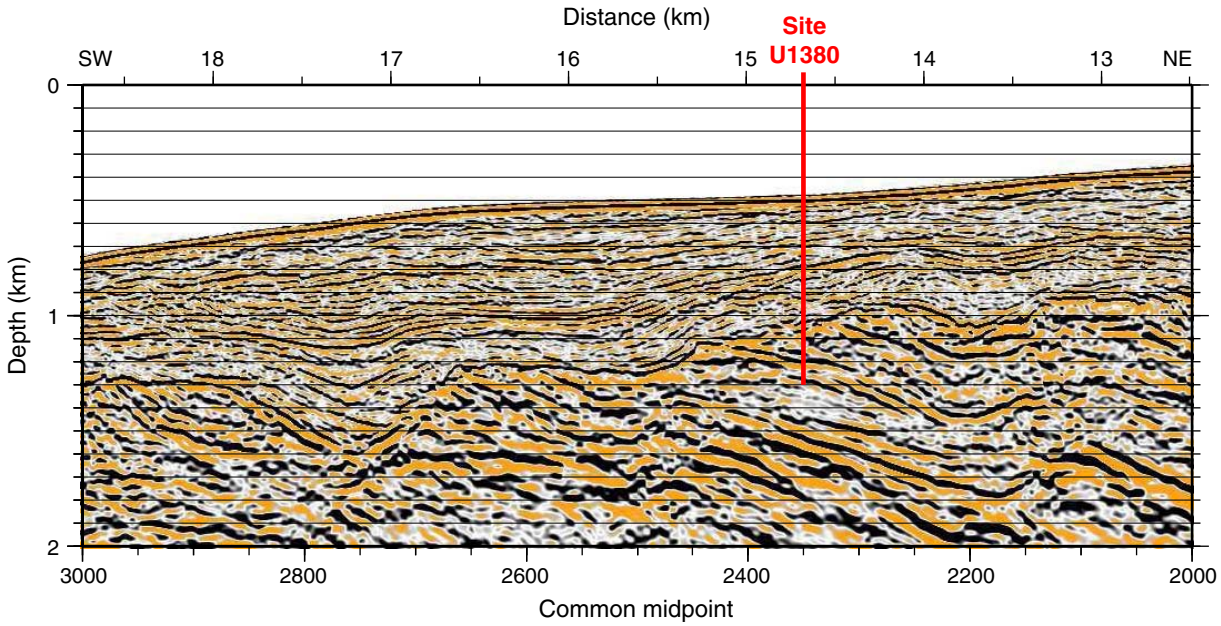

Figure F11. Summary of lithostratigraphic, biostratigraphic, paleomagnetic, physical property, and geochemical data, Site U1380. Orange line shows best-fit exponential porosity-depth relationship obtained from upper 550 m of Sites U1378 and U1380 (porosity = $0.68^{[-0.0008 \times \text{depth}]}$; $R^2 = 0.75$). Nanno = nannofossil, MS = magnetic susceptibility.

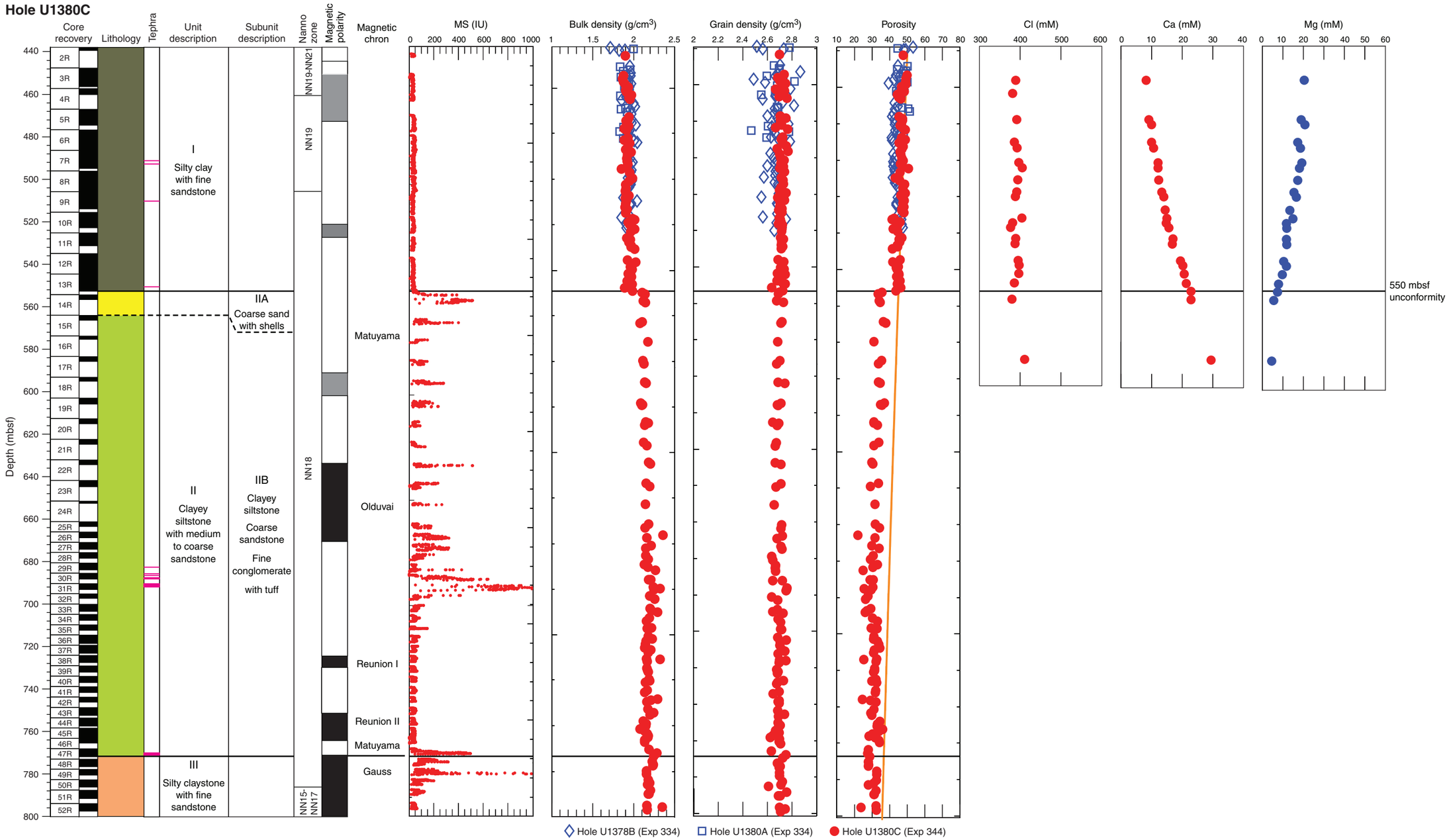

Figure F12. Detail of poststack time-migrated seismic Line BGR99-7 centered at Site U1412. Prestack depth migration from C.R. Ranero (unpubl. data). BSR = bottom-simulating reflector.

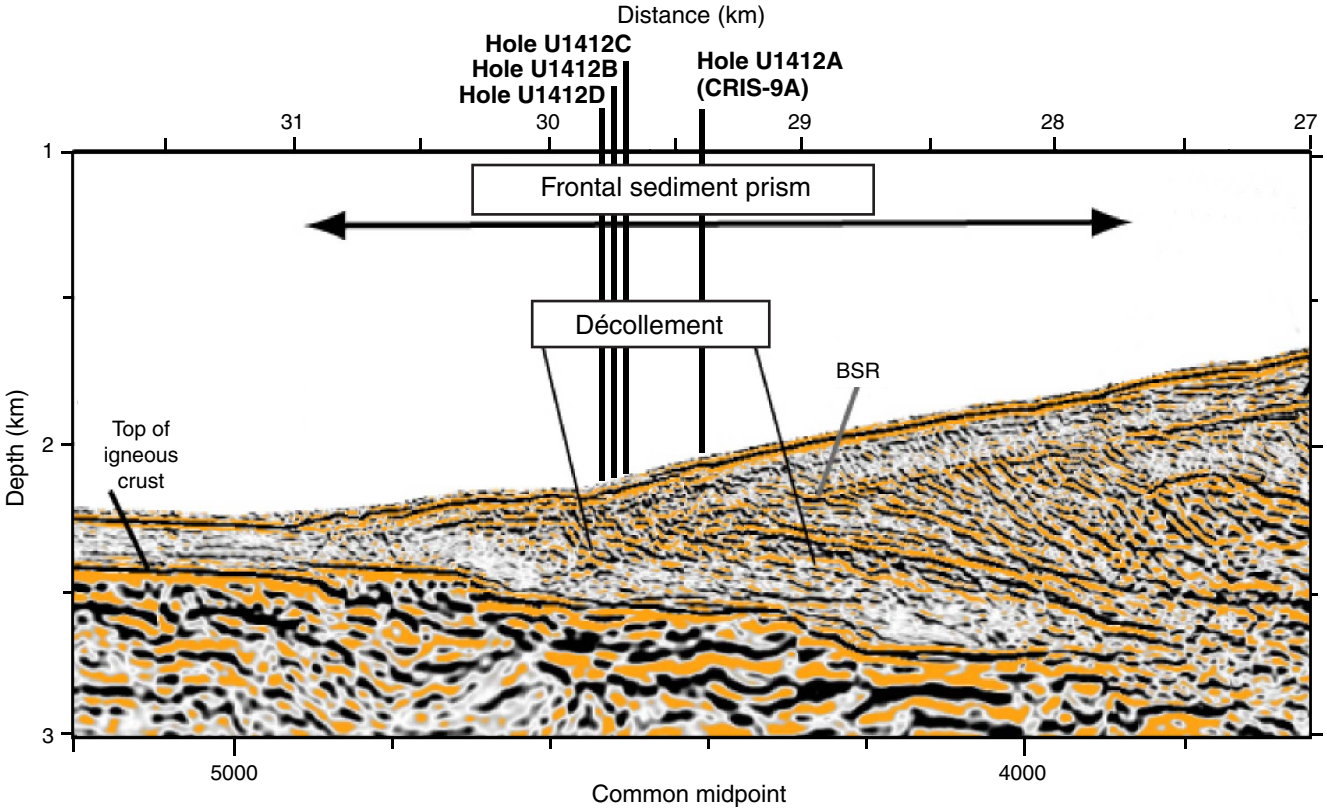

Figure F13. Summary of lithostratigraphic, biostratigraphic, paleomagnetic, physical property, and geochemical data, Site U1412. Nanno = nannofossil, MS = magnetic susceptibility. WRMSL = Whole-Round Multisensor Logger, MAD = moisture and density, BSR = bottom-simulating reflector.

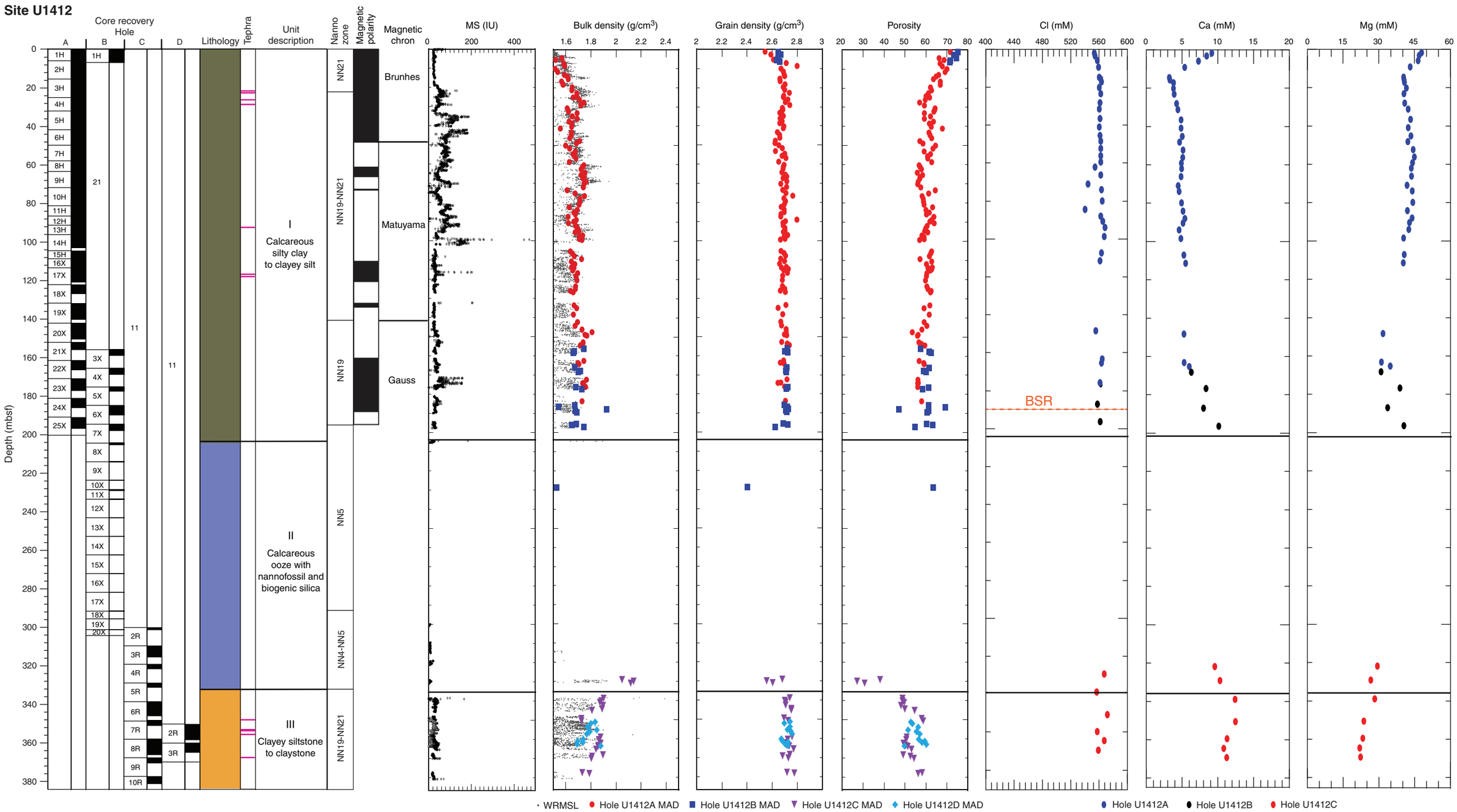

Figure F14. Seismic traveltime section of Line 2466 showing the location of Site U1413.

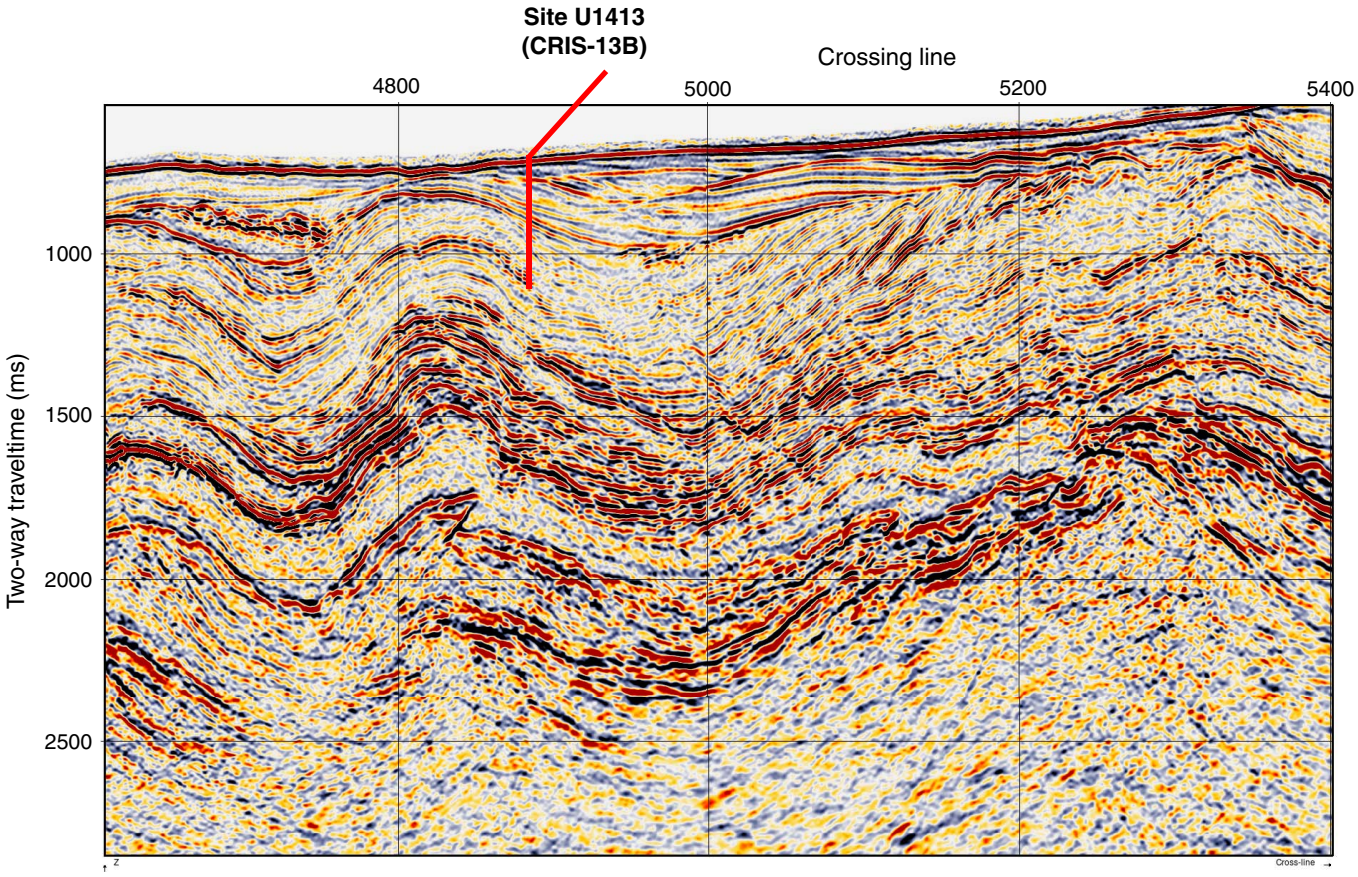

Figure F15. Summary of lithostratigraphic, biostratigraphic, paleomagnetic, physical property, and geochemical data, Site U1413. Nanno = nannofossil, MS = magnetic susceptibility.

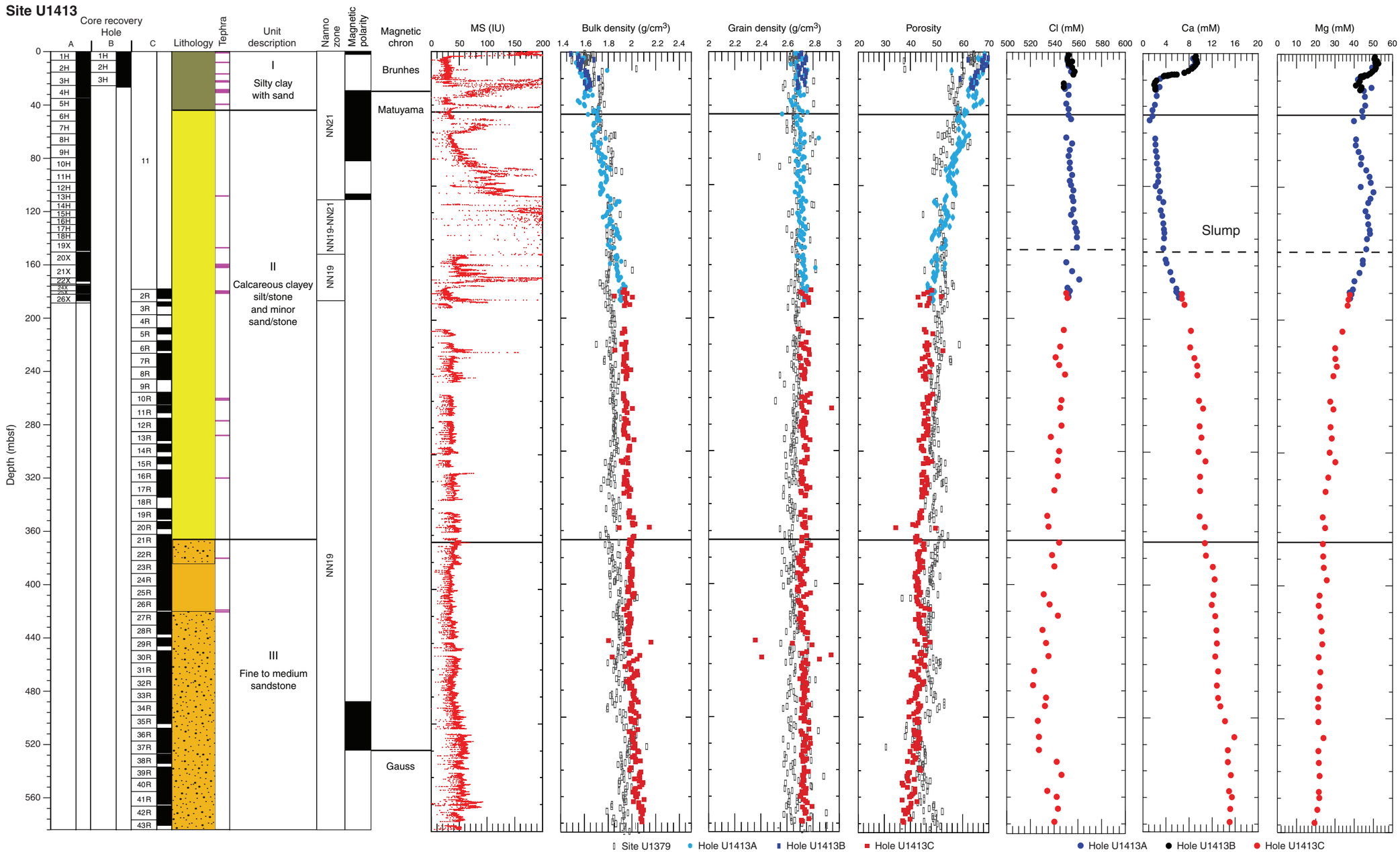

Figure F16. Seismic traveltime section of Line 2497 showing the location of Site U1414.

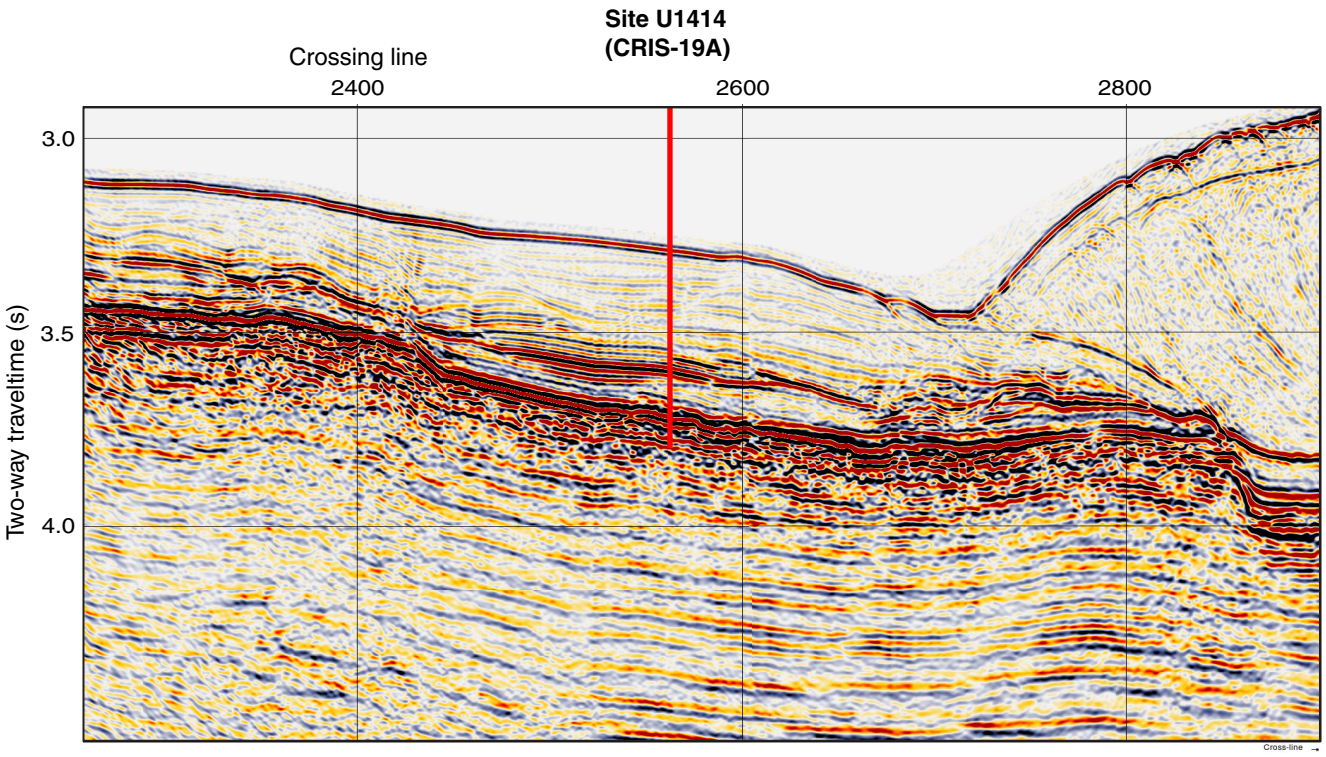

Figure F17. Summary of lithostratigraphic, biostratigraphic, paleomagnetic, physical property, and geochemical data, Site U1414. Nanno = nannofossil, MS = magnetic susceptibility. WRMSL = Whole-Round Multisensor Logger, MAD = moisture and density.

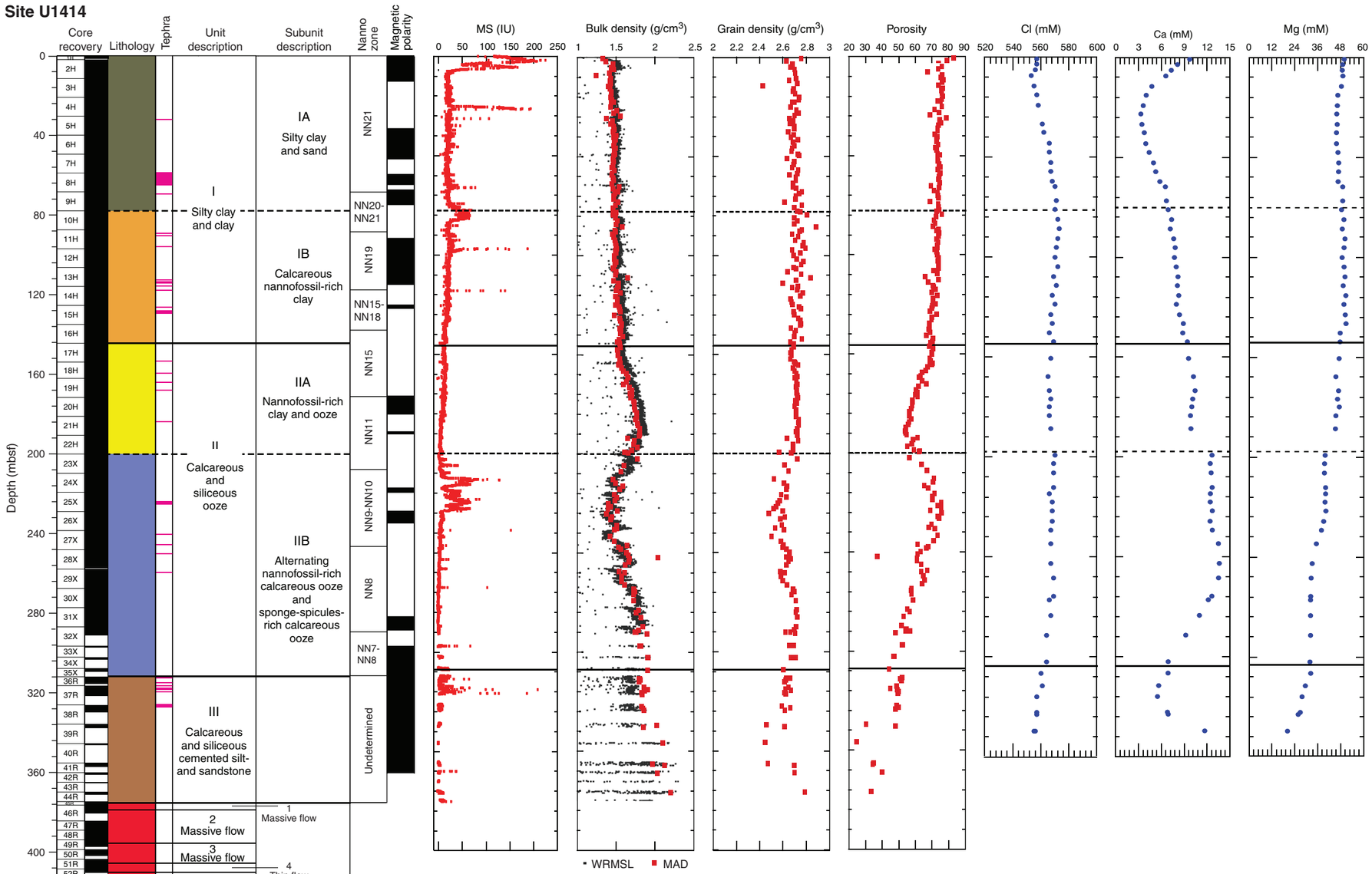

Table T1. Expedition 344 operations summary.

Hole	Latitude	Longitude	Water depth (m)	Total penetration (m)	Drilled interval (m)	Cored interval (m)	Core recovered (m)	Recovery (%)	Total cores (*N*)	APC cores (*N*)	XCB cores (*N*)	RCB cores (*N*)	Start		End		Time on hole (days)
													Date (2012)	Time UTC (h)	Date (2012)	Time UTC (h)	
344-																	
U1380B	8°35.9952′N	84°4.3908′W	502.7	50.0	50.0	—	—	0	0	0	0	0	27 Oct	2315	28 Oct	2130	0.93
U1380C	8°35.9879′N	84°4.3918′W	502.7	800.0	438.0	362.0	202.35	56	51	0	0	51	28 Oct	2130	14 Nov	0700	16.40
		Site U1380 totals:	—	850.0	488.0	362.0	202.35	56	51	0	0	51					17.33
U1381C	8°25.7027′N	84°9.4800′W	2064.6	103.8	—	103.8	109.03	105	13	12	1	0	26 Oct	1215	27 Oct	2145	1.40
		Site U1381 totals:	—	103.8	—	103.8	109.03	105	13	12	1	0					1.40
U1412A	8°29.3294′N	84°7.6686′W	1920.7	200.3	—	200.3	170.03	85	25	15	10	0	14 Nov	0800	16 Nov	2010	2.51
U1412B	8°29.1599′N	84°7.7512′W	1964.9	304.3	149.1	155.2	28.26	18	19	1	18	0	16 Nov	2015	21 Nov	0445	4.35
U1412C	8°29.1700′N	84°7.7467′W	1965.0	387.0	300.0	87.0	36.57	42	9	0	0	9	21 Nov	0445	24 Nov	0400	2.97
U1412D	8°29.1402′N	84°7.7793′W	1973.0	369.2	350.4	18.8	12.25	65	2	0	0	2	1 Dec	0930	3 Dec	0305	1.73
		Site U1412 totals:	—	1260.8	799.5	461.3	247.11	54	55	16	28	11					11.56
U1413A	8°44.4593′N	84°6.8095′W	539.9	189.1	—	189.1	187.28	99	26	18	8	0	24 Nov	0530	26 Nov	0555	2.02
U1413B	8°44.4593′N	84°6.7992′W	540.4	25.6	—	25.6	27.44	107	3	3	0	0	26 Nov	0555	26 Nov	1150	0.25
U1413C	8°44.4482′N	84°6.7993′W	540.4	582.2	178.0	404.2	313.94	78	42	0	0	42	26 Nov	1150	1 Dec	0745	4.83
		Site U1413 totals:	—	796.9	178.0	618.9	528.66	85	71	21	8	42					7.10
U1414A	8°30.2304′N	84°13.5298′W	2458.6	471.6	—	471.6	383.95	84	63	22	13	28	3 Dec	0305	10 Dec	1955	7.96
		Site U1414 totals:	—	471.6	—	471.6	383.95	84	63	22	13	28					7.96
		Expedition 344 totals:	—	3483.1	1465.5	2017.6	1471.1	73	253	71	50	132					45.35

APC = advanced piston corer, XCB = extended core barrel, RCB = rotary core barrel.